ABSTRACT

The vapor pressure of $^{13}CHF_3$ relative to the vapor pressure of $^{12}CHF_3$ has been measured as a function of temperature between 161° K and 205° K through the use of a modified Bigeleisen distillation column. The transient build-up of the isotopic concentration gradient along the length of the packed column during the start-up period was monitored as a function of time by taking samples from the condenser section. The gaseous samples were completely oxidized to carbon dioxide in the presence of a platinum catalyst and a large excess of oxygen at temperatures between 1050° C and 1100° C. The combustion products were gas chromatographically purified and the purified carbon dioxide samples were analyzed in a Nier-type isotope-ratio mass spectrometer. The data of each distillation run were reduced in light of a modified Cohen's theory of the kinetics of a square cascade of close-separation stages.

The vapor pressure isotope effect for carbon substitution in CHF_3 in this temperature range has been found to be an inverse effect. A trend of increasing inverse effect with decreasing temperature has been observed. The relative vapor pressure may be expressed as

$$\ell n \frac{P'}{P} = \frac{(217 \pm 66)}{T} - \frac{(0.89 \pm 0.36)}{T}$$

where P' and P are the vapor pressures of $^{12}CHF_3$ and $^{13}CHF_3$ respectively.

A cell model liquid force field for trifluoromethane has been derived. The accompanying table contains the $\underset{\sim}{F}$ matrix elements fit to the observed vapor pressure isotope effect.

MASTER

DISCLAIMER

This report was prepared as an account of work sponsored by an agency of the United States Government. Neither the United States Government nor any agency Thereof, nor any of their employees, makes any warranty, express or implied, or assumes any legal liability or responsibility for the accuracy, completeness, or usefulness of any information, apparatus, product, or process disclosed, or represents that its use would not infringe privately owned rights. Reference herein to any specific commercial product, process, or service by trade name, trademark, manufacturer, or otherwise does not necessarily constitute or imply its endorsement, recommendation, or favoring by the United States Government or any agency thereof. The views and opinions of authors expressed herein do not necessarily state or reflect those of the United States Government or any agency thereof.

DISCLAIMER

Portions of this document may be illegible in electronic image products. Images are produced from the best available original document.

Liquid and Gaseous $\underset{\sim}{F}$ Matrix for Trifluoromethane

Force Constants	$\underset{\sim}{F}$ Matrix Elements[a]	
	Gas	Liquid
Internal		
Diagonal		
C-H stretch	5.000000	4.814698
C-F stretch	6.017878	6.206256
H-C-F bend	0.491320	0.489509
F-C-F bend	0.764617	0.765351
Interaction		
C-H str x C-F str	1.172021	0.859410
C-F str x C-F str	0.749878	0.474351
C-H str x H-C-F bend	-0.167382	-0.310438
C-H str x F-C-F bend	0.167382	0.310438
C-F str x adj H-C-F bend	0.194294	0.194294
C-F str x opp H-C-F bend	-0.265706	-0.265706
C-F str x adj F-C-F bend	0.256033	0.256033
C-F str x opp F-C-F bend	-0.180848	-0.180848
H-C-F bend x H-C-F bend	0.039340	0.041347
F-C-F bend x F-C-F bend	-0.097309	-0.096575
H-C-F bend x adj F-C-F bend	-0.151667	-0.125241
H-C-F bend x opp F-C-F bend	-0.266667	-0.240241
External		
Diagonal		
Translation	————	0.300000
Rotation	————	0.100000[b]
Internal-External Interaction		
C-H str x T_z	————	-0.840000
C-F str x T_z	————	0.840000
H-C-F bend x T_z	————	0.300000
F-C-F bend x T_z	————	-0.300000

(a) Unless otherwise noted, in units of mdyn/Å.

(b) In units of mdyn-Å.

Thesis Approved by:

Takanobu Ishida
Professor of Chemistry
Thesis Adviser
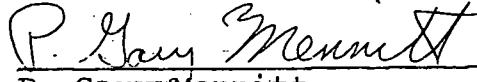
P. Gary Mennitt
Professor of Chemistry
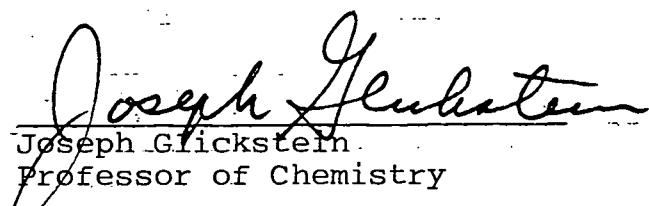
Joseph Glickstein
Professor of Chemistry
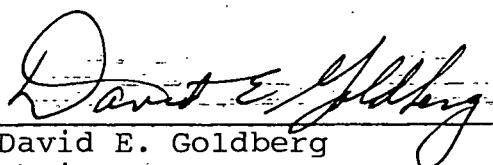
David E. Goldberg
Chairman
Department of Chemistry
Brooklyn College of the
City University of New York

STUDIES OF

CARBON-13 VAPOR PRESSURE ISOTOPE EFFECT

IN CHF_3

A Thesis

Presented to the Graduate Faculty

of the Department of Chemistry

Brooklyn College

City University of New York

In Partial Fulfillment

of the Requirement of the Degree of

Master of Arts

by

Lester Borodinsky

August 1976

I offer this unto That Truth which is Absolute.

TABLE OF CONTENTS

LIST OF TABLES

LIST OF FIGURES

I. INTRODUCTION

The purpose of this study is twofold. The first is to experimentally determine the separation factor for carbon-13 as a function of temperature from its natural abundance by means of low temperature distillation of trifluoromethane, CHF_3. Secondly, this study proposes to investigate theoretically the inverse vapor pressure isotope effect in $^{13}CHF_3/^{12}CHF_3$. This is to be done by a force field study utilizing Wilson's $\underset{\sim}{F}$ and $\underset{\sim}{G}$ matrix method.[29]

Carbon-13 is a stable isotope that naturally occurs at an abundance of 1.11%. The fact that it is not radioactive has recently attracted the interest of biomedical scientists to its potential use as a tracer for carbon in medical and biological studies. Recent advances for detection and/or determination by ^{13}C NMR have made its use particularly attractive. In such tracer studies, this technique will not only trace the path of ^{13}C, but also determine its molecular environment.

^{13}C is currently being enriched up to 95.5%[1] by means of cryogenic distillation of carbon monoxide. It has also been fractionated by the carbon dioxide-carbamate process[2] and the thermal diffusion of methane.[3]

Other methods that have been investigated, but not adapted to production scale, include the following. In the process used by Urey et al, ^{13}C was enriched from its natural abundance by means of a carbon-isotope exchange between an aqueous solution of sodium cyanide and gaseous hydrogen

cyanide;[4]

$$H^{13}CN + {}^{12}CN^- \rightleftharpoons H^{12}CN + {}^{13}CN^- \ .$$
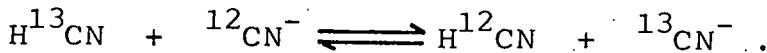
The equilibrium constant was found to be 1.026 at room temperature, but in addition to the obvious toxicity of the substance, polymerization of HCN gradually sets in, leading to an equivalent loss of isotopes in a cascade operation.

A system that consists of a cuprous chloride-ammonium chloride solution and carbon monoxide (COCO system), developed at Oak Ridge National Laboratory, employs thermal reflux at both ends. The stage separation factor for this system is 1.015 at room temperature, and the isotope exchange is rapid enough to obtain a stage height of less than 1.5 times the column diameter.[5]

Another exchange system developed at Oak Ridge consists of a ketone cyanohydrin and aqueous cyanide solution. It has a very high separation factor of about 1.04 but requires a chemical reflux.[5]

The carbon dioxide-carbamate exchange was developed by T. I. Taylor and his students at Columbia University. It has since been scaled up by Mound Laboratory for enriching ^{13}C from its natural abundance to about 93%. The effective stage separation factor depends on temperature, pressure, flow rate, solvent, and the choice of carbamate. The Mound process utilizes carbamate of n-dibutylamine dissolved in triethylamine and yields an effective single stage separation factor of 1.01.[6] Because of the limited solubility of carbamate and the rather high vapor pressure

of the amine, the carbamate process is generally limited to operation at temperatures in the range of 25-40° C.

Unlike processes such as distillation or isotope exchange reactions, thermal diffusion is a non-equilibrium process. Although thermodynamically unfavorable, the thermal diffusion process originally devised by Clausius and Dickel[7] has been widely used for isotope separation purposes. This is due primarily to the simplicity of the aparatus and the relatively large separation factor yielded by the process. This process was used at Mound Laboratory in combination with the carbamate process.

Before proceeding further, it seems appropriate to present the basic nomenclature used in the present study, and to discuss the relative advantages and disadvantages of the various processes. The basic unit of the separation process is the separating stage. Each stage is fed with material of the same composition and produces partially fractionated product streams. When the degree of separation effected by a single stage falls short of the desired separation between product and feed material, it is necessary to connect stages in series. A group of stages connected in series is referred to as a cascade. The degree of separation effected by a unit stage is expressed in terms of the separation factor. Referring to Figure 1, the stage separation factor, α, is defined as

$$\alpha \equiv \frac{\text{Abundance Ratio in Heads}}{\text{Abundance Ratio in Tails}}$$

Figure 1. Separation Stage

STREAM	ATOM FRACTION	ATOM RATIO
Heads	N'	R'
Stage Feed	N	R
Tails	N''	R''

Separation Stage
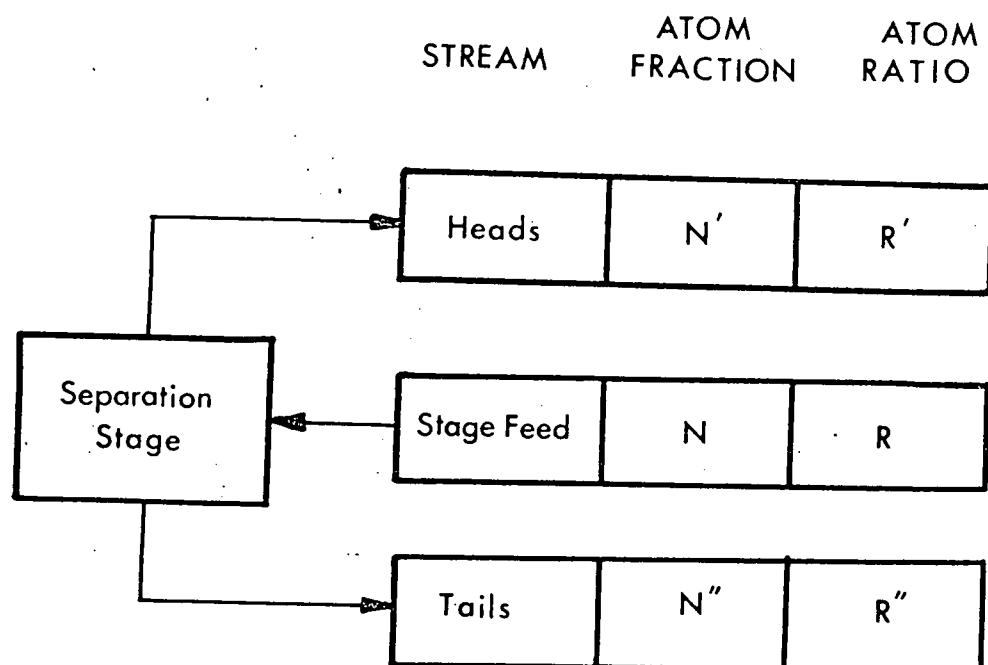
$$= \frac{R'}{R''} = \frac{N}{N''} \frac{1-N''}{N'} \quad . \tag{1}$$

Since α for an isotoped exchange is generally close to unity (except for hydrogen isotopes), it is sometimes convenient to use ϵ, defined as

$$\epsilon \equiv \alpha - 1. \tag{2}$$

For a distillation process, α is equal to the ratio of the vapor pressures of two isotopic molecules at a given temperature. As a rule of thumb, ϵ for a distillation process for enrichment of isotopes of second period elements (Li-F) does not exceed 10^{-2}. At Mound Laboratory, CCl_3F (Halocarbon-11) was distilled at 24° C and the separation factor was found to be 1.0019 ± 0.0003.[3] For an exchange process, the separation factor is proportional to the equilibrium constant. These are not necessarily identical since an isotopic substitution at equivalent atomic positions in a given molecule does not lead to isotopic fractionation.[8] Generally ϵ for an exchange reaction often exceeds $2-3 \times 10^{-2}$ which is attributable to a large change in bond order around the substituted atom as it is exchanged between two chemical species. The disadvantage of the exchange process is that it usually requires a chemical reflux at both ends of the cascade. Such a chemical reflux is necessary to achieve complete conversion of one chemical species into the other at the end of the cascade without any loss of isotopes from the system. This usually leads to costly chemical waste. The carbamate

process achieves the reflux by thermal means, i.e., the carbamate is thermally decomposed at one end of the cascade while carbon dioxide and amine are thermally combined to form carbamate at the other end. Such an exchange process is called an exchange distillation, and has the advantages of both the exchange and distillation processes. The more important merits of a distillation lie in the absence of a chemical reflux and in a large material throughput, the latter being a very important consideration in an industrial size plant. Thus, a distillation plant which handles a substance with a molecular weight of 100 and a density of 2 grams/ml would be 20 times smaller in volume than an exchange plant handling 1 molar solutions.

The recently discovered method of laser-activated isotope separation has a special advantage of being capable of yielding a large separation factor, i.e., of the order of tens and hundreds for α.[9] At this early stage of development, the material throughput is exceedingly limited due to the fact that the laser activation has to be achieved in the gaseous state of very low pressure, typically of the order of 1 torr. This dilute system is a necessary requirement for the achievement of the extremely high selectivity. The future of laser isotope separation seems to depend on ultra-powerful laser technology and a compromise between selectivity and throughput.

In Section I-1 that follows, the general theory of the vapor pressure isotope effect will be presented. Following

it, in Section I-2, will be a discussion of preliminary investigations that lead to the choice of CHF_3 (Halocarbon-23) as the distillation material. The Introduction will be concluded with Section I-3, wherein the outline of the investigation will be presented.

I-1. Theory of Vapor Pressure Isotope Effect

The vapor pressure of a chemically and isotopically pure liquid is determined by the dynamic equilibrium between two species, i.e., the molecules in the gas phase and the molecules in the liquid phase. The vapor pressure of such a substance can be expressed in terms of the partition function of these two species. It follows then that the difference in the vapor pressures of a pair of isotopic liquids of the same substance is expressible in terms of four partition functions, the gas and liquid partion functions for each isotopic species.

Bigeleisen[10] developed a fundamental theory of vapor pressure isotope effect based on the assumptions of the simple cell model of liquids, anf the Born-Oppenheimer approximation. According to this theory, the ratio of the vapor pressures of the lighter isotopic species, P', to that of the heavier isotopic species, P, is given by

$$\ln\left(\frac{P'}{P}\right) = \ln \frac{s}{s'} f_c - \ln \frac{s}{s'} f_g \tag{3}$$

where s' and s are the symmetry numbers of the light and heavy isotopic species respectively, and f_c and f_g are the isotopic ratios of the reduced partition functions in the condensed phase and the gas phase respectively. They are "reduced" in the sense that they are the ratios of the partition functions to their classical limit, i.e.,

$$\frac{s}{s'} f = \frac{\left(Q/Q'\right)_{qm}}{\left(Q/Q'\right)_{cl}} = \frac{\left(Q_{qm}/Q_{cl}\right)}{\left(Q'_{qm}/Q'_{cl}\right)} \tag{4}$$

where Q' and Q are the partition functions of the light and heavy species respectively, and the subscripts qm and cl represent the quantum mechanical and classical respectively.

Within the framework of the Born-Oppenheimer approximation and under the assumption that the potential is harmonic and that the translational and rotational partition functions are classical, $\frac{s}{s'} f$ can be expressed[7] as

$$\frac{s}{s'} f = \prod_{i=1} \frac{u_i}{u_i'} \frac{e^{-u_i/2}\left(1 - e^{-u_i'}\right)}{e^{-u_i'/2}\left(1 - e^{-u_i}\right)} \tag{5}$$

where ther product is taken over all degrees of vibrational freedom, and u is defined as

$$u \equiv \frac{hc\omega}{kT} \tag{6}$$

where h is Planck's constant, c the velocity of light, ω the normal frequency in units of wavenumbers (cm^{-1}), k the Boltzman constant and T the absolute temperature.

When T is very large or when the ω's are small, Equation 5 reduces to

$$\ell n \frac{s}{s'} = \frac{1}{24} \sum_i (u_i'^2 - u_i^2) \qquad (7)$$

$$= \frac{1}{T^2} \frac{1}{24} \left(\frac{hc}{k}\right)^2 \sum_i (\omega_i'^2 - \omega_i^2) \qquad (8)$$

When T is low or when the ω's are large, Equation 5 approaches

$$\ell n \frac{s}{s'} = \sum_i \frac{u_i' - u_i}{2} \qquad (9)$$

$$= \frac{1}{T} \frac{hc}{2k} \sum_i (\omega_i' - \omega_i) \qquad (10)$$

In the simple cell model, $\ell n \frac{s}{s'} f_c$ in Equation 3 is evaluated by associating three translational degrees of freedom, three rotational degrees of freedom, and 3N-6 internal degrees of freedom, with each molecule. Furthermore, the translational and rotational motions are assumed to be oscillatory in nature, a consequence of the cell model assumption that a liquid can be represented by a representative molecule which oscillates independently in an isotropic liquid field. Due to the relatively weak external force (as compared to the forces within the molecule), the frequencies for external oscillation are small; $\omega_{ext} < 200$ cm^{-1}. Thus, $\ell n \frac{s}{s'} f_c$ in Equation 3 can be thought of as consisting of two types of terms, one attributable to the weak external oscillations, which is proportional to $1/T^2$ in accordance with Equation 8, and the other to the internal vibrations in the condensed phase which is proportional to

1/T in agreement with Equation 10. The other term in Equation 3, $\ln \frac{s}{s'}f_g$, of course contributes additional terms which are proportional to 1/T. Consequently, as a first approximation to Equation 3, Bigeleisen derived[10] the following relationship

$$\ln \frac{P'}{P} = \frac{A}{T^2} - \frac{B}{T} \tag{11}$$

where

$$A = \frac{1}{24}\left(\frac{hc}{k}\right)^2 \sum^{6} (\omega'^{2}_{ext} - \omega^{2}_{ext}) \tag{12}$$

and

$$B = \left(\frac{hc}{2k}\right)\left\{ \left[\sum^{3N-6}\omega_g' - \sum^{3N-6}\omega_c' \right]_{int} - \left[\sum^{3N-6}\omega_g - \sum^{3N-6}\omega_c \right]_{int} \right\} \tag{13}$$

It is seen that A depends entirely on the external vibrations, while B represents the isotopic difference in the zero-point energy shift on condensation. It has been shown that A and B are always positive. According to Equation 11, the vapor pressure of the lighter isotope is greater than the heavier isotope at sufficiently low temperatures, while the effect could be reversed as the temperature increases above a certain point. If such a crossover temperature lies within the range of liquid temperature, i.e., at a temperature above the triple point and below the boiling point, then the inverse vapor pressure effect is expected to be advantageous in isotope production. The reason for this will be explained briefly in the following paragraph.

Since isotope separation is a close separation (small ϵ), an isotope separation plant requires a large number of separation stages. At the initial startup of a plant, all stages are charged with material of natural enrichment, and the refluxers on both ends of the column are activated. During the initial transient period, an isotopic concentration gradient is gradually established along the length of the cascade. When the enrichment at the product end of the cascade reaches a steady level, slow product withdrawal is initiated and is accompanied by a corresponding material input at the feed point along the cascade. During the transient period, the cascade is operated at total reflux at both ends, i.e., material is neither withdrawn nor introduced into the system. This transient period increases the holdup (the amount of desired material held up in the system). According to the theory developed by Cohen,[11] the transient period is shorter when ϵ is negative. For a distillation fractionation of ^{13}C, the negative ϵ corresponds to the inverse vapor pressure isotope effect. A preliminary investigation, outlined in the following section, showed that the probability of finding such an inverse effect in the liquid temperature range would be sustantial for fluoromethanes.

I-2. Investigation Leading to the Choice of Fluoromethanes

$^{13}CH_4$ has a lower vapor pressure than $^{12}CH_4$, at liquid methane temperature,[12] while ^{13}C substitution in CCl_4 leads to a slightly inverse isotope effect at 35° C.[13] This is a consequence of the external (translational and rotational) modes approaching negligible levels, as a result of the symmetric substitution of the peripheral positions of heavy chlorine atoms, yielding a small A in Equation 11. The smallness of the inverse effect in CCl_4 is attributable to the high temperature and the prohibited interaction between the rotation and internal motion of a tetrahedral molecule. A high molecular weight and a large magnitude of inertia reduce the magnitude of the $1/T^2$ term of Equation 11, thus favoring the inverse effect at low temperatures. The zero-point energy shift term is enhanced by strong interactions of liquid phase external modes with strongly infrared active internal mode actions, in which the center atom actively participates.[14] Presence of fluorine atoms in a molecule brings the melting and boiling points down to regions that are much lower than those of the corresponding chloro-derivatives, thus raising the possibility of the occurence of the crossover temperature within the liquid range rather than in the solid. One of these compounds, trifluoromethane (Halocarbon-23) has C_{3v} symmetry, which is sufficiently non-symmetric to allow its carbon atom to participate in the normal vibrations that can interact with the external modes in the liquid. It has a melting

point of -155.2° C and a normal boiling point of -82.03° C (see Table I), which can be conveniently handled by the cryogenic distillation column that was generously made available by Prof. Bigeleisen of the University of Rochester. Preliminary calculations[15] on the zero-point energy shift on condensation, based on Wolfsberg's theory[14] of London dispersion forces in liquids, showed that Halocarbon-23 had a good possibility of yielding the inverse isotope effect.

I-3. Outline of Investigation

The separation factor for ^{13}C fractionation in the cryogenic distillation of CHF_3 has been determined in the following manner. A portion of CHF_3 manufactured by Matheson Gas Products, which is 99.0% pure, was purified by repeated bulb-to-bulb distillation and distilled under total reflux in a cryogenic distillation column, which was designed and built by J. Bigeleisen[18] and later modified.[19] The build-up of the ^{13}C enrichment gradient along the column was monitored as a function of time. This transient behavior under total reflux was analyzed according to the theory of K. Cohen,[11] leading to the determination of the stage separation factor and the number of theoretical stages. The separation factor was then obtained as a function of temperature

TABLE I.   Physical Properties of Halocarbon-23[a]

Molecular Formula		CHF_3
Molecular Weight		70.01
Normal Boiling Point		-82.03° C(191.13° K)
Normal Freezing Point		-155.2° C(118.0° K)
Critical Temperature		25.9° C
Critical Pressure		47.7 atm
Critical Volume		133 cc/mol
Critical Density		0.525 g/cm^3
Density of liquid	@ 298° K	0.670 g/cm^3
	@ 200° K	1.409 g/cm^3 [b]
	@ 150° K	1.555 g/cm^3 [b]
Specific Heat of liquid	@ 285° K	0.252 cal/g [b]
	@ 200° K	0.168 cal/g [b]
	@ 180° K	0.162 cal/g [b]
Heat of Vaporization	@ n.B.P.	57.23 cal/g
	@ 200° K	55.58 cal/g [b]
	@ 150° K	64.47 cal/g [b]

(a) Unless otherwise noted, data taken from "Handbook of
Chemistry and Physics", 53rd Edition, Chemical Rubber Co.,
(1972).

(b) Taken from "Handbook of Fundamentals", American Society
of Heating, Refrigerating, and Air-Conditioning Engineers,
(1974)

The data was fit to Bigeleisen's formulae, Equations 3 and 11, and the result was compared with a theoretical calculation based on the theory of the simple cell model. In Chapter II (Experimental), the experimental procedures will be discussed in detail. The method of data reduction by modified Cohen's theory will be presented in Chapter III (Data Reduction). The derivation of the formula used in the data reduction will also be presented in that chapter. An extension of Cohen's theory to accomodate the need of the present investigation which deals primarily with the inverse isotope effect has been developed by Ishida and Wieck.[26] In Chapter IV, the presently obtained data on the $^{12}CHF_3/^{13}CHF_3$ vapor pressure isotope effect will be compared with Bigeleisen's theory, and a cell model liquid force field for trifluoromethane will be derived accordingly.

II. EXPERIMENTAL

The low temperature distillation of Halocarbon-23 (CHF$_3$) necessitated the use of several pieces of apparatus. The two major pieces of apparatus, a low-temperature distillation column and a combustion train, are described in Section II-1, which follows. The acquisition of reliable vapor pressure data for Halocarbon-23 is described in Section II-2. Actual experimental procedures are presented in detail in Section II-3.

II-1. Design and Construction

Design and construction of the experimental apparatus used in this investigation has been fully described by Wieck and Ishida.[19] The following is an exerpt from it, except for several modifications in the design and procedures as noted.

Preliminary purity analyses of Halocarbon-23 were performed on a Perkin-Elmer model 990 gas chromatograph. The resulting chromatograms indicated the presence of significant amounts of impurities. Air, the major impurity, was removed by repeated bulb-to-bulb distillation. The other impurities were shown to be CH$_4$ and SiF$_4$. Low boiling impurities would lead to erroneous interpretations of the

isotopic analyses of the distillate with respect to the distillation column characteristics. In order to bring the level of these impurities down to a more acceptable level, one part in 10^5, further purification was necessary.

The distillation column of the Bigeleisen type was generously donated by its creator, Professor Jacob Bigeleisen of the University of Rochester. Since its movement from Rochester, the column has been cleaned, reassembled and modified.[19]

In order to perform isotope-ratio analyses of the Halocarbon-23 samples withdrawn from the column, the conversion of CHF_3 to carbon dioxide was found to be necessary. This conversion is accomplished by the use of a specially designed and constructed combustion system. Halocarbons, especially highly fluorinated ones, are chemically quite stable. A combustion train similar to that of McKenna, Priest, and Staple[20] with some modification was fabricated in quartz.

A) Distillation Column and Its Support System.

The low-temperature distillation column was originally designed by Bigeleisen and Ribnikar[22] at Brookhaven National Laboratory. It was applied in studies of the vapor pressure isotope effect in N_2O at 184° K. Subsequently, it was used in the distillation studies of C_2H_3D and $^{12}CH_2=^{13}CH_2$ by Bigeleisen, Cragg, and Jeevanandam[12]

for their study of isotopic methanes. This column was transported from the University of Rochester along with its brass housing and service vacuum line. The column has since been modified.[12,19,20,23]

The reassembled column, in the same configuration as that most recently used,[19] had been cleaned, and was repacked with 76 grams of Podbelniak Nichrome Heli-pak No. 2916, which had been cleaned in a Soxhlet extractor with benzene for three days. The reassembled column is depicted in Figure 2 and an enlargement of the boiler is shown in Figure 3.

The entire column and service vacuum line were leak-tested using a highly sensitive (minimum detectable leak is 5×10^{-11} ccNTP/sec) helium leak detector (Dupont Instruments model 25-120 B). It was found that the service line and column were able to attain a vacuum of 10^{-5} torr, a rather good vacuum considering the capillaries involved and the large surface area of the packing. The service vacuum line is schematically represented in Figure 4.

The liquid nitrogen level in the dewar surrounding the column's helium jacket was maintained using a Veeco Instrument's model VLN 30 Liquid Nitrogen Level Controller. The controller, two sensor leads, and a three-way solenoid valve comprise a system (Figure 5) which can maintain a liquid nitrogen level between two predetermined points. The atmosphere above the liquid nitrogen in the liquid nitrogen tank is normally vented through the three-way
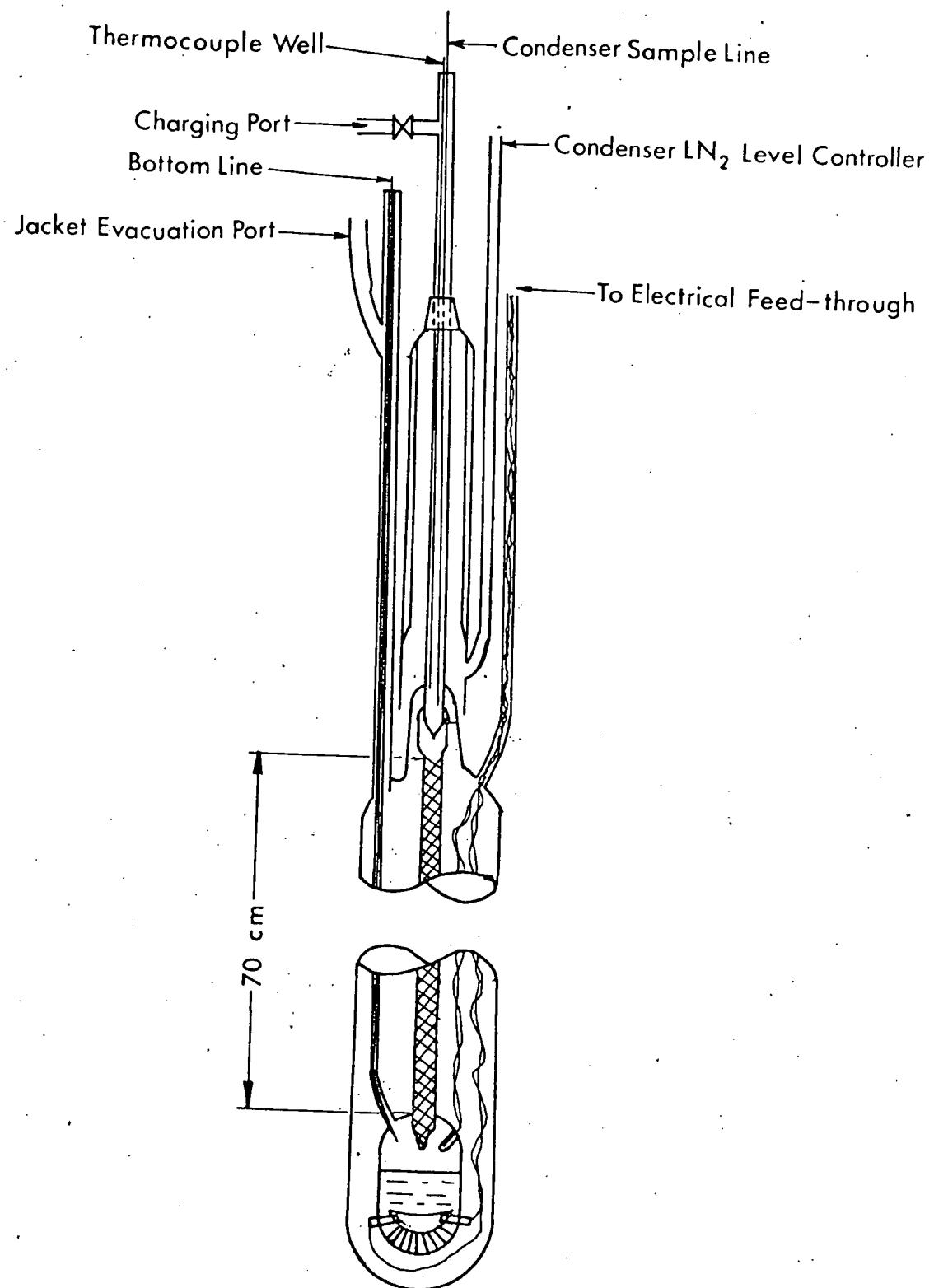
Figure 2. The Cryogenic Distillation Column

Silver Capillary

Platinum Resistance Probe

Heating Element
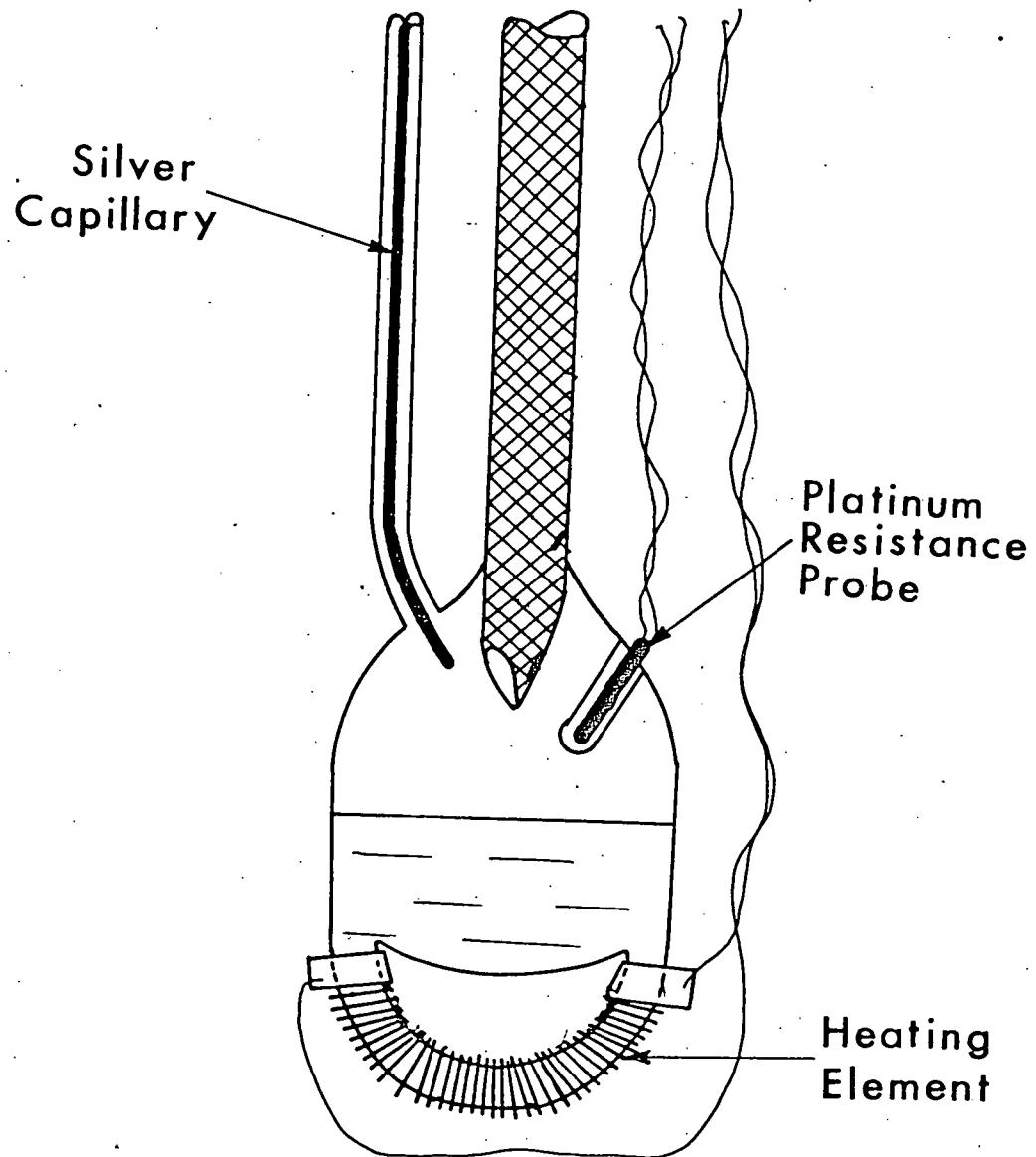
Figure 3. Boiler
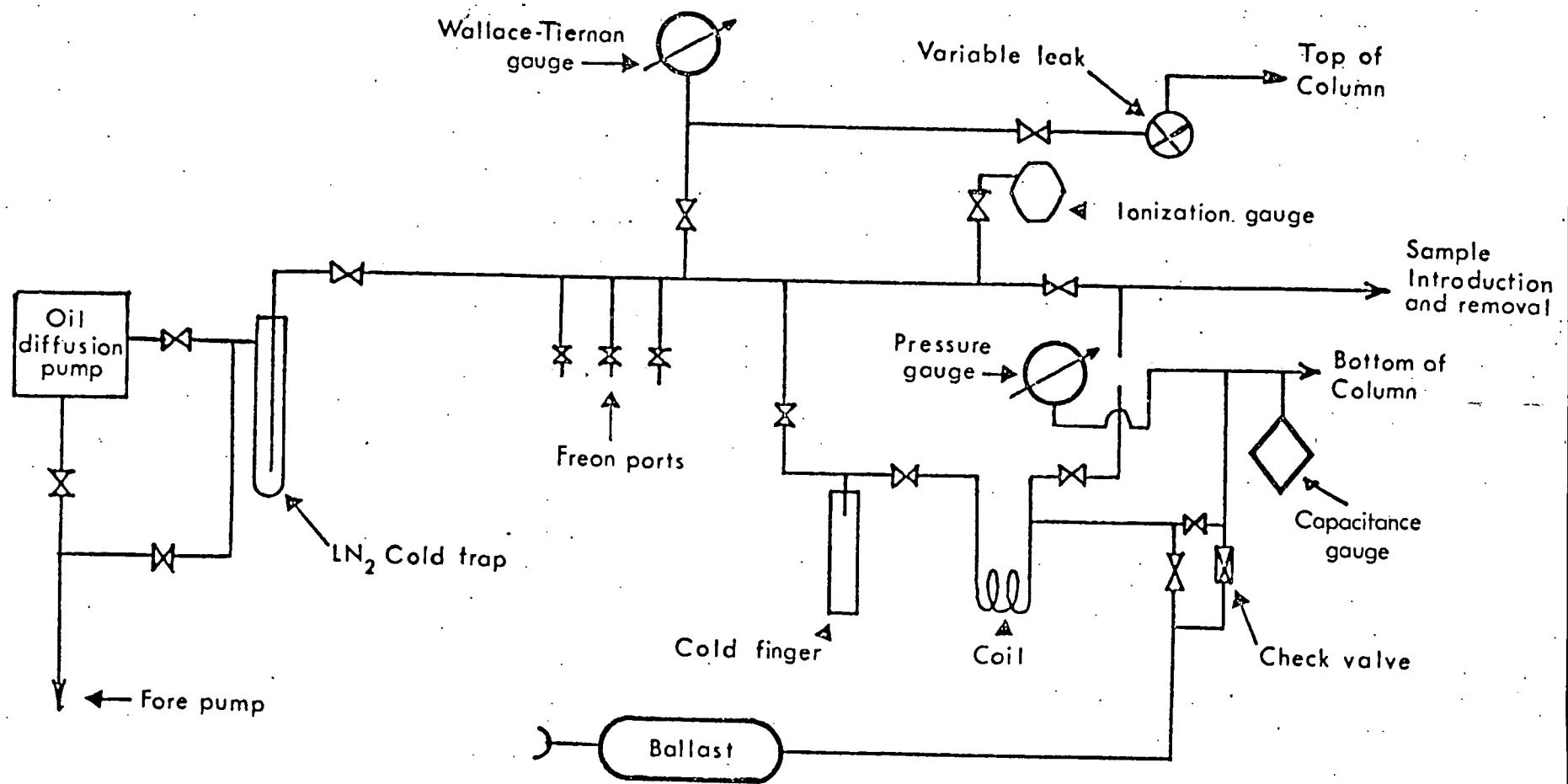
Figure 4. Service Vacuum Line
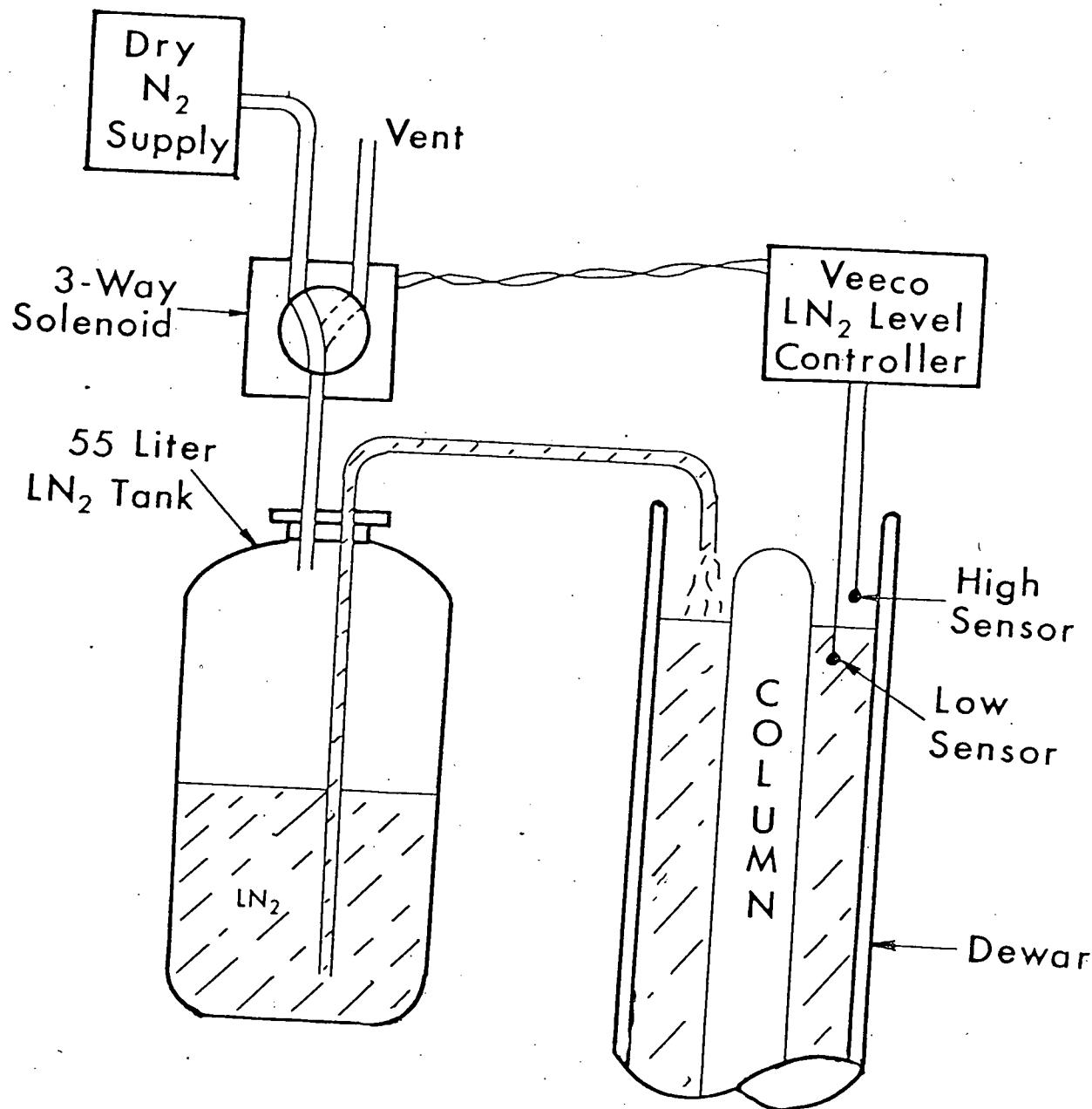
Figure 5. LN$_2$-Level Controller for Distillation Dewar

solenoid valve. When the level of liquid nitrogen drops
below the lower sensor, the three-way solenoid is activated,
the vent closed, and a liquid nitrogen holding tank (Union
Carbide's model UC-55) is pressurized with gaseous nitrogen.
The dewar is filled until the level reaches the higher
sensor. Upon achieving the required level, the holding
tank is vented to the atmosphere. The close control of the
liquid nitrogen level in the dewar is vitally important for
the stable pressure maintenance within the column.

A vacuum system to maintain a high vacuum in the helium
jacket of the column was fabricated primarily of stainless
steel.[19] The system, which is a one-inch vacuum pumping
station, employs a Consolidated Vacuum Corporation type
VMF 21 oil diffusion pump and a Vacuum Instrument
Corporation's BT-20 liquid nitrogen bucket-type cold trap.
The configuration of the system is schematically represented
in Figure 6. The valves are Veeco Instrument's bellows
sealed valves. Vacuum readings are obtained using a model
TG-7 Thermocouple Gauge in conjunction with a model RG-81
Ionization Gauge Controller and model RG-75 Ionization
Gauge Tube, all manufactured by Veeco Instruments, Inc.

Ionization
Gauge

To
Vacuum
Jacket

LN$_2$

Cold

Trap

To
Rough
Pump

Thermocouple
Gauge

Oil
Diffusion
Pump

To
Mechanical
Pump
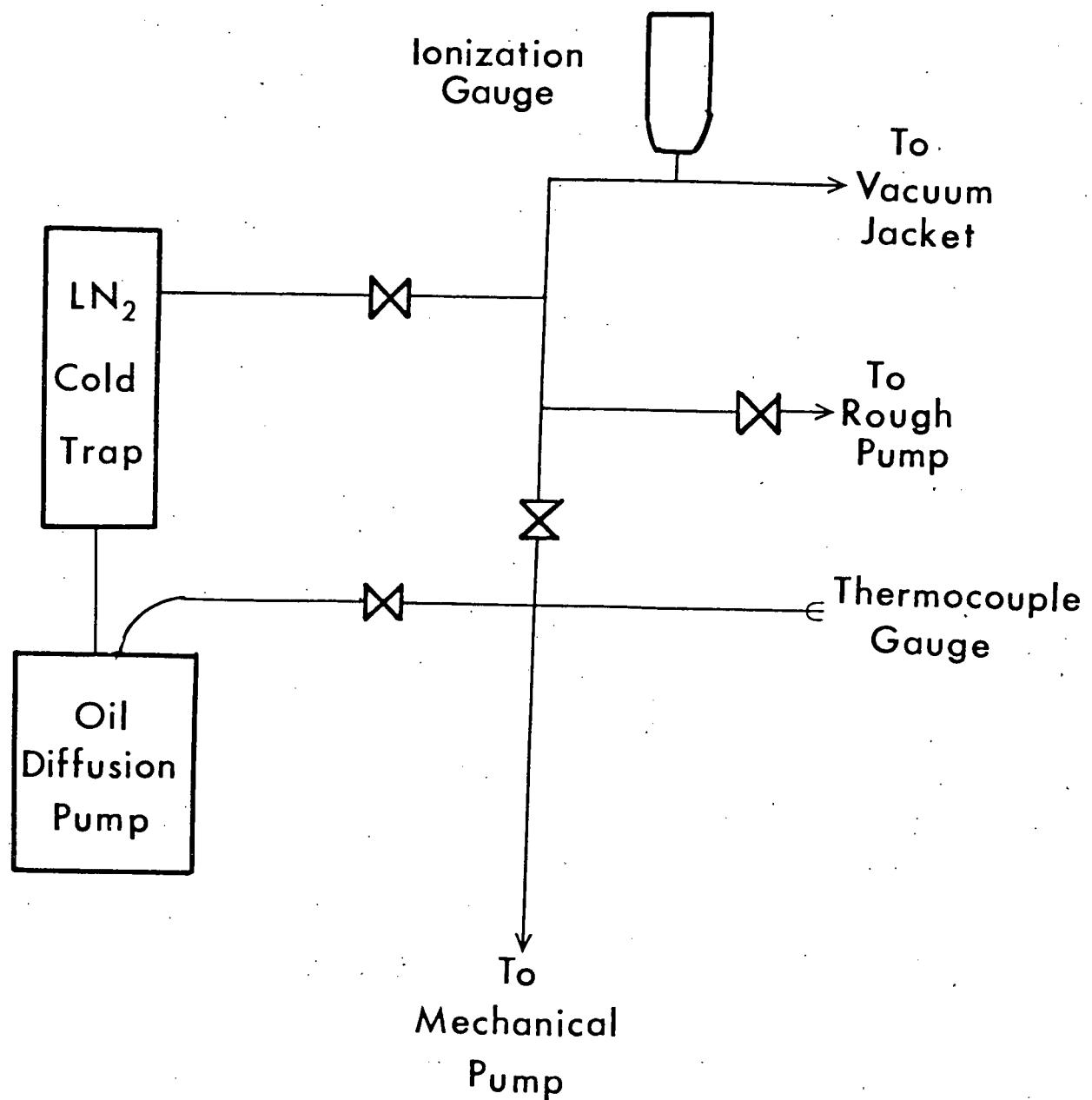
Figure 6. Vacuum System for Vacuum Jacket

B) Combustion Train

The isotopic analysis of the $^{13}C/^{12}C$ ratio is most easily performed on samples of carbon dioxide. A sample of CHF_3 introduced in a mass-spectrometer is hard to completely evacuate out of the system. This therefore necessitated a process for the oxidation of CHF_3 with sufficiently high yield so as to make any corrections for the $^{13}C/^{12}C$ isotope effect unnecessary. It was estimated that a 95% conversion of CHF_3 to CO_2 would limit the uncertainty on the isotopic ratio due to possible carbon isotope fractionation during the chemical conversion to an absolute maximum of ± 0.0001, the limit which can be considered acceptable.

The combustion train consists of three sections (Figure 7). The first section is a quartz tube, 55 cm in length and 10 mm in outside diameter. The tube is packed alternately with platinum gauze and crushed quartz. It is heated by two Lindberg-Hevi Duty ovens, maintained at temperatures between 1000° C and 1050° C. In this temperature region, CHF_3, in the presence of a large excess of oxygen, is decomposed to CO_2, inorganic fluorine compounds (which are eventually converted to SiF_4), and H_2O. The second section of the train is a 10 mm outside diameter pyrex tube, which is packed alternately with pyrex wool and sodium fluoride. This 30 cm length of tubing is maintained at $250 \pm 20^\circ$ C by an oven home-fabricated especially for this use.[30] The sodium fluoride section is employed to absorb SiF_4. The final section is a pyrex U-tube at

To Forepump

To high vacuum pumping system

From O$_2$ Tank

From He Tank
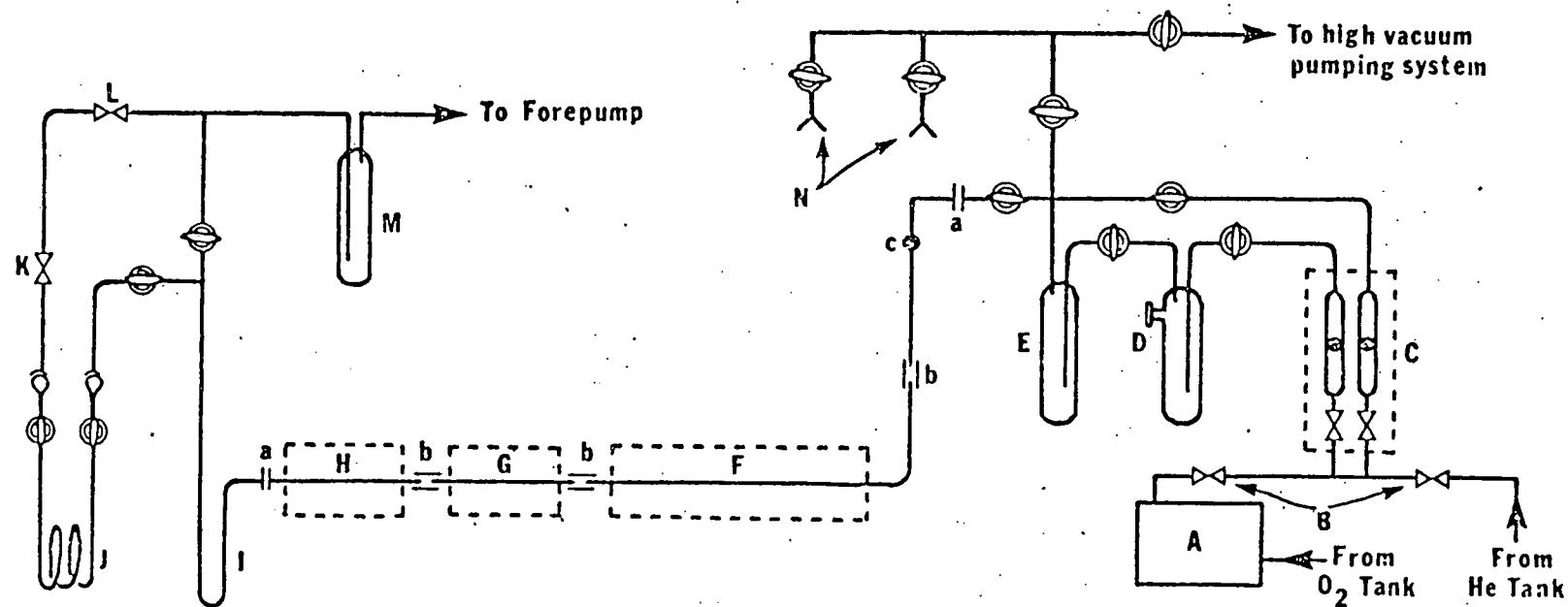
A; Oxygen - purification train
B; Shut - off valves
C; Twin rotometer with needle valves
D; Injection port with silicone rubber
E; Combustion - sample trap
F; Quartz tube with platinum gauze and crushed quartz
G; Pyrex tube with silver wool packing
H; Pyrex tube with NaF packing
I; U- Tube with silica gel packing
J; Removable coiled CO$_2$ trap
K; Metering value
L; Shut - off valve
M; LN$_2$ - trap
N, Combustion sample inlet ports

a; silicone - rubber
  O ring couplings
b; silicone - rubber
  tubing connections
c; constriction

Figure 7. Combustion Train

room temperature filled with silica gel to remove H_2O.

Oxygen used in the train is obtained from a tank and purified by passing the stream through a concentrated H_2SO_4 bubble tower, a Drierite absorption tube, and finally an Ascarite absorption tube. After leaving the purifier, the stream is divided into two legs. One passes through the sample inlet area, thereby driving the sample into the oven and the other leg bypasses this area, flooding the oven with oxygen.

The combustion product, CO_2, thus obtained was trapped in a liquid nitrogen trap. The product contained a small amount (less than one percent) of uncombusted sample plus traces (less than 0.05%) of yet undetermined impurities. The samples of CO_2 were then further purified by means of a home-fabricated gas-chromatograph[30] packed with alumina. After this final purification, the carbon dioxide samples were transferred to glass sample holders for analysis.

II-2. Precision Measurement of the Vapor Pressure of CHF_3

The only data available for the vapor pressure of CHF_3[24] is from an industrial source. In addition, there was no assurance of the accuracy of the temperatures reported by the investigator. Obtaining consistent vapor pressure data was therefore necessitated. For this purpose,

samples of CHF_3 were purified. All impurities in the samples were less than one part in 10^5.

The manometry was performed in a cryostated differential manometer in Prof. J. Bigeleisen's laboratory at the University of Rochester. The cryostat[25] is capable of maintaining cryogenic temperatures to within $\pm 0.001^\circ$ C for several hours at a time. The differential manometry is accomplished through the use of differential capacitance gauges, which are capable of measuring pressure differences up to 50 torr ± 0.1 millitorr. The vapor phase volume in the cryostated sample holder-manometer system is negligible compared to the amount of liquid in the sample holder. The absolute pressure of one of the liquid samples, which in this case was CHF_3, is measured to within ± 1 millitorr by the use of a Texas Instruments' quartz spiral gauge. Vapor pressures of pur CHF_3 were measured in this apparatus at 29 temperatures between 139.3° K and 191.7° K. The results were least-squares fit to a four term equation:

$$\log_{10} P(torr) = \frac{-278.269}{T(^\circ K)} - 4.65910 + 0.0772937T$$

$$- 0.000158127T^2 \qquad (14)$$

The single largest deviation of Equation 14 from an experimental point is 0.004 out of 1.183 in $\log_{10} P$. These results are plotted in Figure 8.

FIGURE 8. VAPOR PRESSURE CURVE FOR CHF_3
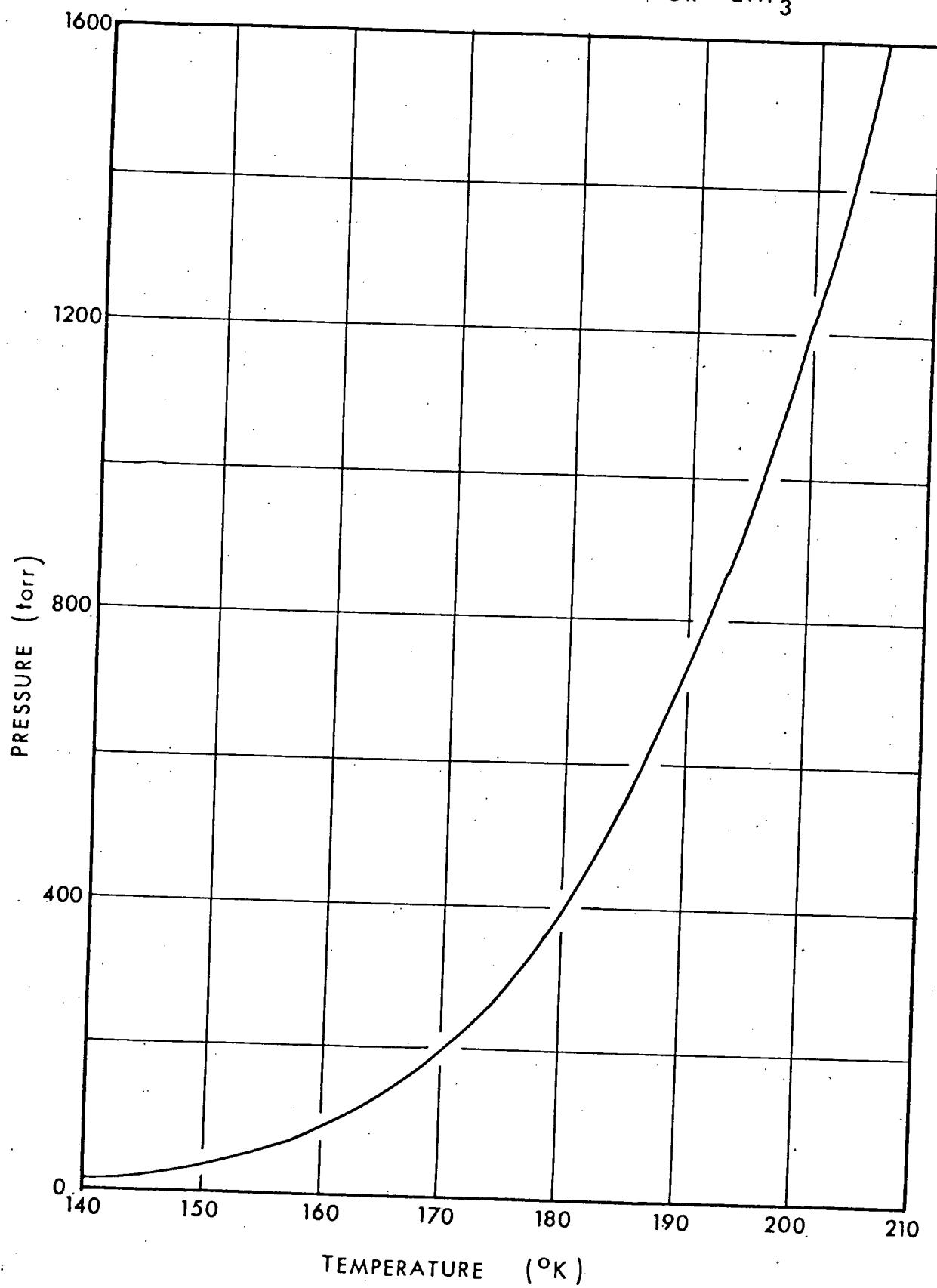
II-3. Experimental Procedure

A) Purification of CHF_3

After the removal of the major impurity, air, by repeated bulb-to-bulb distillation, gas chromatographic analyses, using the Perkin Elmer model 990 gas chromatograph, indicated the presence of 2.7×10^{-4} CH_4 and 1.2×10^{-4} SiF_4. A preliminary low-temperature distillation trial was performed and the resulting material was gas chromatographically analyzed. This procedure indicated that the level of the impurities was significantly reduced. Therefore, the entire supply of trifluoromethane was distilled at low temperature. Gas chromatographic analyses of the resulting material indicated that the CH_4 was reduced to a non-detectable level and that the SiF_4 was present to the extent of 1.7×10^{-5}. This material was then stored as that to be used in the distillation.

B) Distillation

The following paragraphs will outline the preparations for and the execution of a distillation run on the modified Bigeleisen column.

Approximately two days prior to a distillation run, the diffusion pumps on the service line and on the helium jacket line are started up and the liquid nitrogen holding tanks (used as a supply of liquid nitrogen for the cold traps) are filled. Until this point, these vacuum lines

have been kept under rough vacuum. The night before the distillation run is performed, the UC-55 liquid nitrogen holding tank is filled to capacity. The "aging" of this liquid nitrogen was found to be essential, since the liquid nitrogen is shipped at a higher pressure than is maintained in the tanks. Therefore, time must be allowed for it to come to thermal equilibrium in its new environment.

On the morning of the distillation, various preparations are made, including preparation of the CHF_3 sample and cooling of the distillation column. The preparation of the CHF_3 sample involves condensing (using liquid nitrogen) into the cold finger, shown in Figure 4. When approximately ¼ mole (an amount in excess of that which will actually be needed for the distillation) of CHF_3 has been collected in the the cold finger, the liquid nitrogen is removed and replaced with a dry ice-acetone slurry. This maintains the pressure in the cold finger (which is isolated by the use of valves adjcent to each side) at approximately one atmosphere. It was observed that the nearer the temperature of the column was to the actual distillation temperature, the more smoothly the experiment proceeded. At this point, the liquid nitrogen level controller for the dewar surrounding the helium jacket was activated to automatic and the dewar was filled. The temperature within the boiler was monitored with the platinum resistance probe and, as it approached the target temperature for the distillation, the introduction of the CHF_3 into the column

was begun.

From its construction, it can be seen that, in the absence of a conducting gas within the vacuum jacket, the packed section of the column is cooled by the liquid nitrogen by conduction from near the condenser area. Therefore, it follows that a temperature gradient is established as the column temperature is lowered, with the boiler area the warmest and the condenser area the coldest. In order to properly charge and wet the column packing, this gradient was employed. It allowed the charge of CHF_3 to freeze and liquify on the packing rather than condense into the boiler immediately.

This charging procedure is as isothermal as can be hoped for. When the temperature probe in the boiler became near that temperature pre-selected for the run, the valve on the column side of the cold finger and the needle valve leading to the top of the column were slightly opened. As the CHF_3 entered the column, it condensed and warmed the area on which it was condensing, and this "wet" area can be thought of as having travelled along the column towards the boiler. The temperature profile along the column would become more uniform than it was before the charging started. During this time, the rate of addition of CHF_3 entering the column was adjusted using the needle valve in order to keep the temperature of the column as steady as possible by monitoring the pressure in the condenser and the platinum thermometer in the boiler. As the temperature gradient was

removed by the entering CHF_3, the boiler started to fill with the charge and as soon as the level in the boiler was approximately ¼" below the tip of the packed section, corresponding to approximately 20 ml of liquid in the boiler, the column was sealed and the boiler heater current activated. This was the start of the reflux and was time zero for the experimental time measurement. This introduction practice helped minimize the uncertainties on time zero. At this point, the pressure is already stabilized and the column practically at equilibrium due to the "isothermal" charging procedure. Pressure through-out the charging was recorded using the output of the Setra Systems' model 236 differential capacitance gauge connected to the boiler section.

The column was then operated isothermally ($\pm 0.3°$ C) under total reflux, and the buildup of the isotope-enrichment profile along the length of the column was monitored as a function of time by withdrawing gas samples from the condenser section of the column. The condenser samples (approximately 5×10^{-4} mole) were withdrawn through a variable leak into a small manifold of known volume (approximately 75 ml) and the sample pressure of approximately 100 torr was determined by use of a Wallace-Tiernan differential pressure gauge. A sample was usually withdrawn over a period of three to five minutes. Samples were generally taken every 15 minutes during the first hour, and then, succesively, two half-hour samples, two fourty-

five minute samples, and hourly samples, until approximately seven hours after time zero. Pressure and temperature measurements, as well as the current and voltage of the heater, were noted both before and after the extraction of each sample.

Samples of the boiler vapor were withdrawn as a control for the isotopic enrichment. A boiler sample was taken as close to time zero as possible and then at least once more during the course of the distillation. Boiler samples were removed by filling the service manifold, a volume of approximately 425 ml, with CHF_3 through the capillary leading to the boiler, the pressure monitored once again with the Wallace-Tiernan differential pressure gauge.

Samples were stored in 60 ml high vacuum glass gas sample holders.

All samples were now ready for combustion, which will be described in the following Subsection, II-3-C.

In order to apply the modified theory of K. Cohen to the kinetics of the distillation, it was necessary to determine the amount of CHF_3 held up in both the column and the condenser.

The procedure developed to determine the column holdup was essentially a two-stage shut-down of the column. After the last samples were removed from the column during the distillation operation, the line connecting the boiler to the service vacuum line was opened in order to drain the CHF_3 remaining in the boiler. The heater current was

increased to compensate for the additional heat required for the increased rate of vaporization, thereby maintaining pressure in the column at the same constant level as that in the normal distillation operation of the column. When the boiler was emptied, which was checked visually by watching the boiler through an opening in the silver-mirroring on the dewar, the column was sealed and the heater current was deactivated. The liquid nitrogen level controller maintaining the level in the dewar surrounding the column assembly was shut off and the liquid nitrogen allowed to boil off. The liquid nitrogen level in the dewar was allowed to come down to a level below the boiler. This made the boiler the coldest spot of the distillation column, and the CHF_3 originally held in the column packing condensed down into the boiler. The column heater was turned on again and all the material "held up" in the column was collected through the boiler sample line into a high vacuum stainless steel weighing vessel. The vessel was then weighed, its empty weight of 126.02 grams subtracted and thereby the amount of CHF_3 held up in the column was precisely determined.

The holdup in the condenser, another quantity needed for the column kinetics calculations, was determined in a separate series of experiments. The manifold of known volume leading to the column was filled with a known pressure (approximately 500 torr) of CHF_3. The charge was slowly allowed to enter the column until the first drop

appeared at the condenser tip. The remaining pressure in the manifold was the observed. The amount of CHF_3 that entered the condenser before the first drop was determined by applying the ideal gas laws, and this amount was considered to be equal to the condenser holdup.

C) Combustion and Purification

In order to facilitate the isotopic analysis of the CHF_3 samples taken from the column, They were combusted to carbon dioxide, using the apparatus shown in Figure 7 and described in Subsection II-1-B.

Each sample was transferred from its holder into a manifold of known volume, and its pressure was measured using a Wallace-Tiernan differential pressure gauge. The sample was then transferred to the combustion sample trap by condensing the sample into the trap at liquid nitrogen temperature. Oxygen was allowed to flow through the oven for five minutes using the bypass stopcock. At this point, the liquid nitrogen was removed from around the combustion sample trap and oxygen was allowed to flow both through the bypass and to sweep through the sample trap for ten minutes. At the end of this ten minute period, the oxygen flow was halted and five minutes of pump-down time was allowed, followed by two minutes of helium flow to remove any traces of sample from the system. Another ten minute pump-down period was allowed at this point. In all cases, the flow

rate of the gases entering the ovens was 0.05 liters/min. The combustion product, CO_2, was clearly visible at this time in the collector coils. The sample was then transferred to the inlet side of the purification gas chromarograph. Using a flow rate of 20 ml/min at 300° C and an alumina-packed column, the carbon dioxide was purified and collected. The sample pressure was measured in a known volume with a Wallace-Tiernan differential pressure gauge.

D) Mass Spectrometry

An isotopic analysis was performed on each sample using a Consolidated Engineering Corporation's model 21-201 Isotope Ratio Mass Spectrometer. This model is of the Nier type construction. The feature which makes this particular model very attractive for isotopic analysis is its dual collector instrumentation (see Figure 9). In this mass spectrometer, gas molecules enter at low pressure(approximately 10^{-6} torr), are ionized, and accelerated into a magnetic field. In this magnetic field, all particles follow paths which are arcs of circles, with the heavier particles travelling paths of larger radius than the lighter particles. After passing through the magnetic field, each mass (or more correctly, mass-to-charge ratio) is focussed at a different point. The model 21-201's dual collector allows the beam impinging on one of its collectors to be compared with the beam falling on its other collector
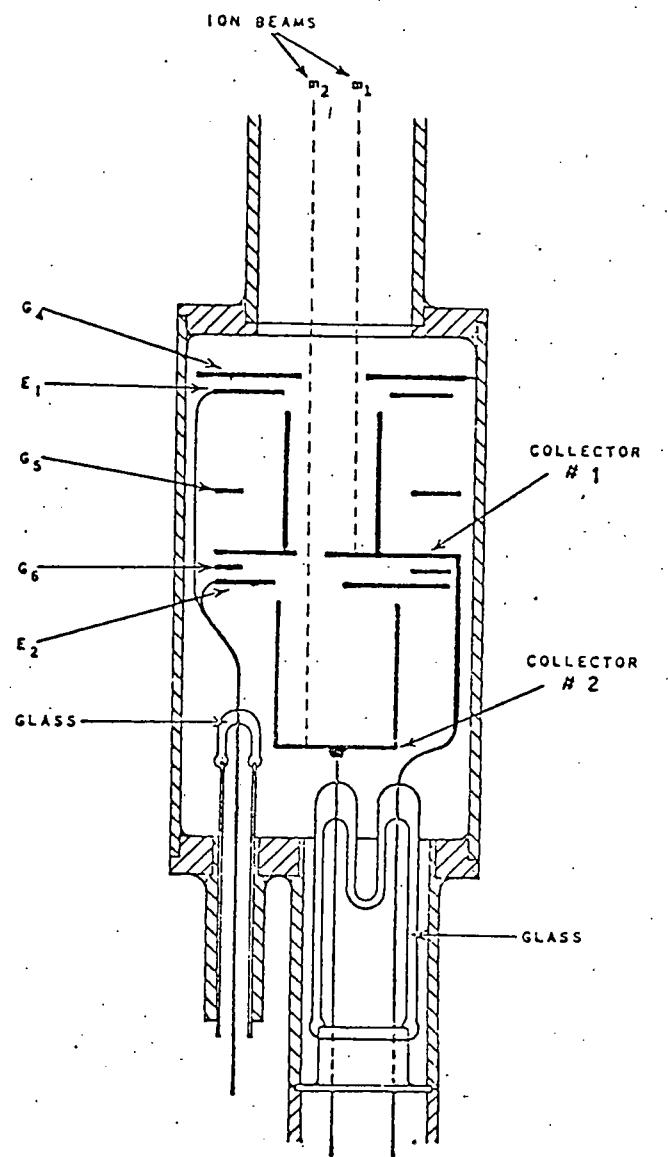
Figure 9. Dual Collector used in the Model 21-201 Mass Spectrometer.

Ion beams enter from top. The higher mass m_1 reaches Collector #2. The lower mass impinges on Collector #1. (Each collector has a box-like shield.) G_5 and G_6 are grounded shields to prevent electrical leakage between E_1 or E_2 and Collector #1. E_1 and E_2 operate at -45 volts with respect to ground and act as suppressors of secondary electrons released by ion bombardment from the collectors. Their slits are large enough so that they intercept no ions.

concurrently. This allows simultaneous recording of the number of ions hitting each collector.

A model 21-201 was generously made available at Brookhaven National Laboratory in the laboratory of Dr. L. Friedman.

Prior to each isotopic analysis, a standard carbon dioxide sample was introduced into the inlet system. With the ion accelerating voltage set at approximately 1175 volts, the magnetic field was scanned and recorded using the number two collecter (narrow slit). Upon detecting the mass 44 and 45 peaks ($^{12}CO_2$ and $^{13}CO_2$ respectively), the field was varied to place the 45 peak on the number two collector. The peak was placed directly on the collector by using the ion accelerating voltage as a fine adjustment. With mass 45 on the number two collector, the number one collector collected masses 42.6 to 46.5. In order to get more accurate data, all samples were analyzed at uniform pressure. Amplifiers were zeroed and checked periodically throughout each analysis session. Adequate time was allowed for pump-out in order to avoid any "memory" from previous samples.

III. DATA REDUCTION

Cohen's theory[11] of the transient kinetics of a square cascade was applied to the data obtained from the mass-spectrometric analyses of the samples from the condenser and boiler in order to determine the relative vapor pressures of the isotopic species. A modification of the theory of long-time kinetics (LTK) was developed,[26] and was used to map the kinetics parameters, A and B, in the ranges of the overall separation and relative (condenser to column) holdups needed for the reduction of the present data. The following Section, III-1, contains an outline of the modified Cohen's theory of long-time kinetics. Section III-2 will outline the method of application of Cohen's theory to the present problem, and Section III-3 will contain a complete set of sample calculations pertaining to the experimental runs.

III-1. Modified Cohen's Theory

The transient behavior of a square, counter-current cascade of close separation stages during the start-up period was theoretically analyzed by K. Cohen[11] in relation to the fractionation of uranium-235. A consideration of the material balance of the desired substance

between the product stage and the s-th stage under conditions of constant flows leads[11] to a partial differential equation:

$$\lambda \frac{\partial N}{\partial t} = \frac{\partial^2 N}{\partial s^2} - \epsilon \frac{\partial}{\partial s}\left[\psi N + N(1-N)\right] \tag{15}$$

where $N = N(s,t)$ is the average mole fraction of the desired substance in the input streams for the s-th stage (cf: Figure 10), counted toward the product end starting from the feed point in the cascade, at time t from the start-up of the cascade. Other quantities used in Equation 15, all dimensionless, are:

$\epsilon = \alpha - 1$, where α is the "head-to-tail" separation factor. This use of α is different from Cohen's, in that the latter α is the "head" or "tail" separation factor. The α used in the present study is twice Cohen's α.[12,22,23,27]

$\lambda = 2h$, where h is the holdup per stage per unit flow, on the average process time per stage.

$\psi = \frac{2P}{\epsilon L}$, where P is the production rate, or the rate of withdrawal of the product at the product-end of the column, and L is the total inter-stage flow rate at stage s. In a square distillation cascade under total reflux, L is also equal to twice the boilup rate.

When the mole fraction of the desired substance is negligibly small compared to unity Equation 15 becomes
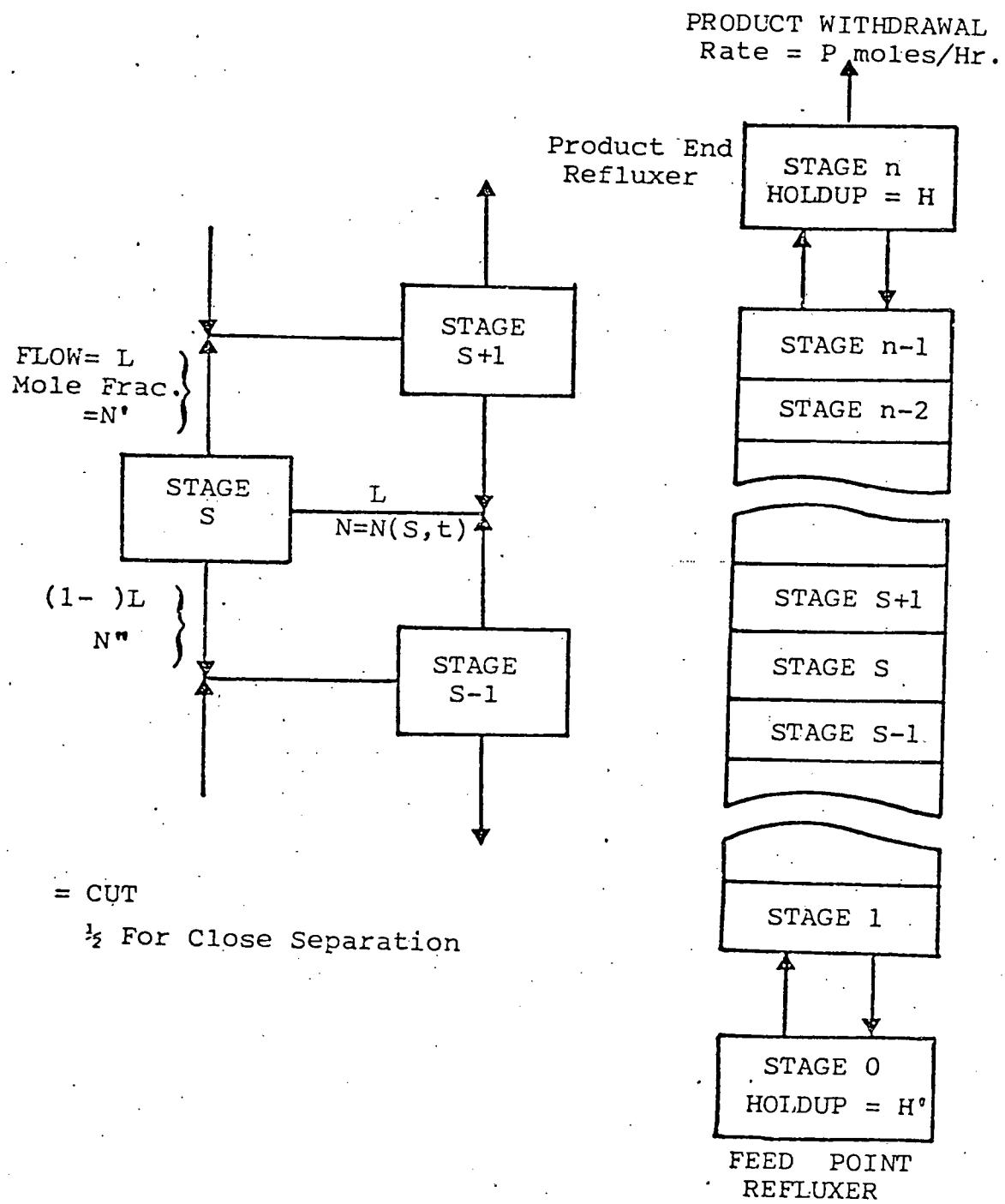
Figure 10. Square Cascade

linear:

$$\lambda \frac{\partial N}{\partial t} = \frac{\partial^2 N}{\partial s^2} - \epsilon (1 + \psi) \frac{\partial N}{\partial s} \tag{16}$$

This would be the case in preliminary fractionation processes of isotopes, such as ^{235}U, D, ^{13}C, and ^{15}N. Cohen solved the equation under the following initial and boundary conditions:

at t = 0 ;   N(s,t=0) = N_O at all s

at s = 0 (feed point); N(0,t) = N_O at all t

at s = n (product end); P = 0   at all t
                        Holdup in refluxer = H

Such a solution is of general interest for two reasons. First, in large-scale production one seeks to minimize the initial start-up period during which the system is operating under total reflux. Second, observation of the transient behavior can be used for evaluating such separation system constants as the number of the theoretical plates and the separation factor.[11]

Cohen's first-order solution of Equation 16 can be expressed in the form

$$\frac{N_\infty - N}{N_\infty - N_O} = Ae^{-B\tau} \tag{17}$$

where τ is the reduced time and is equal to $t/\lambda n^2$, and N_∞ is the mole fraction of the desired substance at $t \longrightarrow \infty$. A and B are Cohen's kinetics parameters, which were tabulated,[11] both dependent on two factors, ϵn and $k/\lambda n$; n is the number of theoretical plates, and k is the ratio of the holdup in the condenser to the boil-up rate.

Thus,

$$\frac{N_\infty}{N_O} = e^{\epsilon n} \tag{18}$$

and

$$\frac{k}{\lambda n} = \frac{\text{Holdup in the condenser } (= H_{cond})}{\text{Total holdup in the column } (= H_{col})} \tag{19}$$

Cohen's solution, Equation 17, was estimated[11] to be valid at large t, satisfying the condition $t > n^2/10$.

The modification[26] of Cohen's LTK theory takes into account the second-order term for the solution of Equation 16 and can be represented as

$$\frac{N_\infty - N}{N_\infty - N_O} = A_1 e^{-B_1 \tau} + A_2 e^{-B_2 \tau} \tag{20}$$

where A_1 and B_1 are Cohen's first-order parameters, A and B respectively, and A_2 and B_2 are the second-order parameters calculated and tabulated by Ishida and Wieck.[26] A_2 and B_2 depend on the same two factors, ϵn and $k/\lambda n$, as do Cohen's parameters. Table XV contains the first-order parameters A_1 and B_1 in the ranges of ϵn and $k/\lambda n$ observed in this study, Table XVI contains the second-order parameters A_2 and B_2 in the same ranges of ϵn and $k/\lambda n$.

The first-order solution, Equation 17, has the advantage of a straight-line least-squares fit: from Equation 17,

$$Y_L(\tau) \equiv \ln \left[\frac{q_\infty - q}{q_\infty - 1} \right] = \ln A - B\tau \tag{21}$$

where

$$q \equiv \frac{N}{N_O} \tag{22}$$

and

$$N = \frac{R}{R + 1} \qquad (23)$$

In this study, in order to take advantage of the linear least-squares fit (LSF) while applying the second-order Equation 20, the second-order term of Equation 20 was used as a correction for the left-hand side of the equation. Thus,

$$y_L(\tau)_{corr} = \ln\left[\frac{q_\infty - q}{q_\infty - 1} - A_2 e^{-B_2\tau}\right] = \ln A_1 - B_1\tau \qquad (24)$$

and the left-hand side of Equation 24 was plotted against time t. A_2 and B_2 were obtained from a knowledge of ϵn, obtained as $\ln q_\infty$, and $k/\lambda n$, obtained from the holdup measurements. A straight line is obtained from the above plot with

$$\text{Intercept} = \ln A_1 \qquad (25)$$

and

$$\text{Slope} = \frac{B_1}{\lambda n^2}$$

$$= \frac{B_1(L/2)}{n\, H_{col}} \qquad (26)$$

Then,

$$n = \frac{(\text{Boil-up rate})(B_1)}{(\text{Column holdup})\,|\text{Slope}|} \qquad (27)$$

By knowing B_1 from Cohen's table, one obtains n and subsequently ϵ.

III-2. Outline of Method of Data Reduction

For each run, the mass-spectrometric data was processed according to the following procedure, outlined schematically in Figure 11.

The raw mass-spectrometric data of the 45/44 relative peak ratio represents the atom ratio, R, of ^{13}C to ^{12}C contained in the CO_2 samples. The overall separation, q, between the top and bottom of the column at time t is given by Equation 22.

Thus, from the isotopic ratio of $^{13}C/^{12}C$, R, of a condenser sample, and the isotopic ratio of $^{13}C/^{12}C$, R_o, of a boiler sample, N was calculated by Equation 23. Then, q was calculated from Equation 22, and both $\ln (q_\infty - q)/(q_\infty - 1)$ and $\ln \left[(q_\infty - q)/(q_\infty - 1) - A_2 e^{-B_2 \tau} \right]$ were plotted as a function of time t. The plots were fit to a linear function of t, using equal weights for all points: the possible error in the plotted quantity due to uncertainties of $\pm 2.2 \times 10^{-5}$ in the isotopic ratio measurements are of the order of 0.014 and do not vary significantly from point to point, so that their effect on the slope of the least-squares fit line going through these points is insignificant. The errors on the LSF parameters, the slope and the intercept, were estimated based on the root-mean-square error (RSME) of the actual scatter of the experimental points around the best-fit line.[28] The points with the largest deviations were eliminated until the estimate of error on the slope became no more than 10% of the absolute

FIGURE 11.   FLOW CHART OF DATA REDUCTION
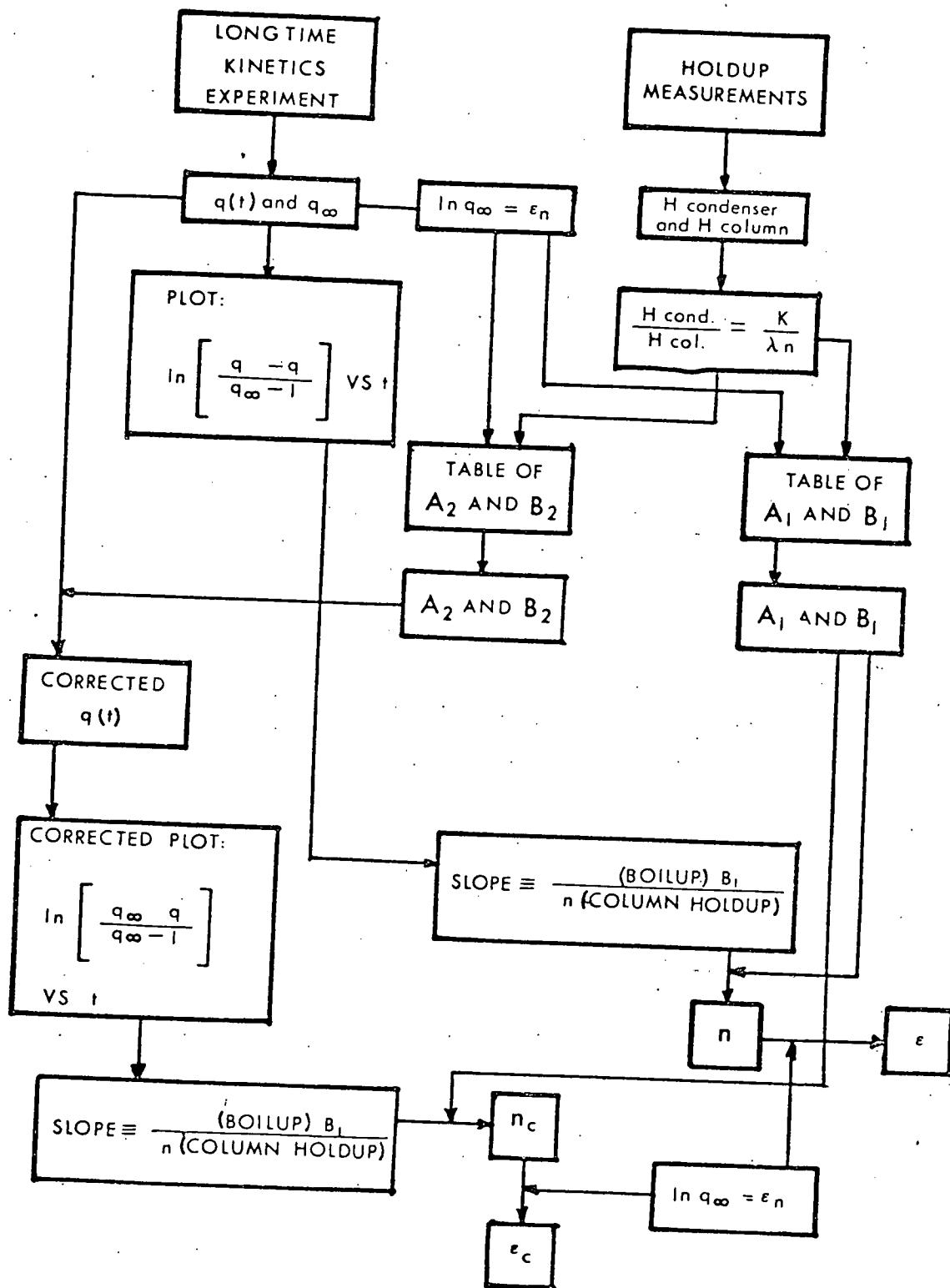
magnitude of the slope. It was found that the values of the slope are rather insensitive to decisions to retain or discard points, while the intercept is very sensitive to such decisions. Therefore, the slope would lend to relatively objective evaluations of n and ϵ, despite the rather arbitrary decisions made on the experimental points. It was also found that the intercept of the LTK plot, which is equal to $\ln A_1$, is too sensitive to relatively small uncertainties in time zero. Thus, for example, referring to Table XIV(C), the intercept for Run LD-10 is -0.554, whereas the value determined from ϵn and $k/\lambda n$ (i.e., $\ln A_1$) is -0.173. The latter value of the intercept could have been obtained if time zero were set approximately 15 minutes earlier than time zero actually used.

III-3. Sample Calculations

As an illustrative example, run LD-10 will be used. The average R of the boiler samples is equal to 0.011759.

$$\therefore N_{Boiler} = N_o = \frac{0.011759}{1 + 0.011759} = 0.011622$$

The equilibrium value of separation (or the overall separation value) is equal to 0.012189.

$$\therefore N_\infty = \frac{0.012189}{1 + 0.012189} = 0.012042$$

For condenser sample #1:

$$N = \frac{0.011879}{1 + 0.011879} = 0.011740$$

$$q = \frac{N}{N_O} = \frac{0.011740}{0.011622} = 1.0101$$

$$q_\infty = \frac{N_\infty}{N_O} = \frac{0.012042}{0.011622} = 1.0361$$

$$\therefore \dot{Y}_L(\tau) = \ln\left[\frac{q_\infty - q}{q_\infty - 1}\right] = -0.3279$$

Since $k/\lambda n$ is equal to 0.0374 and ϵn has a value of 0.03551, the following values of the "correctional" LTK parameters, A_2 and B_2 are obtained from Table XVI as:

$$A_2 = 0.0879$$

$$B_2 = 20.5846$$

$$\therefore Y_L(\tau)_{corr} = \ln\left[\frac{q_\infty - q}{q_\infty - 1} - A_2 e^{-B_2 \tau}\right] = -0.2940$$

These corrected $Y_L(\tau)$ were then least-squares fit (LSF), yielding

Slope $= -0.00772 \pm 0.00080$

Intercept $= -0.580 \pm 0.297$

The values of $Y_L(\tau)$ calcaluated from this LSF are compared to their corresponding experimental values under the column "First LSF" in Table II. Since the RMSE of the above slope is more than 10% of the absolute magnitude of the slope, the experimental points No. 7, 10, and 12 were removed. Another linear LSF was then performed on the remaining eleven points. The Second LSF yielded

Slope $= -0.00787 \pm 0.00075$

Intercept $= -0.554 \pm 0.220$

TABLE II.   SAMPLE CALCULATION OF RUN LD-10

| | EXP $Y_L(\tau)$ | FIRST LSF | | SECOND LSF | |
| | | CALC $Y_L(\tau)$ | EXP-CALC $Y_L(\tau)$ | CALC $Y_L(\tau)$ | EXP-CALC $Y_L(\tau)$ |
SAMPLE					
1	-0.294039	-0.663129	0.369	-0.688027	0.394
2	-0.917590	-0.790411	-0.127	-0.806163	-0.111
3	-0.963767	-0.931827	-0.032	-0.932176	-0.032
4	-1.169525	-1.051503	-0.118	-1.050313	-0.119
5	-1.357729	-1.308424	-0.049	-1.302338	-0.055
6	-1.609364	-1.516499	-0.093	-1.514984	-0.094
7	-0.600317	-1.981516	1.381	———	———
8	-2.862201	-2.587957	-0.274	-2.578214	-0.284
9	-3.207041	-2.902441	-0.305	-2.877494	-0.330
10	-4.728409	-3.419253	-1.309	———	———
11	-3.332205	-3.721396	0.389	-3.696575	0.364
12	-2.666173	-4.187942	1.522	———	———
13	-3.401197	-4.436931	1.036	-4.413271	1.012
14	-6.040255	-5.243201	-0.797	-5.295358	-0.745

and the values of $y_L(\tau)$ calculated thusly are arrayed in Table II under the column headed "Second LSF". The experimental values of $y_L(\tau)$ are plotted versus time in Figure 12, and the line drawn is according to the calculation of the Second LSF.

Since ϵn and $k/\lambda n$ are equal to 0.03551 and 0.0374 respectively, A_1 and B_1 are obtained from Table XV as 0.8411 and $\widehat{2}$.2589 respectively.

$$\therefore n = \frac{(1.2922)(2.2589)}{(6.762)|-0.00787|} = 54.8$$

The error on n is assumed to be due to that on the slope of the linear LSF only. Therefore,

$$\sigma_n = 54.8 \frac{(0.00075)}{(0.00787)} = 5.2$$

Knowing the value of ϵn and n, ϵ can subsequently be ascertained:

$$\epsilon = \frac{\epsilon n}{n} = \frac{0.03551}{54.8} = 0.000647$$

and

$$\sigma_\epsilon = 0.000647 \frac{(0.00075)}{(0.00787)} = 0.000061$$

Thus

$$\alpha = \frac{1}{1 + \epsilon} = \frac{1}{1 + 0.000647} = 0.999352$$

In order to observe the effect of the second-order correction term of $y_L(\tau)$ in Equation 24, run LD-02 will be used as an example.

Since ϵn and $k/\lambda n$ have values of 0.03565 and 0.0400 respectively, values of A_1 and B_1 (from Table XV) as well as A_2 and B_2 (from Table XVI) are as follows:
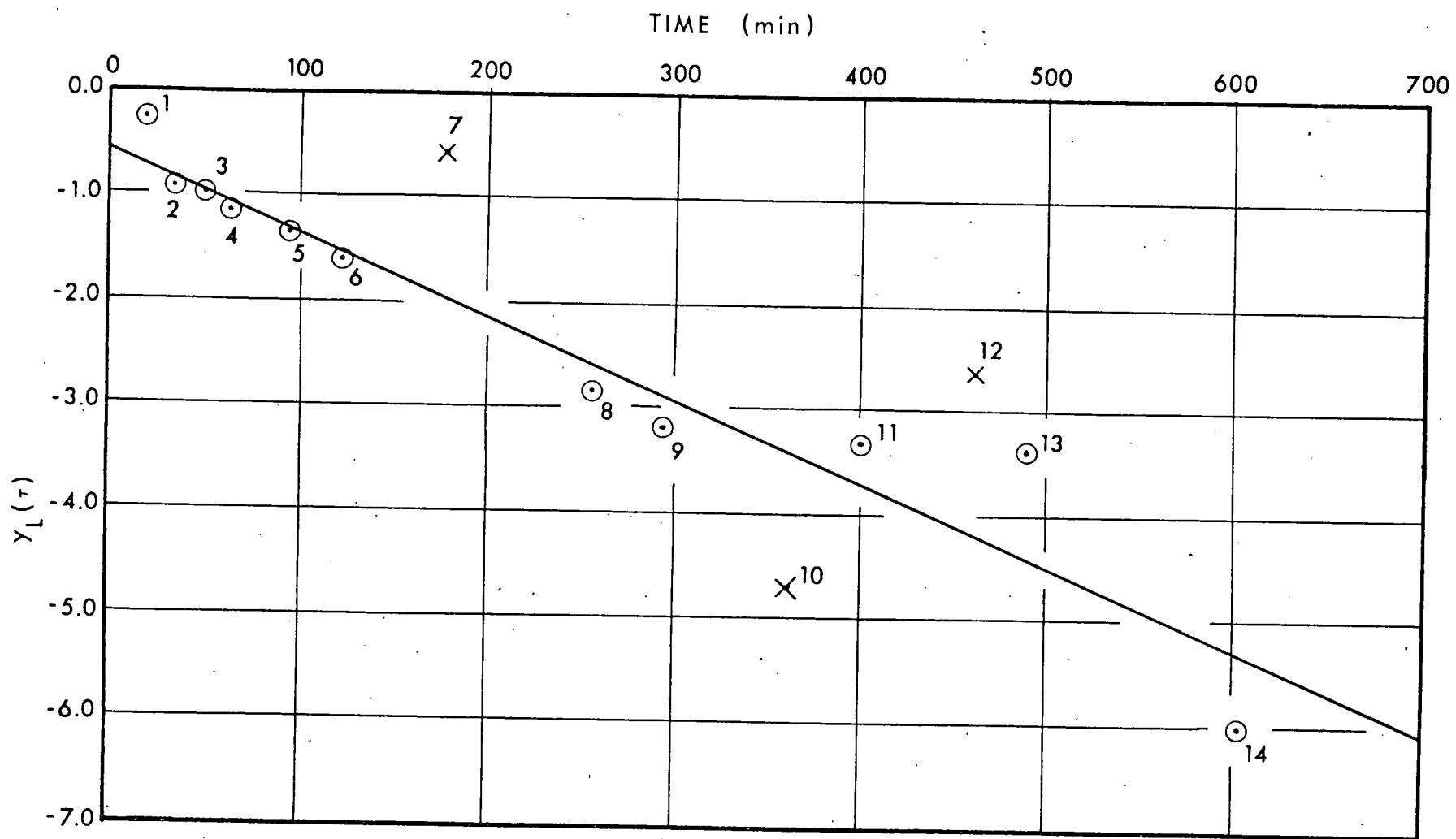
FIGURE 12. LONG TIME KINETICS PLOT OF RUN LD-10

A_1 = 0.8428

B_1 = 2.2475

A_2 = 0.0877

B_2 = 20.4830

Both Equation 21 and Equation 24 are least-squares fit using the above information.

For the uncorrected fit (Equation 21), the LSF yields

Slope = -0.01335

Intercept = -0.629

For the corrected fit (Equation 24), the LSF yields

Slope = -0.01456

Intercept = -0.538

Both the LSF of Equation 21 (dashed line) and the LSF of Equation 24 (solid line) are plotted in Figure 24. It can be seen that the effect of the second-order term in Equation 24 is that of an improvement of the fit to the experimental points.

IV. RESULTS AND DISCUSSION

This chapter is comprised of two parts. Section IV-1, which follows, will contain the results of the experimental aspect of this study and a discussion thereof. In the second part of this chapter, Section IV-2, the cell-model force field calculations will be developed.

IV-1. Experimental Results of the Separation Factor as a Function of Temperature

Results of the mass-spectrometric analyses of the samples for all eleven runs are presented in Tables III to XIII, one table for each distillation run. Tables XIV(A) through XIV(D) summarize the calculations of the number of theoretical stages, n, and the separation factor, ϵ (= $\alpha-1$).

The headings in Tables III to XIII are self-explanatory. In Table XIV(A), the heading "T ($^{\circ}$K) from P" was obtained using Equation 14 and the pressure, tabulated under "P (torr) from W-T gauge", read from the Wallace-Tiernan differential pressure gauge. Using the Platinum Resistance Thermometer (PRT) readings, the temperature is additionally obtained through a calibration traceable to the National Bureau of Standards. The least-squares fit formula for the calibration is:

TABLE III.   Data for Run LD-02

N_{Boiler} = 0.011610   Epsilon x n = 0.03565

$N_{Infinity}$ = 0.012031 $Q_{Infinity}$ = 1.0363

Column Holdup = 6.320 grams   Boilup Rate = 0.7049 grams/min.

$N_{Reading}$	$Q_{Reading}$	$Y_L(\tau)$ uncorr.	$Y_L(\tau)$ corr.	Time (min)
0.011784	1.0150	-0.5340	-0.5145	17
0.011837	1.0196	-0.7743	-0.7713	33
0.011871	1.0225	-0.9677	-0.9668	48
0.011923	1.0270	-1.3581	-1.3603	62
0.011960	1.0302	-1.7771	-1.7799	82
0.011995	1.0332	-2.4570	-2.4591	102
0.012002	1.0338	-2.6664	-2.6753	122
0.012004	1.0339	-2.7356	-2.7468	152
0.012016	1.0349	-3.2962	-3.3346	182
0.012023	1.0355	-3.8710	-3.9632	242
0.012030	1.0361	-5.3763	-6.0426	302
0.012027	1.0359	-4.4600	-4.6563	358

TABLE IV.   Data for Run LD-03

N_{Boiler} = 0.011635   Epsilon x n =0.05377

$N_{Infinity}$ = 0.012277 $Q_{Infinity}$ = 1.0552

Column Holdup = 6.421 grams   Boilup Rate = 0.7538 grams/min.

$N_{Reading}$	$Q_{Reading}$	$y_L(\tau)$ uncorr.	$y_L(\tau)$ corr.	Time (min.)
0.011815	1.0155	-0.3287	-0.3017	17
0.011971	1.0289	-0.7406	-0.7371	47
0.012076	1.0380	-1.1623	-1.1595	62
0.012104	1.0403	-1.3084	-1.3109	82
0.012139	1.0433	-1.5344	-1.5372	102
0.012169	1.0459	-1.7807	-1.7824	122
0.012179	1.0468	-1.8752	-1.8796	153
0.012218	1.0501	-2.3794	-2.3871	183
0.012227	1.0509	-2.5389	-2.5526	242
0.012263	1.0540	-3.7815	-3.8255	302
0.012272	1.0547	-4.6978	-4.8552	367

TABLE V.   Data for Run LD-04

N_{Boiler} = 0.011855   Epsilon x n = 0.02731

$N_{Infinity}$ = 0.012183 $Q_{Infinity}$ = 1.0277

Column Holdup = 6.234 grams   Boilup Rate = 0.6313 grams/min.

$N_{Reading}$	$Q_{Reading}$	$Y_L(\tau)$ uncorr.	$Y_L(\tau)$ corr.	Time (min.)
0.011878	1.0020	-0.0749	-0.0502	17
0.011932	1.0065	-0.2689	-0.2604	33
0.011985	1.0110	-0.5048	-0.5020	47
0.012085	1.0195	-1.2129	-1.2079	92
0.012125	1.0228	-1.7405	-1.7326	122
0.012113	1.0218	-1.5555	-1.5445	155
0.012135	1.0237	-1.9264	-1.9218	182
0.012145	1.0245	-2.1546	-2.1554	243
0.012152	1.0251	-2.3528	-2.3590	302
0.012180	1.0274	-4.7232	-4.6944	405

TABLE VI.   Data for Run LD-05

N_{Boiler} = 0.011506   Epsilon x n = 0.05039

$N_{Infinity}$ = 0.012101 $Q_{Infinity}$ = 1.0517

Column Holdup = 6.309 grams   Boilup Rate = 0.8838 grams/min.

$N_{Reading}$	$Q_{Reading}$	$y_L(\tau)$ uncorr.	$y_L(\tau)$ corr.	Time (min.)
0.011710	1.0177	-0.4155	-0.3894	18
0.011787	1.0245	-0.6319	-0.6268	32
0.011844	1.0294	-0.8272	-0.8349	47
0.011917	1.0357	-1.1543	-1.1717	62
0.011958	1.0393	-1.3982	-1.4255	92
0.012032	1.0457	-2.0915	-2.1545	152
0.012072	1.0491	-2.8389	-3.0213	183
0.012085	1.0503	-3.3310	-3.6160	242
0.012096	1.0513	-4.0247	-4.7791	302
0.012095	1.0512	-3.9376	-4.5968	417
0.012100	1.0516	-4.4788	-6.3886	738

TABLE VII.   Data for Run LD-06

N_{Boiler} = 0.011495   Epsilon x n = 0.04899

$N_{Infinity}$ = 0.012072 $Q_{Infinity}$ = 1.0502

Column Holdup = 6.884 grams   Boilup Rate = 0.9861 grams/min.

$N_{Reading}$	$Q_{Reading}$	$y_L(\tau)$ uncorr.	$y_L(\tau)$ corr.	Time (min.)
0.011658	1.0141	-0.3299	-0.2867	17
0.011752	1.0223	-0.5890	-0.5642	32
0.011857	1.0314	-0.9840	-0.9727	49
0.011860	1.0317	-0.9976	-0.9942	62
0.011945	1.0391	-1.5071	-1.5108	87
0.011930	1.0378	-1.3986	-1.4019	142
0.012020	1.0456	-2.3933	-2.4066	272
0.012030	1.0465	-2.5983	-2.6202	302
0.012032	1.0467	-2.6689	-2.6690	362
0.012060	1.0491	-3.8178	-3.8729	422

TABLE VIII. Data for Run LD-07

N_{Boiler} = 0.011440   Epsilon x n = 0.04894

$N_{Infinity}$ = 0.012014 $Q_{Infinity}$ = 1.0502

Column Holdup = 6.473 grams   Boilup Rate = 1.0547 grams/min.

$N_{Reading}$	$Q_{Reading}$	$Y_L(\tau)$ uncorr.	$Y_L(\tau)$ corr.	Time (min.)
0.011573	1.0117	-0.2645	-0.2217	17
0.011733	1.0256	-0.7132	-0.6844	31
0.011788	1.0304	-0.9388	-0.9171	47
0.011824	1.0335	-1.1032	-1.0980	62
0.011889	1.0392	-1.5242	-1.5224	94
0.011944	1.0440	-2.0996	-2.1035	122
0.011943	1.0439	-2.0859	-2.0899	182
0.011948	1.0444	-2.1568	-2.1630	212
0.011970	1.0463	-2.5696	-2.5684	287
0.011976	1.0468	-2.7130	-2.7150	317
0.012011	1.0499	-5.2756	-5.2540	437
0.012008	1.0496	-4.5843	-4.5609	629

TABLE IX.   Data for Run LD-08

N_{Boiler} = 0.011567   Epsilon x n = 0.05427

$N_{Infinity}$ = 0.012212 $Q_{Infinity}$ = 1.0558

Column Holdup = 5.765 grams   Boilup Rate = 0.5051 grams/min.

$N_{Reading}$	$Q_{Reading}$	$y_L(\tau)$ uncorr.	$y_L(\tau)$ corr.	Time (min.)
0.011715	1.0128	-0.2609	-0.2187	20
0.011821	1.0219	-0.4995	-0.4743	35
0.011985	1.0361	-1.0426	-1.0318	62
0.012032	1.0402	-1.2788	-1.2725	92
0.012059	1.0425	-1.4375	-1.4378	122
0.012091	1.0453	-1.6734	-1.6731	152
0.012101	1.0461	-1.7576	-1.7596	182
0.012125	1.0483	-2.0052	-2.0033	212
0.012154	1.0508	-2.4163	-2.4088	244
0.012165	1.0517	-2.6226	-2.6191	302
0.012197	1.0545	-3.7864	-3.7612	350
0.012203	1.0550	-4.2968	-4.2720	390
0.012210	1.0556	-5.8002	-5.7761	752

TABLE X. Data for Run LD-09

N_{Boiler} = 0.011456   Epsilon x n = 0.04490

$N_{Infinity}$ = 0.011982 $Q_{Infinity}$ = 1.0459

Column Holdup = 7.282 grams   Boilup Rate = 1.4197 grams/min.

$N_{Reading}$	$Q_{Reading}$	$y_L(\tau)$ uncorr.	$y_L(\tau)$ corr.	Time (min.)
0.011473	1.0015	-0.0334	-0.0224	18
0.011616	1.0140	-0.3650	-0.3599	32
0.011710	1.0222	-0.6618	-0.6590	49
0.011906	1.0393	-1.9327	-1.9342	62
0.011917	1.0403	-2.1000	-2.0909	94
0.011943	1.0425	-2.6005	-2.6017	122
0.011959	1.0440	-3.1542	-3.1298	188
0.011960	1.0441	-3.1985	-3.1743	226
0.011970	1.0449	-3.8050	-3.7804	252
0.011977	1.0455	-4.6819	-4.6559	304
0.011980	1.0458	-5.6005	-5.5722	364
0.011981	1.0458	-6.2824	-6.2653	422

TABLE XI. Data for Run LD-10

N_{Boiler} = 0.011622   Epsilon x n = 0.03551

$N_{Infinity}$ = 0.012042 $Q_{Infinity}$ = 1.0361

Column Holdup = 6.762 grams   Boilup rate = 1.2922 grams/min.

$N_{Reading}$	$Q_{Reading}$	$y_L(\tau)$ uncorr.	$y_L(\tau)$ corr.	Time (min.)
0.011740	1.0101	-0.3279	-0.2940	17
0.011878	1.0220	-0.9407	-0.9176	32
0.011883	1.0225	-0.9709	-0.9638	48
0.011912	1.0250	-1.1743	-1.1695	63
0.011934	1.0268	-1.3552	-1.3577	95
0.011958	1.0289	-1.6104	-1.6094	122
0.012018	1.0340	-2.8466	-2.8622	257
0.012025	1.0346	-3.1744	-3.2070	295
0.012027	1.0348	-3.2929	-3.3322	399
0.012028	1.0349	-3.3574	-3.4012	490
0.012041	1.0361	-6.0654	-6.0403	602

TABLE XII.   Data for Run LD-11

N_{Boiler} = 0.011726   Epsilon x n = 0.04456

$N_{Infinity}$ = 0.012260 $Q_{Infinity}$ = 1.0456

Column Holdup = 7.289 grams   Boilup Rate = 0.3927 grams/min.

$N_{Reading}$	$Q_{Reading}$	$Y_L(\tau)$ uncorr.	$Y_L(\tau)$ corr.	Time (min.)
0.011906	1.0154	-0.4108	-0.3808	18
0.011980	1.0217	-0.6459	-0.6331	32
0.012078	1.0301	-1.0797	-1.0715	49
0.012177	1.0385	-1.8628	-1.8612	93
0.012218	1.0420	-2.5443	-2.5427	167
0.012220	1.0422	-2.5921	-2.5915	208
0.012243	1.0442	-3.4719	-3.4472	243
0.012252	1.0449	-4.2261	-4.2010	303
0.012255	1.0452	-4.6944	-4.6710	373
0.012253	1.0450	-4.3593	-4.3345	413
0.012255	1.0452	-4.6944	-4.6710	517
0.012259	1.0455	-6.3085	-6.2804	654

TABLE XIII. Data for Run LD-12

N_{Boiler} = 0.011701   Epsilon x n = 0.04276

$N_{Infinity}$ = 0.012212 $Q_{Infinity}$ = 1.0437

Column Holdup = 7.219 grams   Boilup Rate = 1.1930 grams/min.

$N_{Reading}$	$Q_{Reading}$	$Y_L(\tau)$ uncorr.	$Y_L(\tau)$ corr.	Time (min.)
0.011776	1.0064	-0.1582	-0.1314	17
0.011934	1.0199	-0.6084	-0.6050	49
0.012026	1.0278	-1.0087	-1.0086	62
0.012035	1.0286	-1.0625	-1.0600	92
0.012080	1.0324	-1.3558	-1.3535	122
0.012131	1.0368	-1.8423	-1.8419	193
0.012159	1.0392	-2.2722	-2.2661	222
0.012167	1.0399	-2.4324	-2.4297	274
0.012190	1.0418	-3.1253	-3.1453	302
0.012187	1.0415	-3.0029	-3.0175	362
0.012192	1.0419	-3.2163	-3.2406	435
0.012201	1.0428	-3.8621	-3.8385	487
0.012211	1.0436	-6.2548	-6.2364	632

TABLE XIV(A).   Summary of Distillation Data for Halocarbon 23

Run No.	P (torr) from W-T gauge	T (°K) from P	PRT (ohms)	T (°K) from PRT	Column Holdup (q)	Boilup Rate (q/min)
LD-11	$93^{+}_{-}11$	161.2 ± 0.9	55.4 ± 0.5	161.1 ± 0.9	7.287	0.3927
LD-08	153 ± 11	167.3 ± 0.9	57.9 ± 0.4	167.2 ± 0.8	5.765	0.5051
LD-04	265 ± 13	174.7 ± 0.8	61.0 ± 0.3	174.9 ± 0.6	6.234	0.6313
LD-02	366 ± 11	179.3 ± 0.4	62.8 ± 0.3	179.3 ± 0.6	6.320	0.7049
LD-03	428 ± 12	181.7 ± 0.7	63.8 ± 0.2	181.8 ± 0.4	6.421	0.7538
LD-05	592 ± 16	186.8 ± 0.5	65.9 ± 0.2	187.0 ± 0.5	6.309	0.8838
LD-06	730 ± 14	190.4 ± 0.5	67.3 ± 0.3	190.5 ± 0.6	6.884	0.9861
LD-07	846 ± 29	193.0 ± 0.7	68.1 ± 0.3	192.5 ± 0.5	6.473	1.0547
LD-12	1015 ± 24	196.5 ± 0.5	70.0 ± 0.2	197.2 ± 0.3	7.219	1.1930
LD-10	1225 ± 33	200.2 ± 0.5	71.4 ± 0.3	200.6 ± 0.5	6.762	1.2922
LD-09	1497 ± 38	204.6 ± 0.5	72.7 ± 0.2	204.0 ± 0.3	7.282	1.4197

TABLE XIV(B). Summary of Distillation Data for Halocarbon-23

Run No.	$k/\lambda n$	Epsilon x n	A_1	B_1	A_2	B_2
LD-11	0.0347	0.04456	0.8400	2.2621	0.0872	20.6734
LD-08	0.0439	0.05427	0.8466	2.2132	0.0859	20.3046
LD-04	0.0406	0.02731	0.8425	2.2528	0.0884	20.4757
LD-02	0.0400	0.03565	0.8428	2.2475	0.0877	20.4830
LD-03	0.0394	0.05377	0.8438	2.2330	0.0862	20.4741
LD-05	0.0401	0.05039	0.8440	2.2331	0.0865	20.4531
LD-06	0.0368	0.04899	0.8417	2.2489	0.0868	20.5898
LD-07	0.0391	0.04894	0.8432	2.2389	0.0866	20.4764
LD-12	0.0350	0.04276	0.8400	2.2625	0.0874	20.6650
LD-10	0.0374	0.03551	0.8411	2.2589	0.0879	20.5846
LD-09	0.0347	0.04490	0.8400	2.2618	0.0872	20.6547

TABLE XIV(C). Summary of Distillation Data for Halocarbon-23

Run No.	Negative of Slope of LTK (uncorr) $(\min^{-1})$	Negative of Intercept of LTK (uncorr)	Negative of Slope of LTK (corr) $(\min^{-1})$	Negative of Intercept of LTK (corr.)
LD-11	0.00883 ±0.00072	0.813 ±0.232	0.00880 ±0.00072	0.803 ±0.233
LD-08	0.00781 ±0.00054	0.470 ±0.160	0.00780 ±0.00054	0.459 ±0.160
LD-04	0.01019 ±0.00108	0.022 ±0.214	0.01019 ±0.00102	0.014 ±0.144
LD-02	0.01335 ±0.00128	0.629 ±0.225	0.01456 ±0.00135	0.538 ±0.214
LD-03	0.01151 ±0.00161	0.254 ±0.114	0.01188 ±0.00116	0.216 ±0.100
LD-05	0.00870 ±0.00089	0.839 ±0.289	0.00814 ±0.00080	0.820 ±0.271
LD-06	0.00713 ±0.00058	0.482 ±0.131	0.00727 ±0.00061	0.459 ±0.138
LD-07	0.00749 ±0.00091	0.645 ±0.247	0.00750 ±0.00072	0.634 ±0.228
LD-12	0.00842 ±0.00057	0.218 ±0.176	0.00842 ±0.00056	0.215 ±0.175
LD-10	0.00781 ±0.00077	0.564 ±0.225	0.00787 ±0.00075	0.554 ±0.220
LD-09	0.01438 ±0.00092	0.311 ±0.204	0.01432 ±0.00094	0.308 ±0.206

TABLE XIV(D).   Summary of Distillation Data for Halocarbon-23

Run No.	n (uncorr)	ε (uncorr)	n (corr)	ε (corr)	Holdup per Stage (q)
LD-11	13.7 ±1.1	0.00323 ±0.00026	13.8 ±1.1	0.00322 ±0.00026	0.527
LD-08	24.8 ±1.7	0.00218 ±0.00015	24.8 ±1.7	0.00218 ±0.00015	0.231
LD-04	22.3 ±2.3	0.00122 ±0.00012	22.3 ±2.2	0.00122 ±0.00012	0.278
LD-02	18.7 ±1.8	0.00189 ±0.00018	17.2 ±1.5	0.00207 ±0.00019	0.367
LD-03	22.7 ±12.1	0.00236 ±0.00125	22.0 ±2.1	0.00243 ±0.00023	0.290
LD-05	35.5 ±3.6	0.00141 ±0.00014	35.7 ±3.5	0.00140 ±0.00014	0.176
LD-06	46.1 ±3.7	0.00108 ±0.00008	44.2 ±3.7	0.00110 ±0.00009	0.155
LD-07	48.6 ±5.9	0.00100 ±0.00012	48.6 ±4.6	0.00100 ±0.00009	0.133
LD-12	44.4 ±3.0	0.00096 ±0.00006	44.3 ±2.9	0.00096 ±0.00006	0.162
LD-10	55.2 ±5.4	0.00064 ±0.00006	54.8 ±5.2	0.00064 ±0.00006	0.123
LD-09	30.6 ±1.9	0.00146 ±0.00009	30.7 ±2.0	0.00145 ±0.00009	0.236

TABLE XV. First Order Term Kinetics Parameters A_1 and B_1

ϵn		0.035	0.036	0.037	0.038	0.039	0.040	0.041	0.042	0.043	0.044
0.027	A=	0.8387	0.8394	0.8401	0.8407	0.8414	0.8421	0.8427	0.8434	0.8440	0.8447
	B=	2.2776	2.2732	2.2688	2.2644	2.2601	2.2557	2.2514	2.2470	2.2427	2.2384
0.028	A=	0.8388	0.8395	0.8402	0.8408	0.8415	0.8421	0.8428	0.8435	0.8441	0.8447
	B=	2.2766	2.2722	2.2678	2.2635	2.2591	2.2548	2.2504	2.2461	2.2418	2.2375
0.029	A=	0.8389	0.8396	0.8402	0.8409	0.8416	0.8422	0.8429	0.8435	0.8442	0.8448
	B=	2.2757	2.2713	2.2669	2.2625	2.2581	2.2538	2.2495	2.2451	2.2408	2.2365
0.030	A=	0.8390	0.8396	0.8403	0.8410	0.8416	0.8423	0.8430	0.8436	0.8443	0.8449
	B=	2.2747	2.2703	2.2659	2.2616	2.2572	2.2529	2.2485	2.2442	2.2399	2.2356
0.031	A=	0.8391	0.8397	0.8404	0.8411	0.8417	0.8424	0.8430	0.8437	0.8443	0.8450
	B=	2.2738	2.2694	2.2650	2.2606	2.2562	2.2519	2.2476	2.2433	2.2389	2.2347
0.032	A=	0.8391	0.8398	0.8405	0.8411	0.8418	0.8425	0.8431	0.8438	0.8444	0.8451
	B=	2.2728	2.2684	2.2640	2.2597	2.2553	2.2510	2.2466	2.2423	2.2380	2.2337
0.033	A=	0.8392	0.8399	0.8406	0.8412	0.8419	0.8425	0.8432	0.8438	0.8445	0.9451
	B=	2.2719	2.2675	2.2631	2.2587	2.2543	2.2500	2.2457	2.2414	2.2371	2.2328
0.034	A=	0.8393	0.8400	0.8406	0.8413	0.8420	0.8426	0.8433	0.8439	0.8446	0.8452
	B=	2.2709	2.2665	2.2621	2.2578	2.2534	2.2491	2.2447	2.2404	2.2361	2.2318
0.035	A=	0.8394	0.8400	0.8407	0.8414	0.8420	0.8427	0.8433	0.8440	0.8446	0.8453
	B=	2.2699	2.2656	2.2612	2.2568	2.2524	2.2481	2.2438	2.2395	2.2352	2.2309
0.036	A=	0.8394	0.8401	0.8408	0.8415	0.8421	0.8428	0.8434	0.8441	0.8447	0.8454
	B=	2.2690	2.2646	2.2602	2.2559	2.2515	2.2472	2.2428	2.2385	2.2342	2.2299

TABLE XV. (Continued)

ϵn		$k/\lambda n$									
		0.035	0.036	0.037	0.038	0.039	0.040	0.041	0.042	0.043	0.044
0.037	A=	0.8395	0.8402	0.8409	0.8415	0.8422	0.8428	0.8435	0.8441	0.8448	0.8454
	B=	2.2680	2.2636	2.2593	2.2549	2.2506	2.2462	2.2419	2.2376	2.2333	2.2290
0.038	A=	0.8396	0.8403	0.8409	0.8416	0.8423	0.8429	0.8436	0.8442	0.8449	0.8455
	B=	2.2671	2.2627	2.2583	2.2540	2.2496	2.2453	2.2409	2.2366	2.2323	2.2280
0.039	A=	0.8397	0.8404	0.8410	0.8417	0.8423	0.8430	0.8437	0.8443	0.8449	0.8456
	B=	2.2661	2.2617	2.2574	2.2530	2.2487	2.2443	2.2400	2.2357	2.2314	2.2271
0.040	A=	0.8398	0.8404	0.8411	0.8418	0.8424	0.8431	0.8437	0.8444	0.8450	0.8457
	B=	2.2652	2.2608	2.2564	2.2521	2.2477	2.2434	2.2391	2.2347	2.2304	2.2262
0.041	A=	0.8398	0.8405	0.8412	0.8418	0.8425	0.8432	0.8438	0.8445	0.8451	0.8457
	B=	2.2642	2.2598	2.2555	2.2511	2.2468	2.2424	2.2381	2.2338	2.2295	2.2252
0.042	A=	0.8399	0.8406	0.8413	0.8419	0.8426	0.8432	0.8439	0.8445	0.8452	0.8458
	B=	2.2633	2.2589	2.2545	2.2502	2.2458	2.2415	2.2372	2.2329	2.2286	2.2243
0.043	A=	0.8400	0.8407	0.8413	0.8420	0.8427	0.8433	0.8440	0.8446	0.8453	0.8459
	B=	2.2623	2.2579	2.2536	2.2492	2.2449	2.2405	2.2362	2.2319	2.2276	2.2233
0.044	A=	0.8401	0.8407	0.8414	0.8421	0.8427	0.8434	0.8440	0.8447	0.8453	0.8460
	B=	2.2614	2.2570	2.2526	2.2483	2.2439	2.2396	2.2353	2.2310	2.2267	2.2224
0.045	A=	0.8402	0.8408	0.8415	0.8422	0.8428	0.8435	0.8441	0.8448	0.8454	0.8461
	B=	2.2604	2.2560	2.2517	2.2473	2.2430	2.2386	2.2343	2.2300	2.2257	2.2215
0.046	A=	0.8402	0.8409	0.8416	0.8422	0.8429	0.8435	0.8442	0.8448	0.8455	0.8461
	B=	2.2595	2.2551	2.2507	2.2464	2.2420	2.2377	2.2334	2.2291	2.2248	2.2205

TABLE XV. (Continued)

$k/\lambda n$

ϵn		0.035	0.036	0.037	0.038	0.039	0.040	0.041	0.042	0.043	0.044
0.047	A=	0.8403	0.8410	0.8416	0.8423	0.8430	0.8436	0.8443	0.8449	0.8456	0.8462
	B=	2.2858	2.2541	2.2498	2.2454	2.2411	2.2368	2.2324	2.2281	2.2239	2.2196
0.048	A=	0.8404	0.8411	0.8417	0.8424	0.8430	0.8437	0.8443	0.8450	0.8456	0.8463
	B=	2.2576	2.2532	2.2488	2.2445	2.2401	2.2358	2.2315	2.2272	2.2229	2.2186
0.049	A=	0.8405	0.8411	0.8418	0.8425	0.8431	0.8438	0.8444	0.8451	0.8457	0.8464
	B=	2.2566	2.2523	2.2479	2.2435	2.2392	2.2349	2.2306	2.2263	2.2220	2.2177
0.050	A=	0.8405	0.8412	0.8419	0.8425	0.8432	0.8439	0.8445	0.8451	0.8458	0.8464
	B=	2.2557	2.2513	2.2469	2.2426	2.2382	2.2339	2.2296	2.2253	2.2210	2.2168
0.051	A=	0.8406	0.8413	0.8420	0.8426	0.8433	0.8439	0.8446	0.8452	0.8459	0.8465
	B=	2.2547	2.2504	2.2460	2.2416	2.2373	2.2330	2.2287	2.2244	2.2201	2.2158
0.052	A=	0.8407	0.8414	0.8420	0.8427	0.8434	0.8440	0.8447	0.8453	0.8459	0.8466
	B=	2.2538	2.2494	2.2450	2.2407	2.2364	2.2320	2.2277	2.2234	2.2191	2.2149
0.053	A=	0.8408	0.8414	0.8421	0.8428	0.8434	0.8441	0.8447	0.8454	0.8460	0.8467
	B=	2.2528	2.2485	2.2441	2.2398	2.2354	2.2311	2.2268	2.2225	2.2182	2.2139
0.054	A=	0.8409	0.8415	0.8422	0.8428	0.8435	0.8442	0.8448	0.8455	0.8461	0.8467
	B=	2.2519	2.2475	2.2432	2.2388	2.2345	2.2302	2.2258	2.2216	2.2173	2.2130
0.055	A=	0.8409	0.8416	0.8423	0.8429	0.8436	0.8442	0.8449	0.8455	0.8462	0.8468
	B=	2.2509	2.2466	2.2422	2.2379	2.2335	2.2292	2.2249	2.2206	2.2163	2.2121
0.056	A=	0.8410	0.8417	0.8423	0.8430	0.8437	0.8443	0.8450	0.8456	0.8463	0.8469
	B=	2.2500	2.2456	2.2413	2.2369	2.2326	2.2283	2.2240	2.2197	2.2154	2.2111

TABLE XVI. Second Order Term Kinetics Parameters A_2 and B_2

ϵn		k/λn									
		0.035	0.036	0.037	0.038	0.039	0.040	0.041	0.042	0.043	0.044
0.027	A=	0.0885	0.0885	0.0885	0.0884	0.0884	0.0884	0.0884	0.0883	0.0883	0.0883
	B=	20.6977	20.6579	20.6180	20.5782	20.5374	20.4976	20.4629	20.4273	20.3916	20.3560
0.028	A=	0.0885	0.0884	0.0884	0.0883	0.0883	0.0883	0.0883	0.0882	0.0882	0.0882
	B=	20.6958	20.6560	20.6162	20.5764	20.5366	20.4968	20.4611	20.4255	20.3898	20.3542
0.029	A=	0.0884	0.0883	0.0883	0.0882	0.0882	0.0882	0.0882	0.0881	0.0881	0.0881
	B=	20.6940	20.6542	20.6144	20.5746	20.5348	20.4950	20.4593	20.4237	20.3880	20.3524
0.030	A=	0.0883	0.0883	0.0883	0.0882	0.0882	0.0882	0.0882	0.0881	0.0881	0.0881
	B=	20.6922	20.6524	20.6126	20.5728	20.5330	20.4932	20.4575	20.4219	20.3862	20.3506
0.031	A=	0.0882	0.0882	0.0882	0.0881	0.0881	0.0881	0.0881	0.0880	0.0880	0.0880
	B=	20.6904	20.6506	20.6108	20.5710	20.5312	20.4914	20.4557	20.4201	20.3844	20.3488
0.032	A=	0.0881	0.0881	0.0881	0.0880	0.0880	0.0880	0.0880	0.0879	0.0879	0.0879
	B=	20.6886	20.6488	20.6090	20.5692	20.5294	20.4896	20.4539	20.4183	20.3826	20.3470
0.033	A=	0.0881	0.0881	0.0881	0.0880	0.0880	0.0880	0.0880	0.0879	0.0879	0.0879
	B=	20.6867	20.6469	20.6072	20.5674	20.5276	20.4878	20.4521	20.4165	20.3808	20.3452
0.034	A=	0.0880	0.0880	0.0880	0.0879	0.0879	0.0879	0.0879	0.0878	0.0878	0.0877
	B=	20.6849	20.6451	20.6054	20.5656	20.5258	20.4860	20.4503	20.4147	20.3790	20.3434
0.035	A=	0.0879	0.0879	0.0879	0.0878	0.0878	0.0878	0.0878	0.0877	0.0877	0.0877
	B=	20.6831	20.6433	20.6036	20.5638	20.5240	20.4842	20.4486	20.4130	20.3773	20.3417
0.036	A=	0.0878	0.0878	0.0878	0.0877	0.0877	0.0877	0.0877	0.0876	0.0876	0.0876
	B=	20.6813	20.6415	20.6017	20.5619	20.5222	20.4824	20.4468	20.4112	20.3755	20.3399

TABLE XVI. (Continued)

						$k/\lambda n$					
ϵn		0.035	0.036	0.037	0.038	0.039	0.040	0.041	0.042	0.043	0.044
0.037	A=	0.0877	0.0877	0.0877	0.0876	0.0876	0.0876	0.0876	0.0875	0.0875	0.0875
	B=	20.6795	20.6397	20.5999	20.5601	20.5204	20.4806	20.4450	20.4044	20.3737	20.3381
0.038	A=	0.0877	0.0877	0.0877	0.0876	0.0876	0.0876	0.0876	0.0875	0.0875	0.0874
	B=	20.6776	20.3678	20.5981	20.5583	20.5186	20.4788	20.4432	20.4076	20.3719	20.3363
0.039	A=	0.0876	0.0876	0.0876	0.0875	0.0875	0.0875	0.0875	0.0874	0.0874	0.0873
	B=	20.6758	20.6360	20.5963	20.5565	20.5168	20.4770	20.4414	20.4058	20.3701	20.3345
0.040	A=	0.0875	0.0875	0.0875	0.0874	0.0874	0.0874	0.0874	0.0873	0.0873	0.0872
	B=	20.6740	20.6342	20.5945	20.5547	20.5150	20.4752	20.4396	20.4040	20.3683	20.3327
0.041	A=	0.0874	0.0874	0.0874	0.0873	0.0873	0.0873	0.0873	0.0872	0.0872	0.0871
	B=	20.6722	20.6324	20.5927	20.5529	20.5132	20.4734	20.4378	20.4021	20.3663	20.3306
0.042	A=	0.0873	0.0873	0.0873	0.0872	0.0872	0.0872	0.0872	0.0871	0.0871	0.0870
	B=	20.6704	20.6306	20.5909	20.5511	20.5114	20.4616	20.4359	20.4001	20.3643	20.3285
0.043	A=	0.0872	0.0872	0.0872	0.0871	0.0871	0.0871	0.0871	0.0870	0.0870	0.0869
	B=	20.6686	20.6288	20.5891	20.5493	20.5096	20.4698	20.4340	20.3982	20.3622	20.3264
0.044	A=	0.0871	0.0871	0.0871	0.0870	0.0870	0.0870	0.0870	0.0869	0.0869	0.0868
	B=	20.6668	20.6270	20.5873	20.5475	20.5078	20.4681	20.4322	20.3962	20.3602	20.3243
0.045	A=	0.0871	0.0871	0.0871	0.0870	0.0870	0.0870	0.0869	0.0868	0.0868	0.0867
	B=	20.6650	20.6252	20.5855	20.5457	20.5060	20.4663	20.4303	20.3943	20.3582	20.3222
0.046	A=	0.0870	0.0870	0.0870	0.0869	0.0869	0.0869	0.0868	0.0867	0.0867	0.0866
	B=	20.6632	20.6235	20.5838	20.5440	20.5043	20.4645	20.4284	20.3424	20.3562	20.3201

TABLE XVI. (Continued)

k/λn

εn		0.035	0.036	0.037	0.038	0.039	0.040	0.041	0.042	0.043	0.044
0.047	A=	0.0869	0.0869	0.0869	0.0868	0.0868	0.0868	0.0867	0.0866	0.0866	0.0865
	B=	20.6614	20.6217	20.5820	20.5422	20.5025	20.4628	20.4265	20.3904	20.3542	20.3180
0.048	A=	0.0868	0.0868	0.0868	0.0867	0.0867	0.0867	0.0866	0.0865	0.0865	0.0864
	B=	20.6596	20.6199	20.5802	20.5404	20.5007	20.4610	20.4247	20.3885	20.3521	20.3159
0.049	A=	0.0867	0.0867	0.0867	0.0866	0.0866	0.0866	0.0865	0.0864	0.0864	0.0863
	B=	20.6578	20.6181	20.5784	20.5386	20.4989	20.4592	20.4229	20.3865	20.3501	20.3138
0.050	A=	0.0866	0.0866	0.0866	0.0865	0.0865	0.0865	0.0864	0.0863	0.0863	0.0862
	B=	20.6560	20.6163	20.5766	20.5368	20.4971	20.4574	20.4210	20.3846	20.3481	20.3117
0.051	A=	0.0865	0.0865	0.0865	0.0864	0.0864	0.0864	0.0863	0.0862	0.0862	0.0861
	B=	20.6542	20.6145	20.5748	20.5350	20.4953	20.4556	20.4192	20.3829	20.3464	20.3100
0.052	A=	0.0864	0.0864	0.0864	0.0863	0.0863	0.0863	0.0862	0.0861	0.0861	0.0860
	B=	20.6524	20.6127	20.5730	20.5333	20.4936	20.4539	20.4175	20.3811	20.3446	20.3082
0.053	A=	0.0864	0.0864	0.0864	0.0863	0.0863	0.0863	0.0862	0.0861	0.0861	0.0860
	B=	20.6506	20.6109	20.5712	20.5315	20.4918	20.4521	20.4157	20.3794	20.3429	20.3065
0.054	A=	0.0863	0.0863	0.0863	0.0862	0.0862	0.0862	0.0861	0.0860	0.0860	0.0859
	B=	20.6489	20.6092	20.5695	20.5298	20.4901	20.4504	20.4140	20.3776	20.3411	20.3047
0.055	A=	0.0862	0.0862	0.0862	0.0861	0.0861	0.0861	0.0860	0.0859	0.0859	0.0858
	B=	20.6471	20.6074	20.5677	20.5280	20.4883	20.4486	20.4122	20.3759	20.3394	20.3030
0.056	A=	0.0861	0.0861	0.0861	0.0860	0.0860	0.0860	0.0859	0.0858	0.0858	0.0857
	B=	20.6453	20.6056	20.5659	20.5262	20.4865	20.4468	20.4104	20.3741	20.3377	20.3013

$$T \ (^\circ K) = \frac{-0.59608}{R \ (\text{ohm})} + 31.028 + 2.279R$$

$$+ \ 2.432 \times 10^{-1}R^2 - 4.9494 \times 10^{-4}R^3 \quad (28)$$

The discrepancy between the two temperature readings is an indication of the reliability of the Wallace-Tiernan gauge, which is excellent. In Table XIV(D), the last column, entitled "Holdup per Stage (g)" is an indication of the degree of wetness of the column packing.

The data of Tables III to XIII have been plotted in Figures 13 to 23, one figure for each distillation run. These figures are the plots of the overall separation, q, as a function of time, t, and the solid lines through the figures correspond to the second-order corrected long-time kinetics, Equation 24.

The data from runs LD-02, LD-03, LD-06, and LD-10 have been plotted in Figures 24 to 27 respectively in order to demonstrate the effect of the second-order correction term of Equation 24. In each of these figures, the solid line represents the solution of the second-order corrected Equation 24, while the dashed line represents the first-order solution, Equation 21. The effect is observable only within approximately the first 100 minutes of each distillation run, since the second term in the left-hand side of Equation 24 becomes insignificant for large values of τ, which is equal to $t/\lambda n^2$.

The mass spectrometric analyses of these distillation experiments indicates that all the data attests to the inverse vapor pressure isotope effect.

FIGURE 13. SEPARATION AS A FUNCTION OF TIME, RUN-02
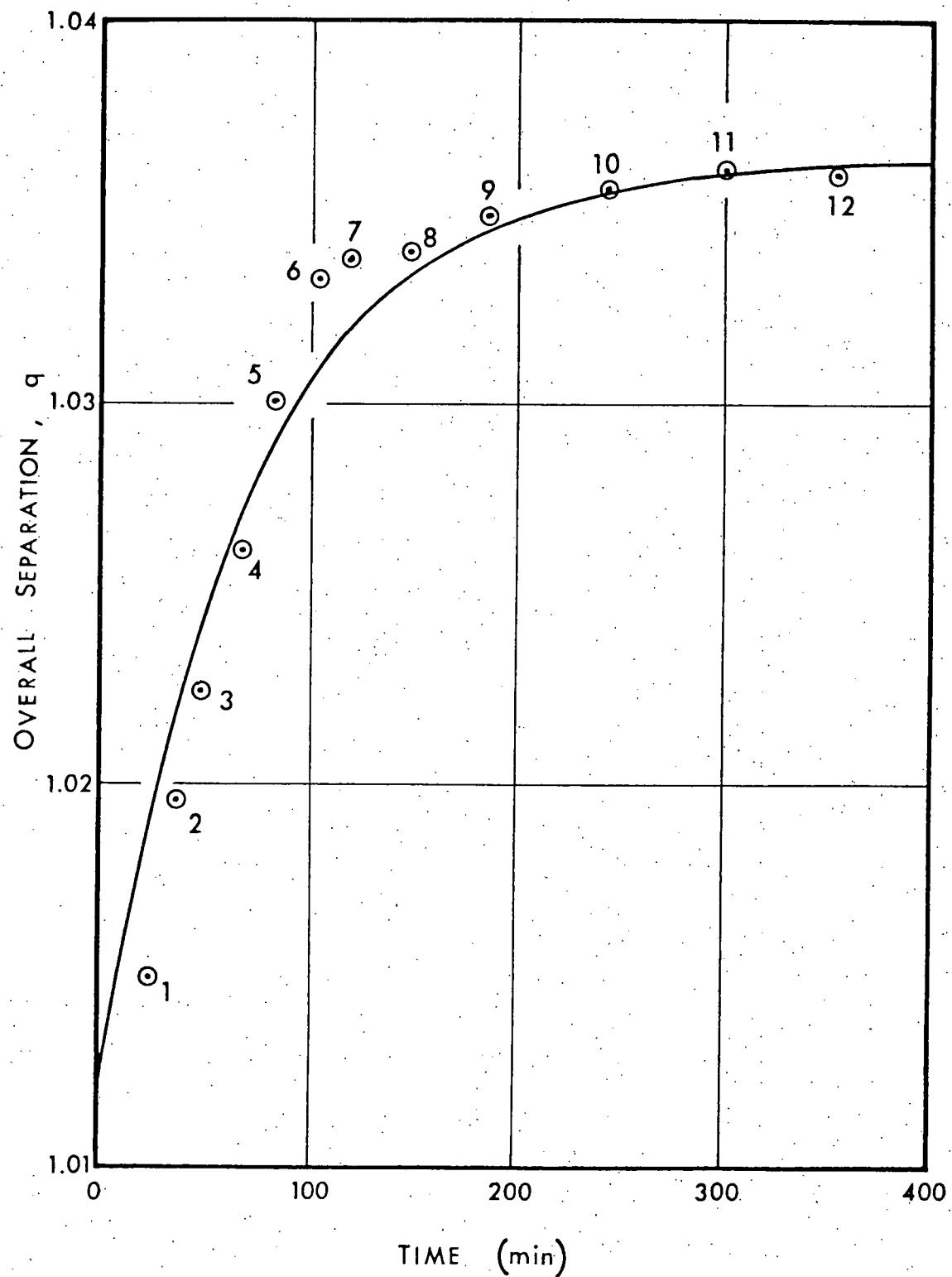
FIGURE 14. SEPARATION AS A FUNCTION OF TIME, RUN LD-03
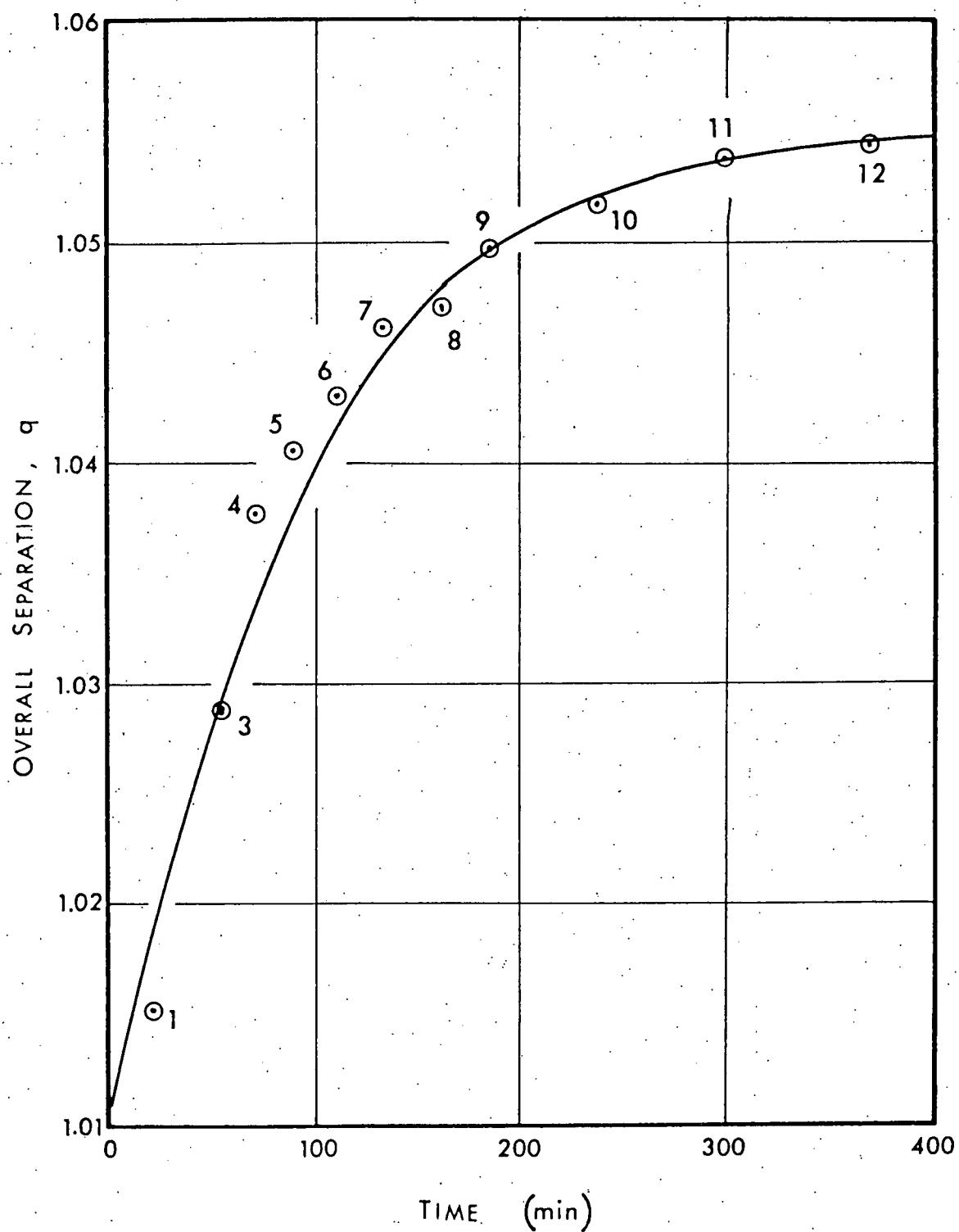
FIGURE 15. SEPARATION AS A FUNCTION OF TIME, RUN LD-04
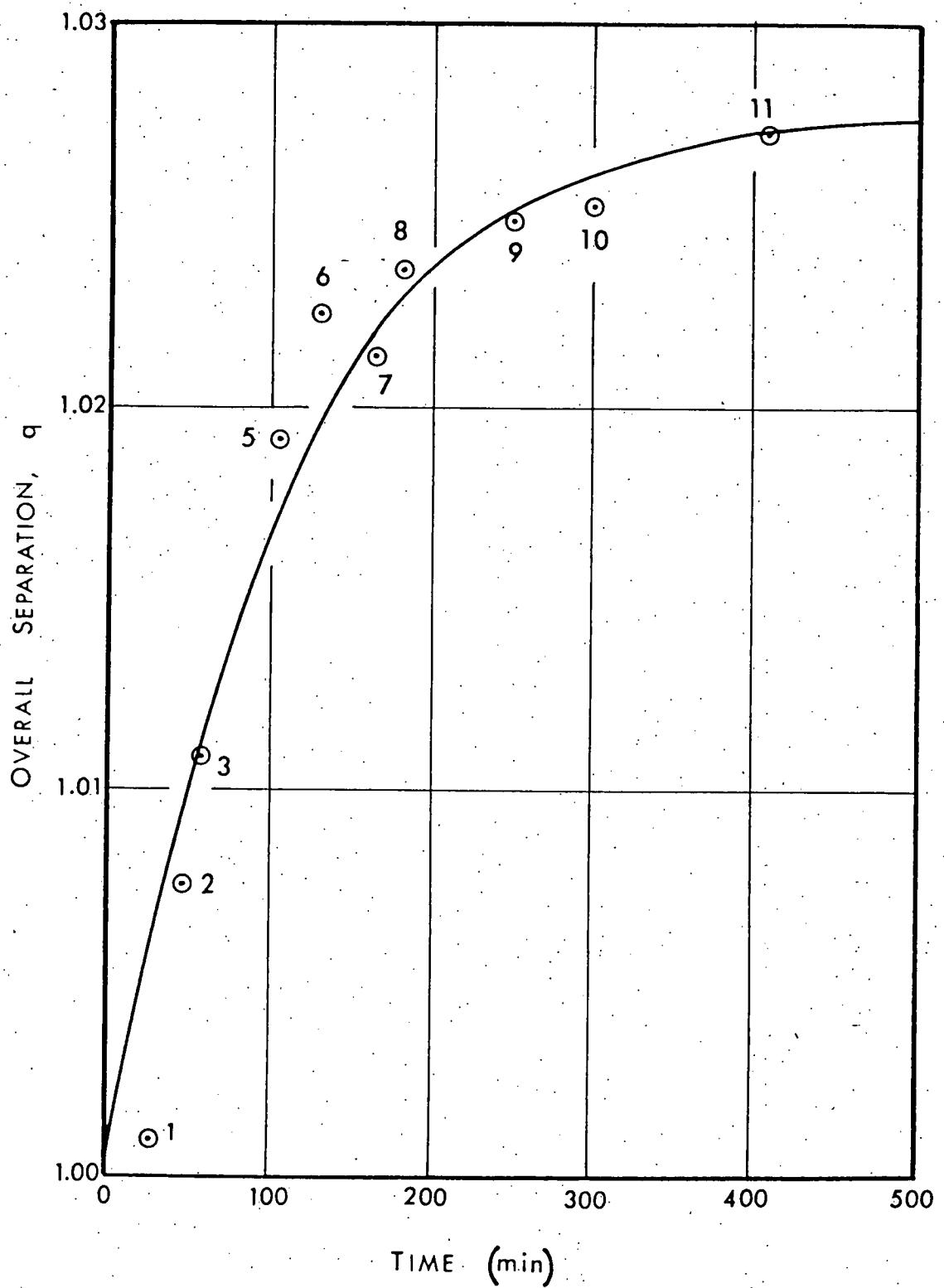
FIGURE 16. SEPARATION AS A FUNCTION OF TIME, RUN LD-05
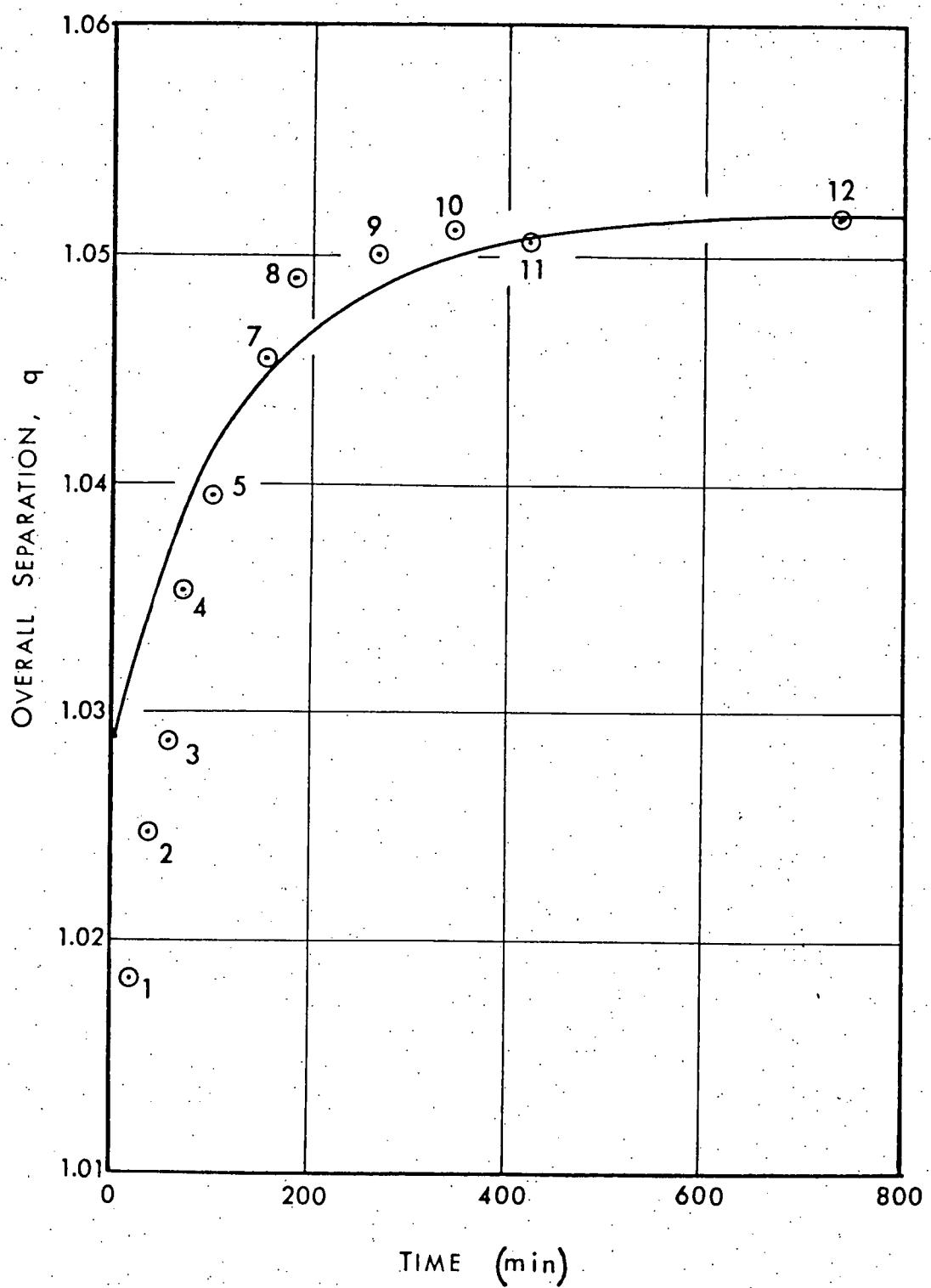
FIGURE 17. SEPARATION AS A FUNCTION OF TIME, RUN LD-06
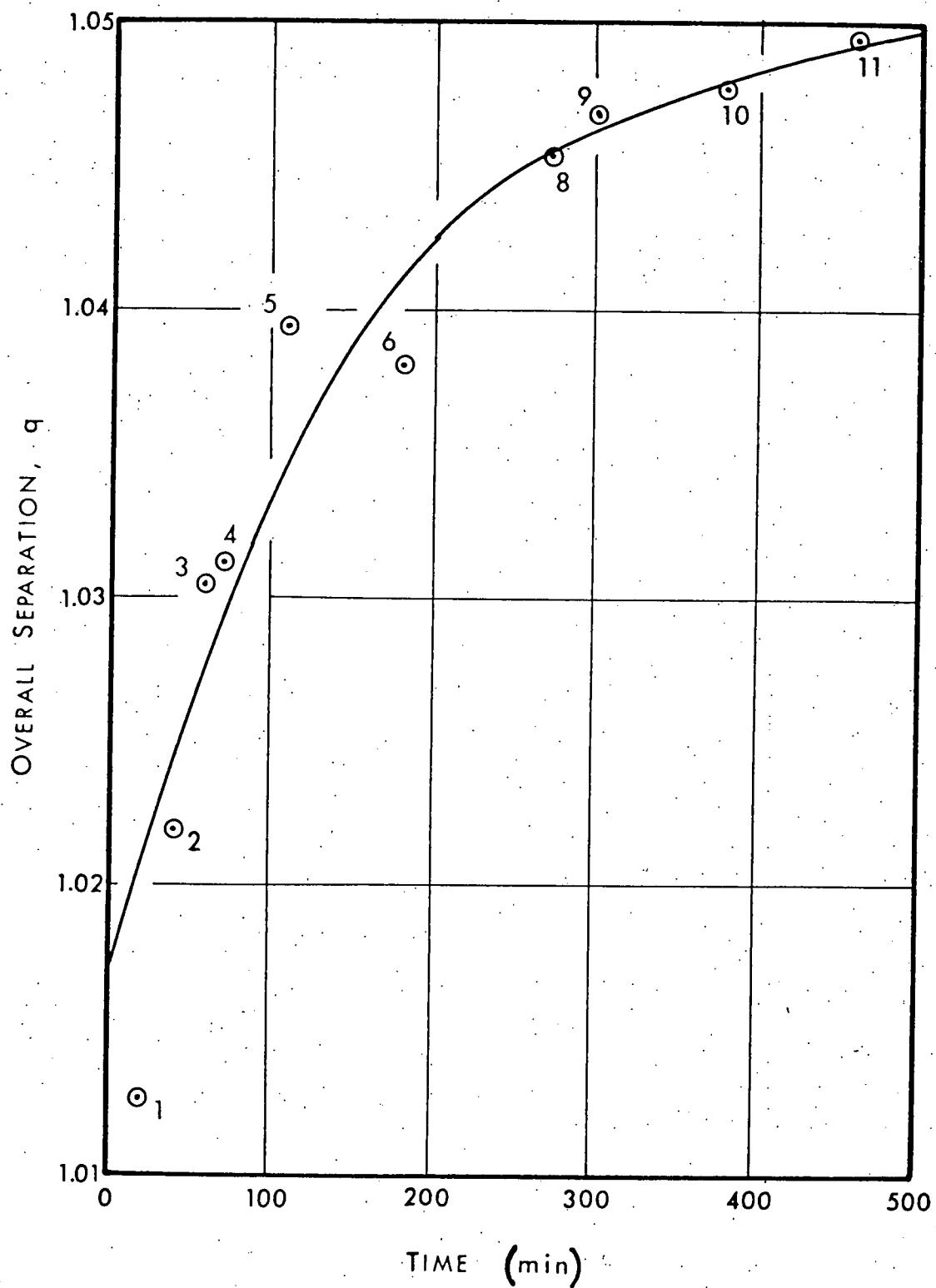
FIGURE 18. SEPARATION AS A FUNCTION OF TIME, RUN LD-07
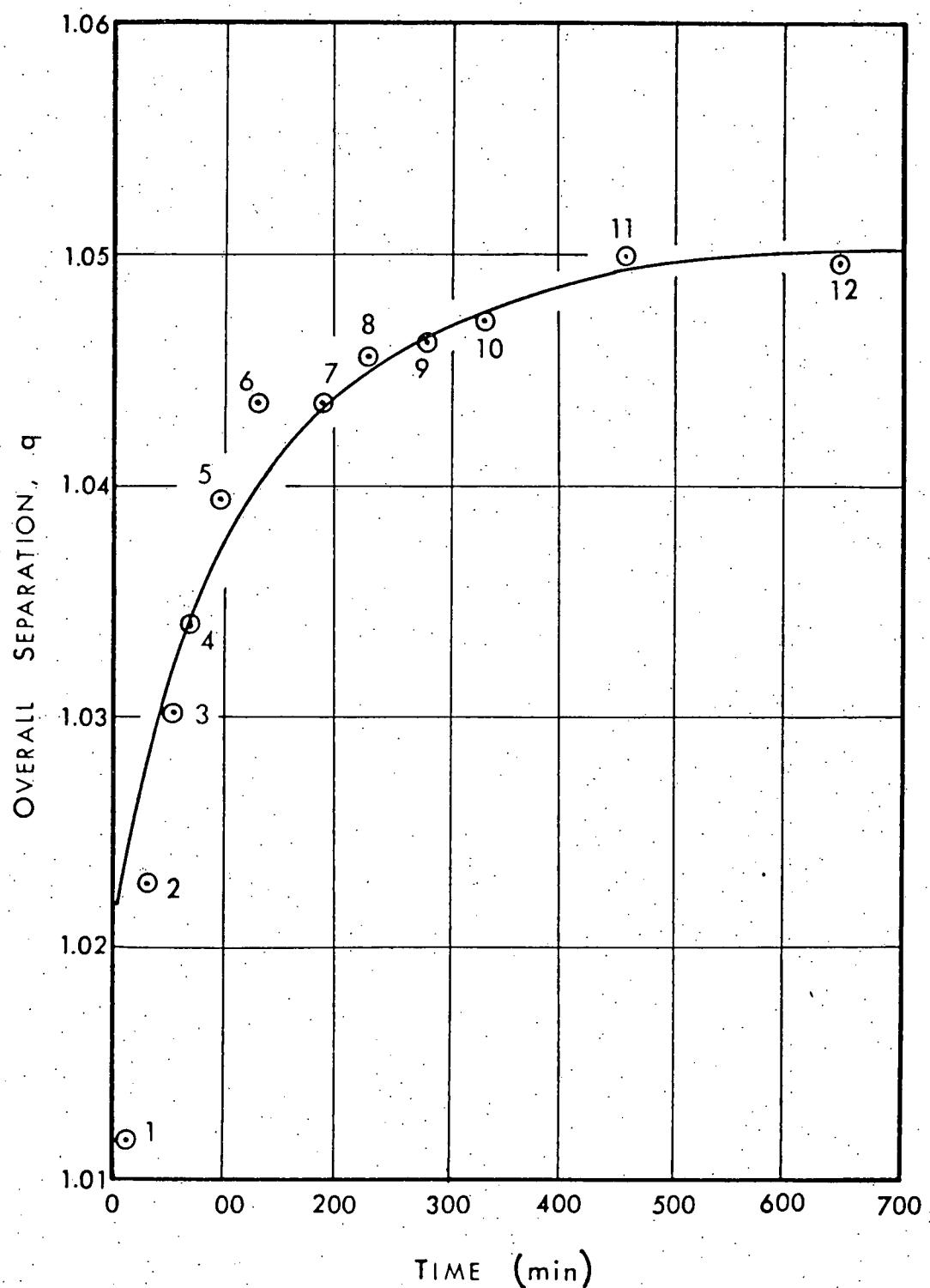
FIGURE 19. SEPARATION AS A FUNCTION OF TIME, RUN LD-08
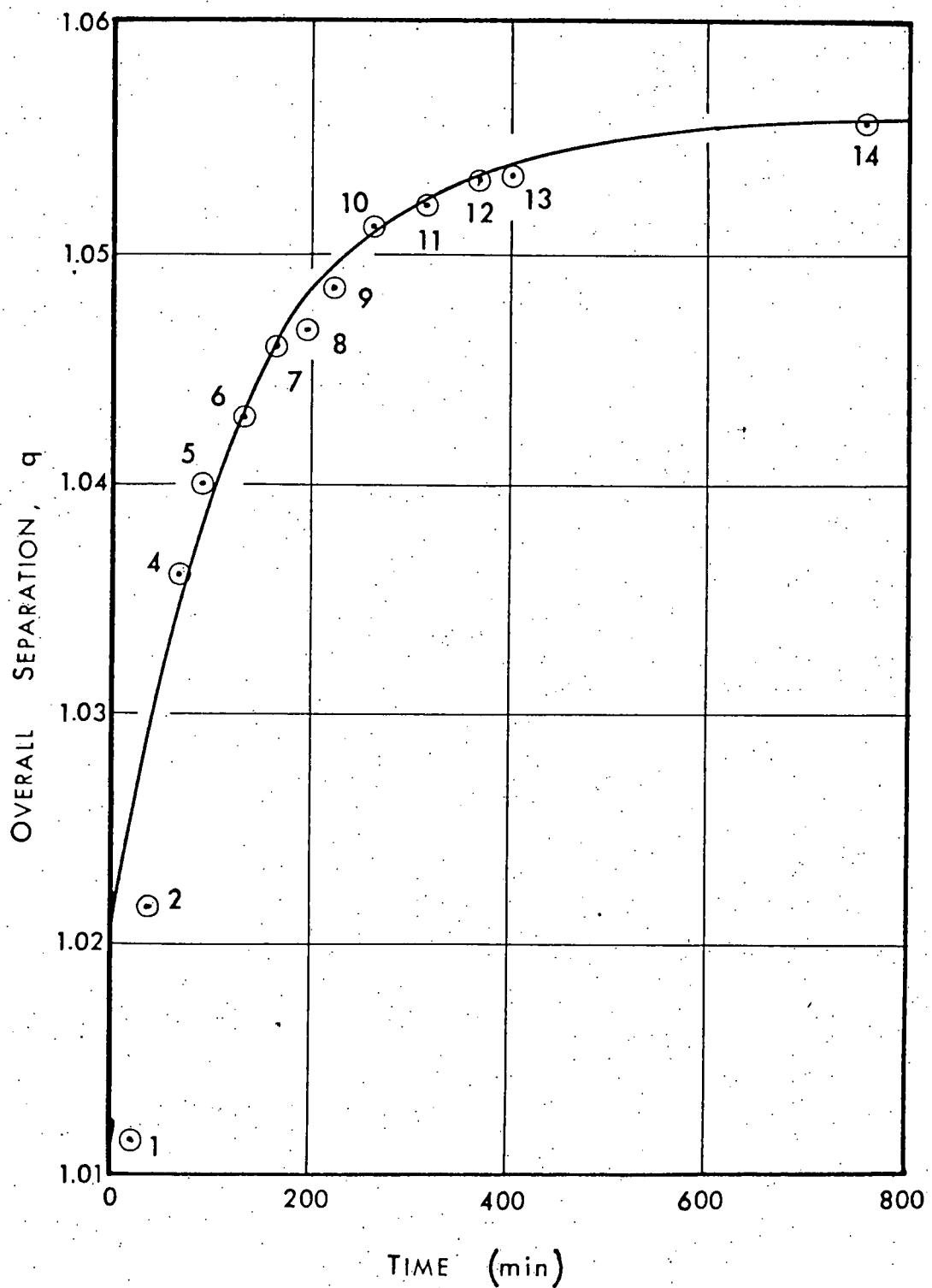
FIGURE 20. SEPARATION AS A FUNCTION OF TIME, RUN LD-09
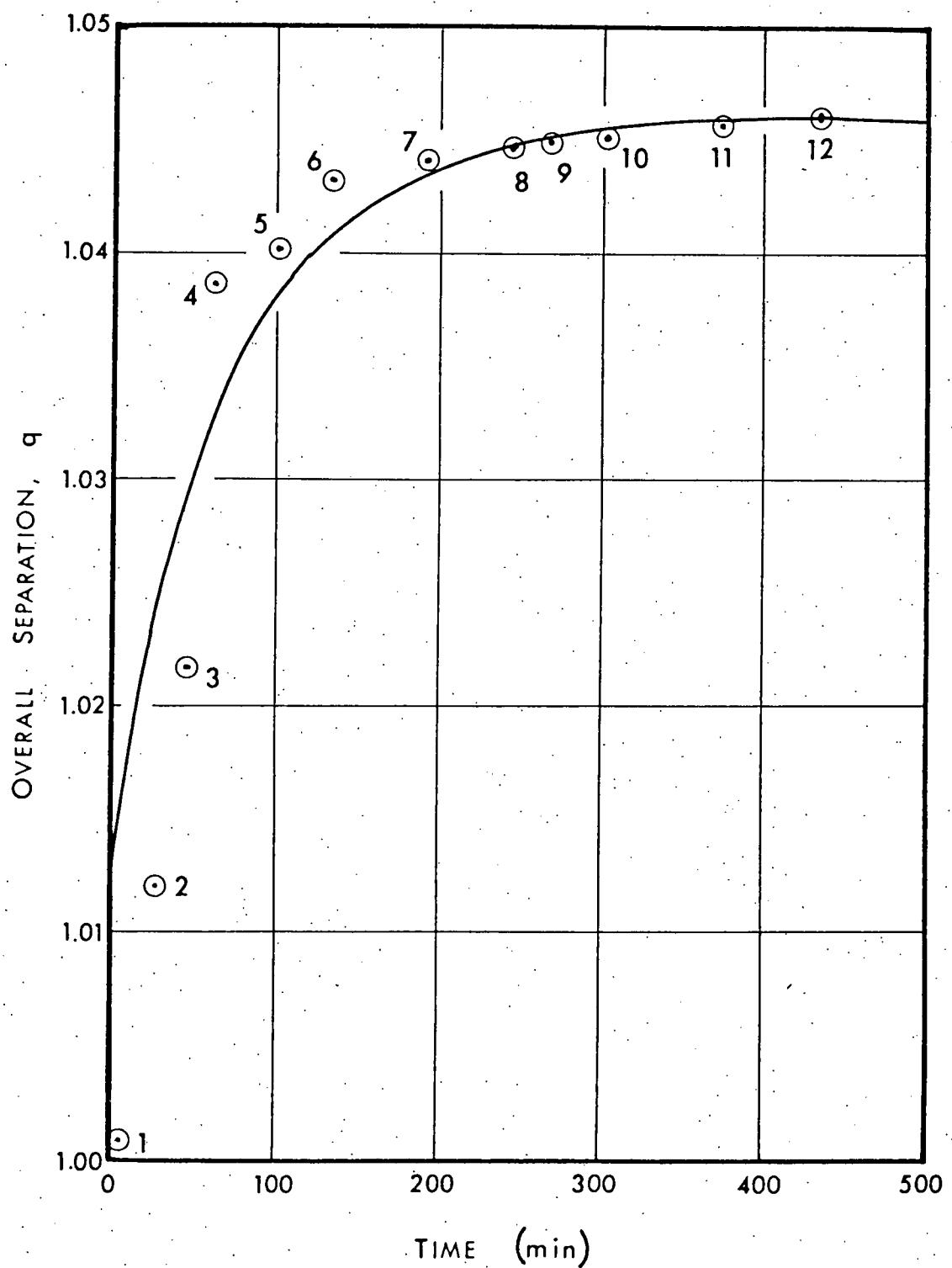
FIGURE 21. SEPARATION AS A FUNCTION OF TIME, RUN LD-10
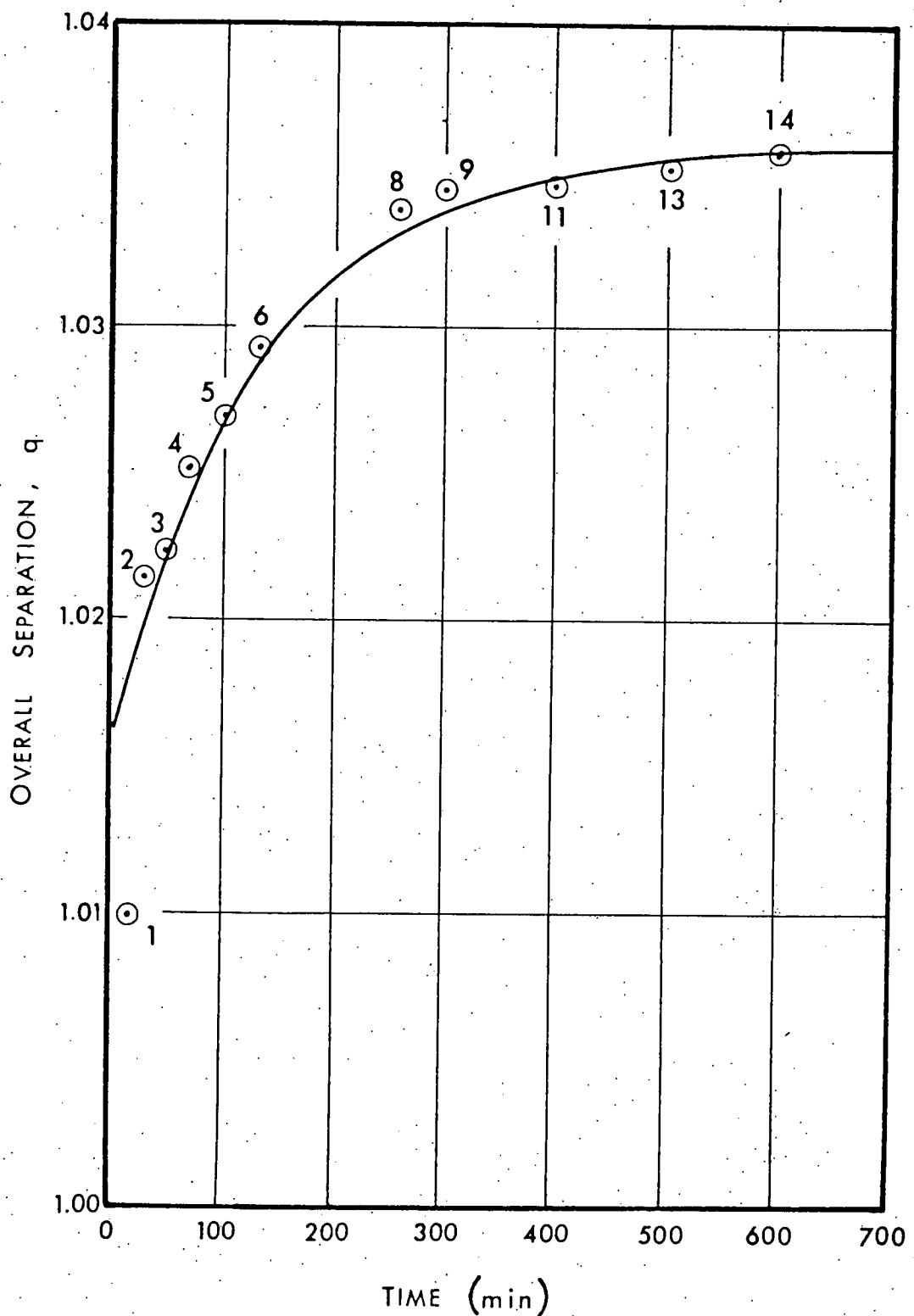
FIGURE 22. SEPARATION AS A FUNCTION OF TIME, RUN LD-11
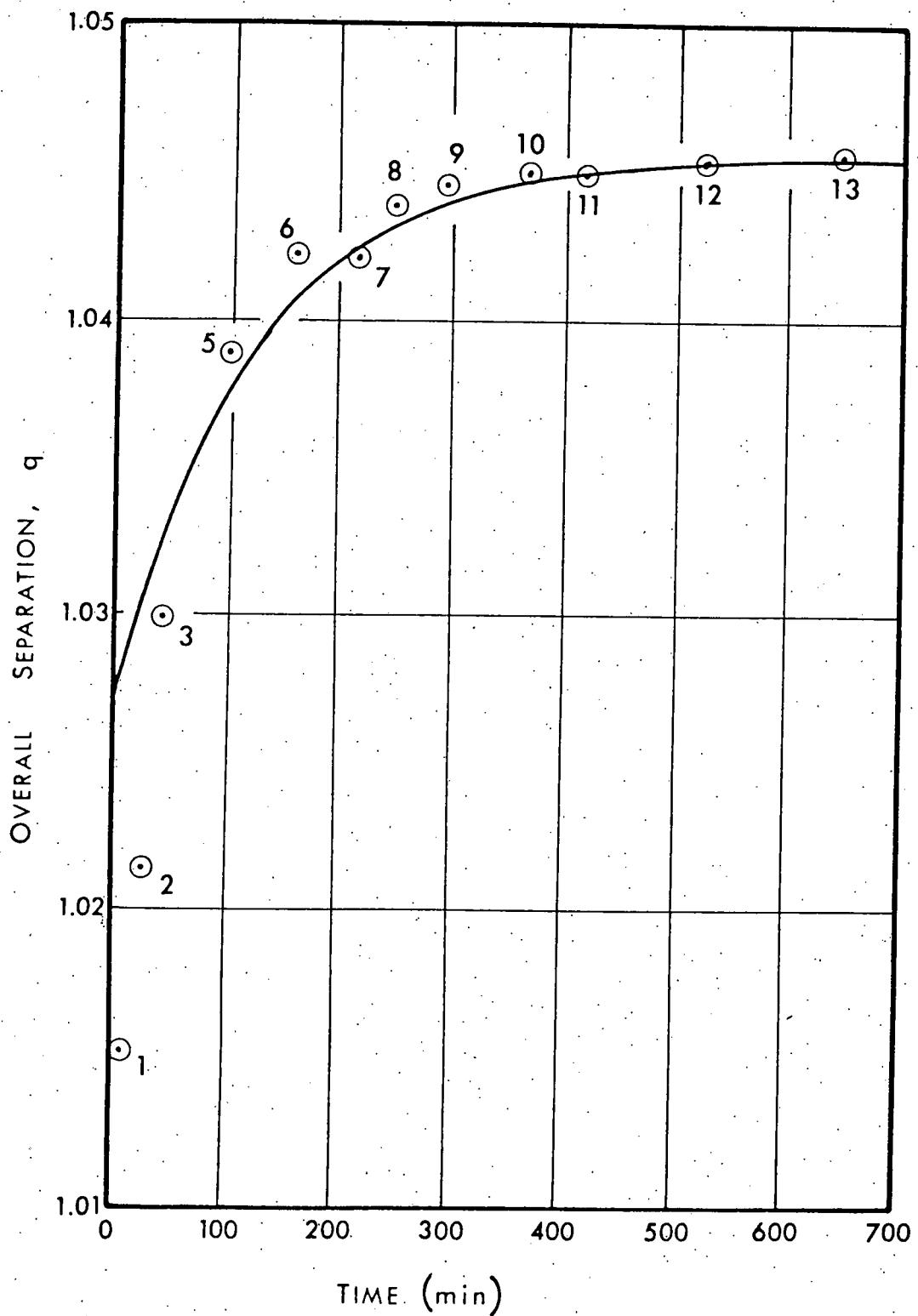
FIGURE 23. SEPARATION AS A FUNCTION OF TIME, RUN LD-12
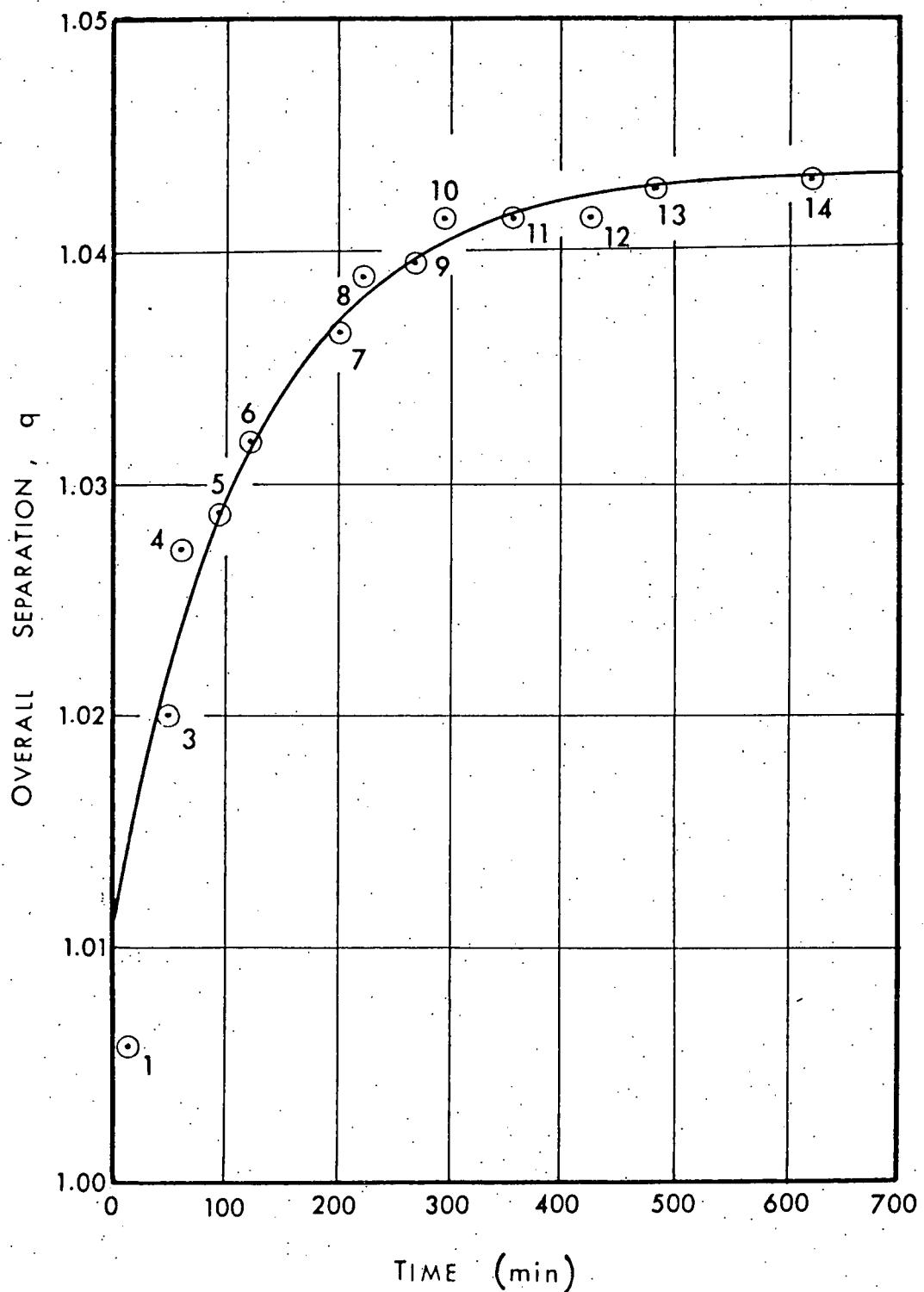
FIGURE 24. SECOND ORDER CORRECTION OF $y_L(\tau)$, LD-02
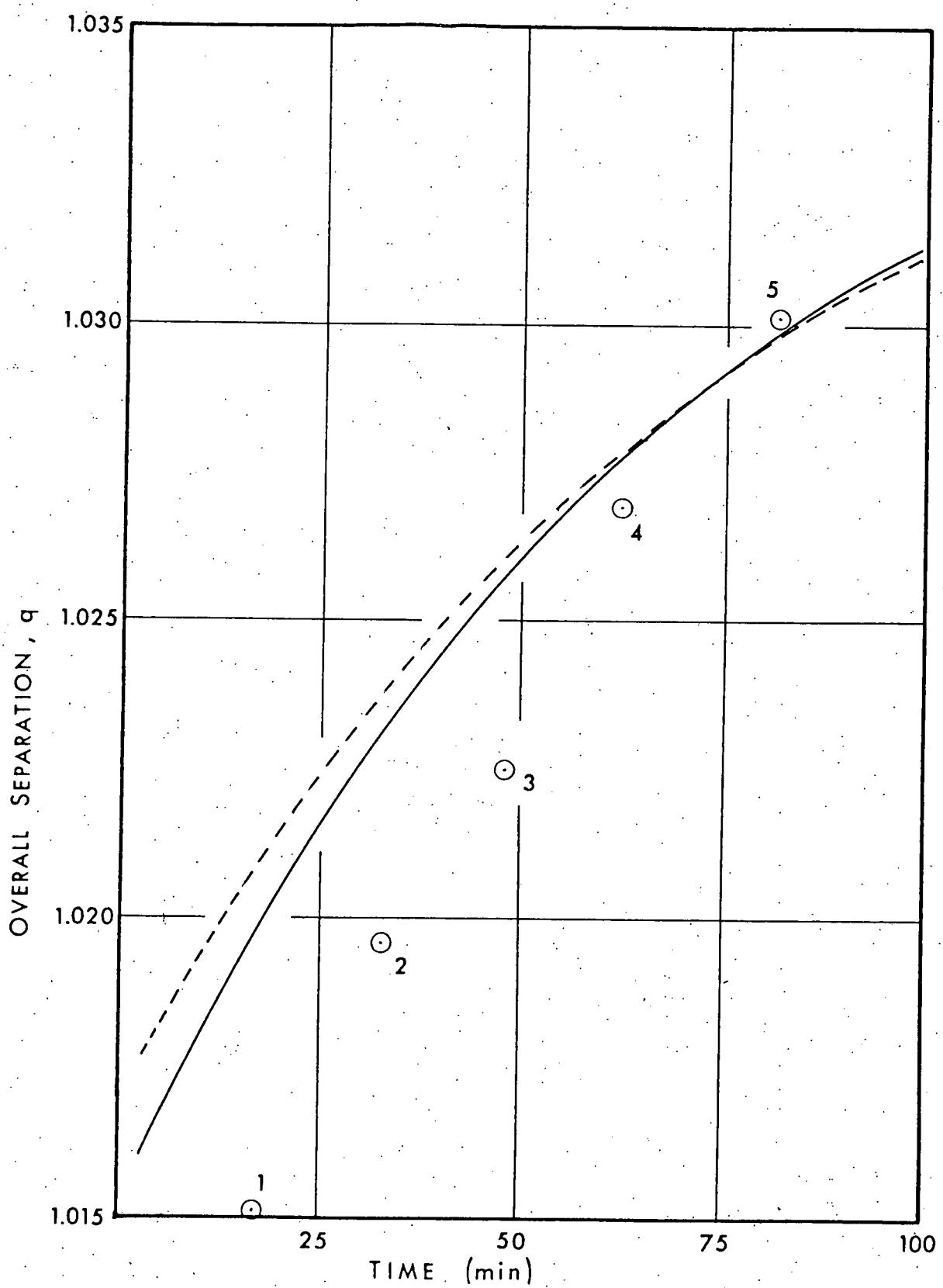
FIGURE 25. SECOND ORDER CORRECTION OF $y_L(\tau)$, LD-03
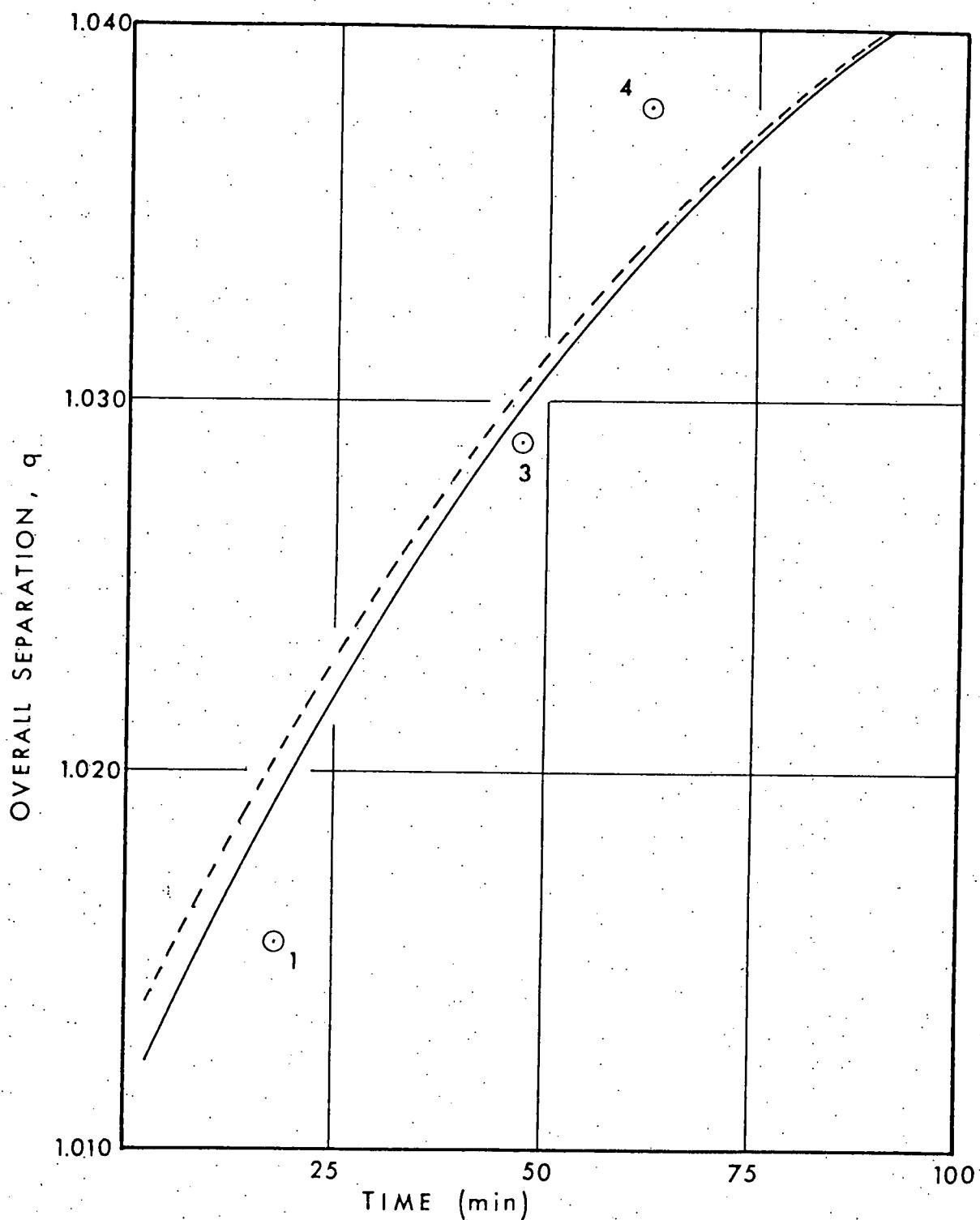
FIGURE 26. SECOND ORDER CORRECTION OF $y_L(\tau)$, LD-06
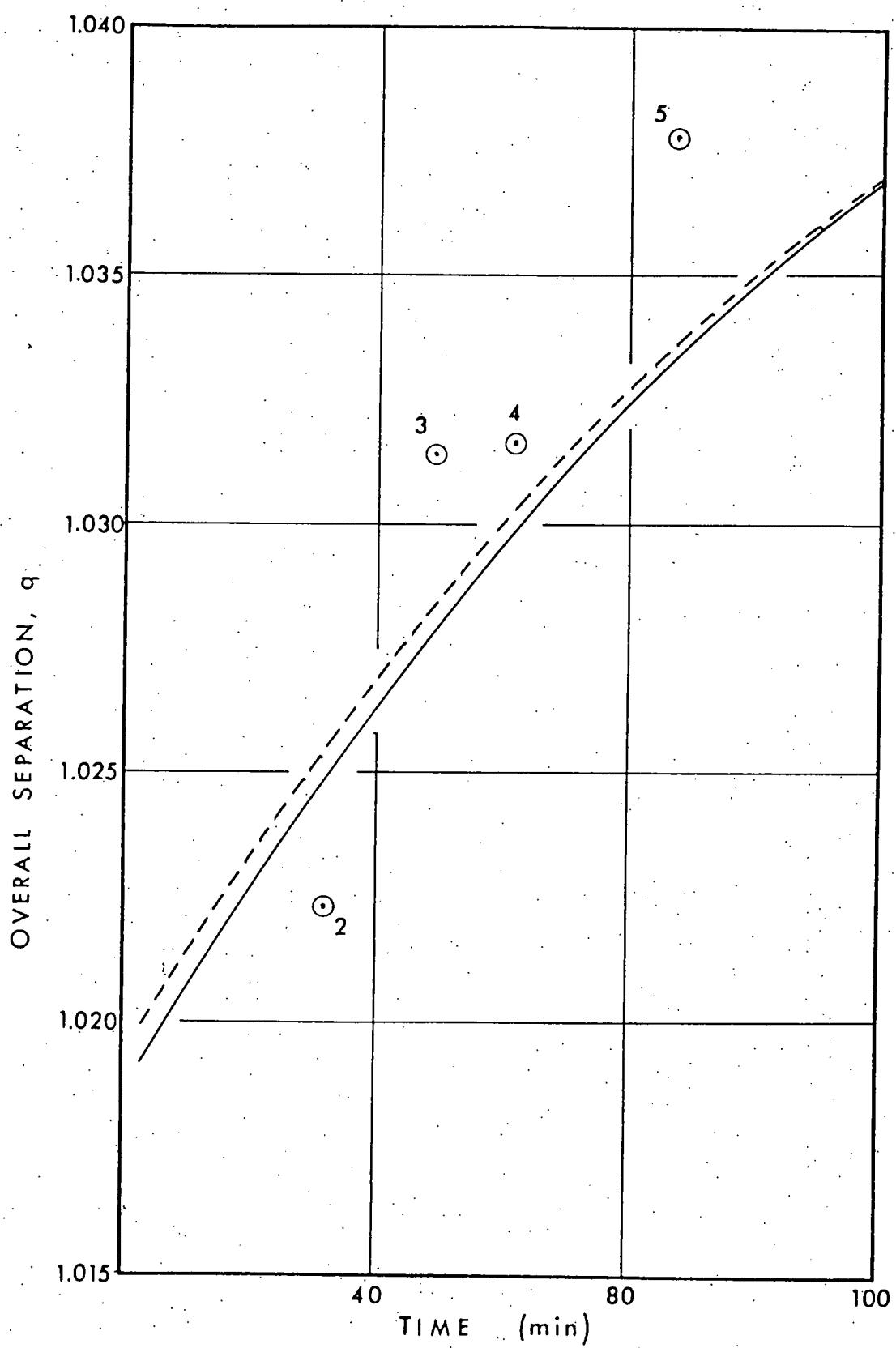
FIGURE 27. SECOND ORDER CORRECTION OF $y_L(\tau)$, LD-10
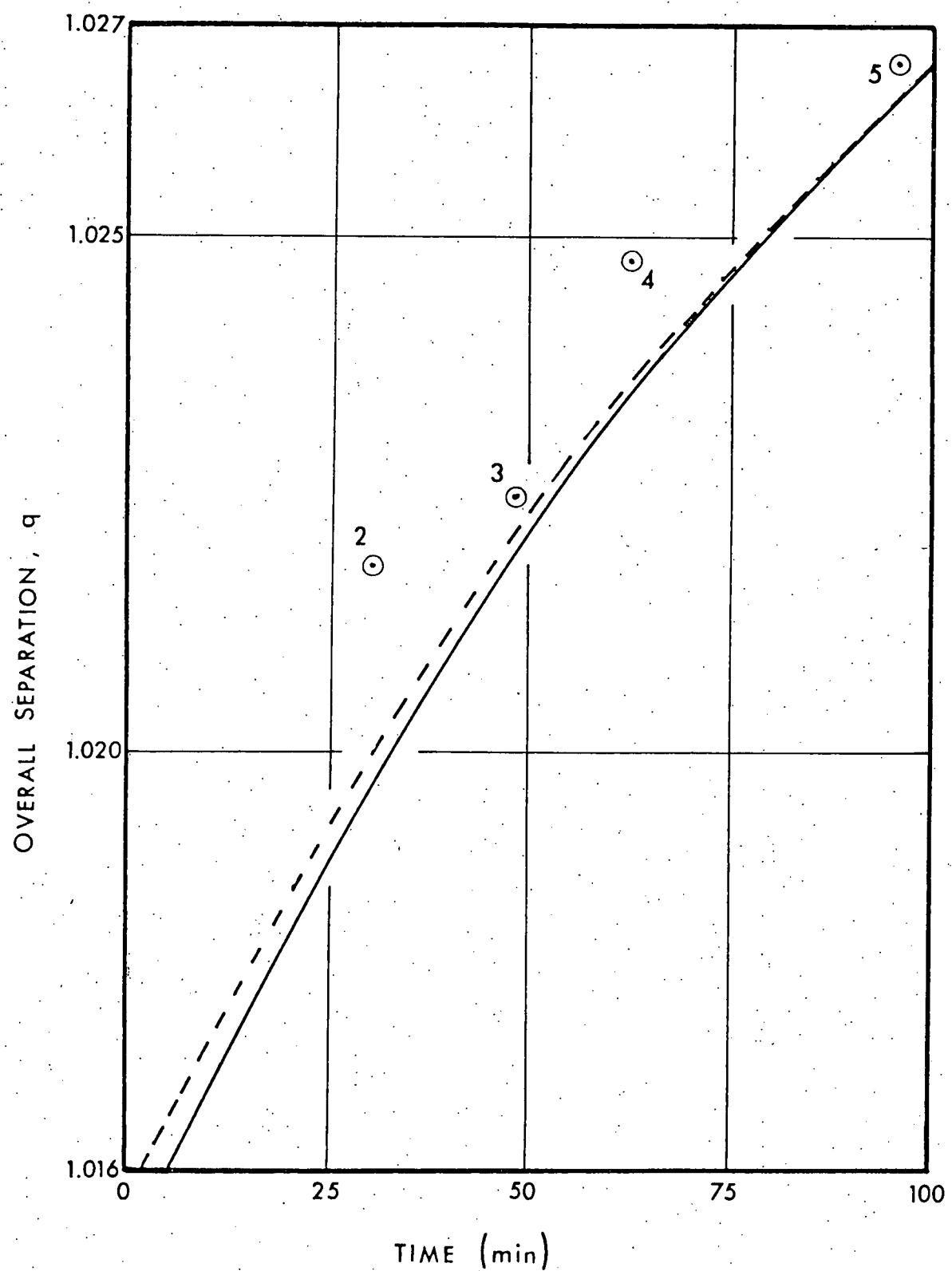
The results on ϵ summarized in Table XIV(D) were least-squares fit to two functional forms:

$$\ln\left(\frac{P'}{P}\right) = \frac{A}{T^2} - \frac{B}{T} \tag{11}$$

$$\ln\left(\frac{P'}{P}\right) = \frac{A'}{T} - B' \tag{29}$$

where P' and P are the vapor pressures of the $^{12}CHF_3$ and $^{13}CHF_3$ molecules respectively, so that

$$\ln\left(\frac{P'}{P}\right) \approx \ln \alpha = \ln (1 + \epsilon) \approx \epsilon \tag{30}$$

Equation 11 is Bigeleisen's first-order approximation[10] for the relative vapor pressures of the isotopic molecules under the assumptions of the Born-Oppenheimer approximation, harmonic potentials, and the liquid cell model. According to this theory, A represents the isotopic difference in the first quantum correction for the loose external oscillations of liquid molecules, and B represents the isotope effect in the shift of the zero-point energy upon condensation. Both A and B are positive according to this approximation.[38]

For $^{13}CHF_3/^{12}CHF_3$, it has been found that

$$\left.\begin{array}{l} A = 217 \pm 66 \\ B = 0.89 \pm 0.36 \end{array}\right\} \tag{31a,b}$$

and

$$\left.\begin{array}{l} A' = 1.49 \pm 0.38 \\ B' = (6.49 \pm 2.06) \times 10^{-3} \end{array}\right\} \tag{32a,b}$$

The errors quoted in Equations 31 and 32 are the root-mean-squares deviation of the experimental points around the least- squares fit curve. Figure 28 depicts the comparison
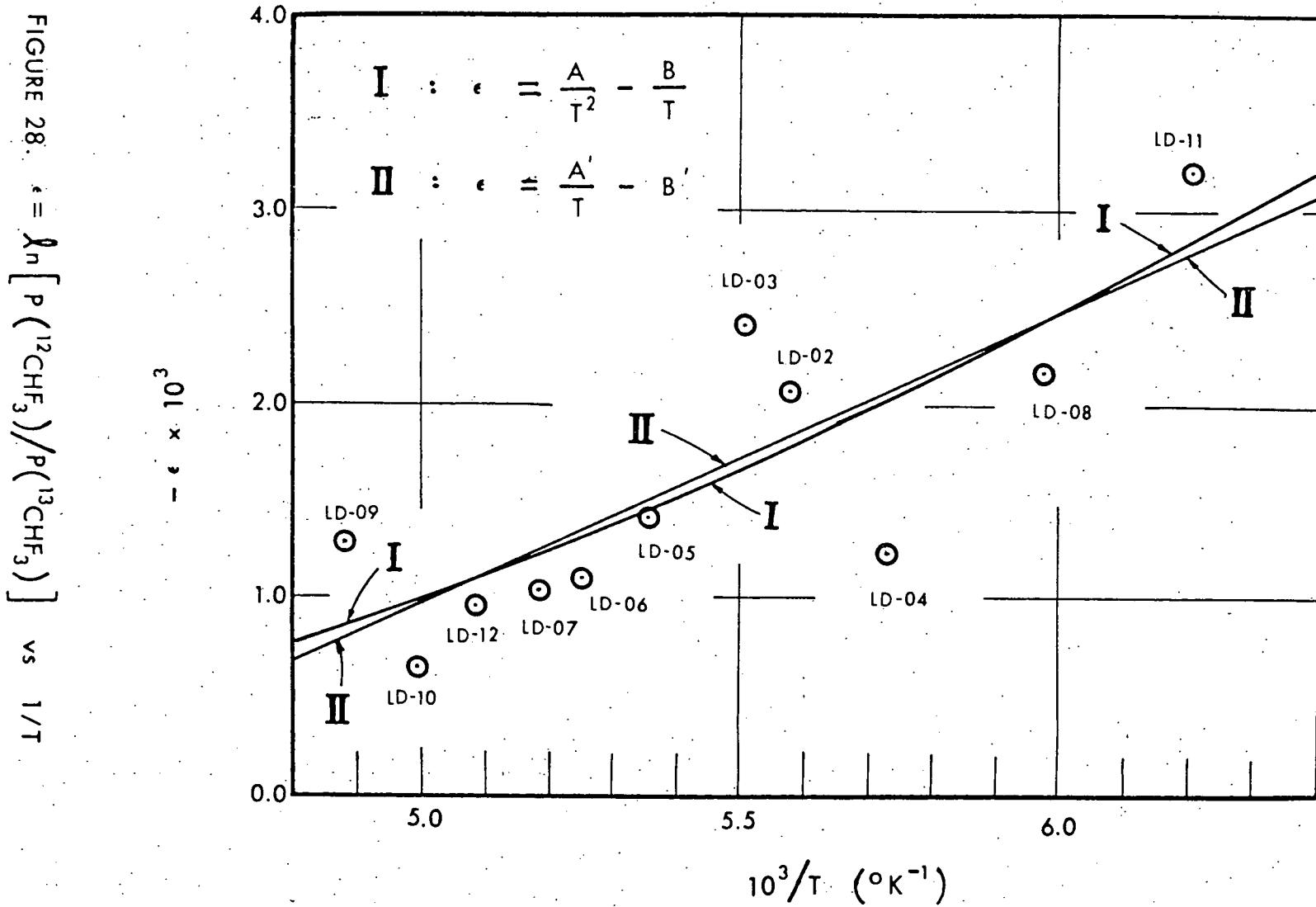
FIGURE 28. $\epsilon = \ell_n \left[P(^{12}CHF_3)/P(^{13}CHF_3) \right]$ vs 1/T

I : $\epsilon = \dfrac{A}{T^2} - \dfrac{B}{T}$

II : $\epsilon = \dfrac{A'}{T} - B'$

-93-

of these least-squares fits obtainable by the two functional forms, Equation 11 (curve I) and Equation 29 (curve II) as a function of 1/T, and Figure 29 represents Equation 11 (solid line) and Equation 29 (dashed line) plotted as a function of T. Aside from the physical meaning that may be attached to the constants A and B, Equation 11 is able to account for the existence of curvature in the plot of $\ln (P'/P)$ vs 1/T, Figure 28.

The ratio of A to A' is 145, while the ratio of B to B' is 137. Therefore, the functional form of Equation 29 can be thought of as a variation of Equation 11 in which A/T_{av} is set equal to a constant A' and B/T_{av} is set equal to B'. However, there is little difference between the line given by Equations 11 and 31 and the one represented by Equations 29 and 32, as seen in Figure 28.

Bigeleisen, Cragg, and Jeevanandam[12] reported that, for the $^{13}C/^{12}C$ sffect in liquid methane, A = 93.8 $\pm$ 6.1 and B = 0.535 $\pm$ 0.06, according to Equation 11. The value of A = 217 $\pm$ 66 for $^{13}CHF_3/^{12}CHF_3$ is considerably greater than A = 93.8 $\pm$ 6.1 for $^{13}CH_4/^{12}CH_4$. This must be due to the larger intermolecular forces in the polar CHF_3 liquid.

In order to further investigate the intermolecular forces in the liquid CHF_3, a cell-model calculation has been performed to reproduce the observed vapor pressure isotope effect in $^{13}CHF_3/^{12}CHF_3$ within the framework of the Bigeleisen-Stern-Van Hook-Wolfsberg theory. The result is presented in the next section, Section IV-2.

FIGURE 29. $\epsilon = \ln\left[P\left(^{12}CHF_3\right)\middle/P\left(^{13}CHF_3\right)\right]$ vs TEMPERATURE
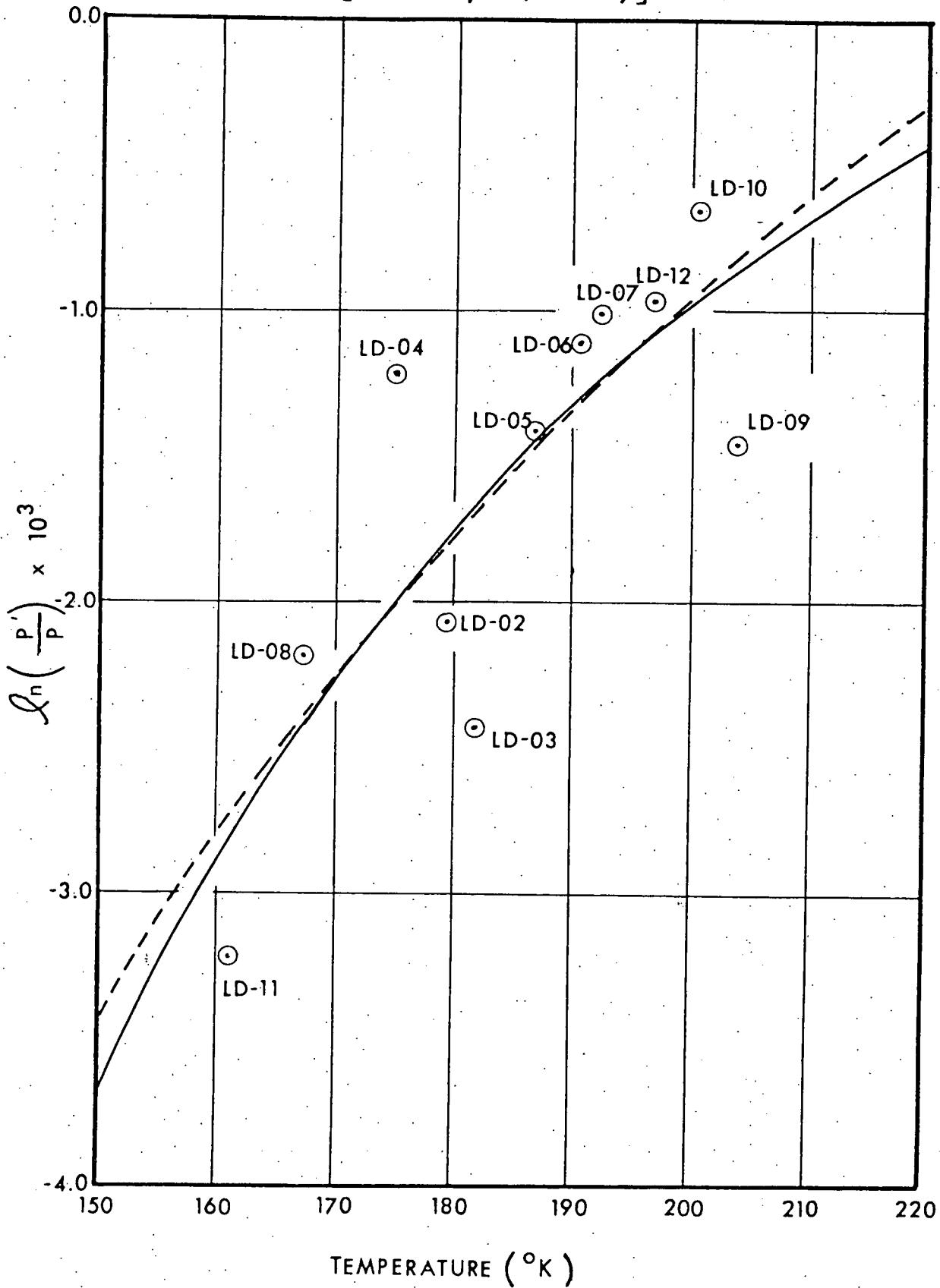
IV-2. Cell Model Calculations

The utility of the cell model lies in the fact that, under the harmonic force field assumptions, all degrees of freedom of a liquid molecule can be treated by the standard method of normal coordinate analysis. Wilson's $\underset{\sim}{F}\ \underset{\sim}{G}$ matrix method[29] provides a mathematical procedure necessary for such molecular vibration problems. In this section, this $\underset{\sim}{F}\ \underset{\sim}{G}$ matrix method and its application to high speed computer programming originally developed by Schachtschneider and Snyder[31] will first be described. The application of the method to the present problem of gaseous and liquid trifluoromethane for the purpose of fitting the $\underset{\sim}{F}$ matices to observed vapor pressure isotope effect as well as the internal frequencies will be presented in the latter subsections.

A) Wilson's $\underset{\sim}{F}\ \underset{\sim}{G}$ Matrix Method

Wilson's $\underset{\sim}{F}\ \underset{\sim}{G}$ matrix method is based on classical mechanics. If $(q_1,\ q_2,\ \cdots\ q_f)$ is a complete set of f coordinates, where f is the degree of freedom of a molecular system (f may be 3N, 3N-5, or 3N-6), the potential energy V can be expressed in the form of an f-dimensional Taylor expansion:

$$V = V_o + \sum_{i=1}^{f}\left(\frac{\partial V}{\partial q_i}\right)_c q_i + \frac{1}{2}\sum_{i=1}^{f}\sum_{j=1}^{f}\left(\frac{\partial^2 V}{\partial q_i \partial q_j}\right)_o q_i q_j$$

$$+ \text{(higher terms)}, \tag{33}$$

where the subscript "o" refers to the value of the appropriate function at the origin. In isotope effect studies, the origin is chosen to be at the minimum of the potential function. Then, $V_o = 0$ and $\left(\frac{\partial V}{\partial q_i}\right)_o = 0$ for all i. In the harmonic approximation, the "(higher terms)" of Equation 33 vanish. Thus

$$2V = \sum_{i=1}^{f}\sum_{j=1}^{f}\left(\frac{\partial^2 V}{\partial q_i \partial q_j}\right)_o q_i q_j \tag{34}$$

or

$$2V = \sum_{i=1}^{f}\sum_{j=1}^{f} f_{ij} q_i q_j \tag{35}$$

where

$$f_{ij} \equiv \left(\frac{\partial^2 V}{\partial q_i \partial q_j}\right)_o \tag{36}$$

The kinetic energy T in cartesian coordinates is

$$2T = \sum_{i=1}^{3N} m_i \dot{q}_i{}^{c^2} \tag{37}$$

where m_i is the atomic mass associated with the i-th cartesian coordinate $q_i{}^c$. If the coordinate transformation between this coordinate and a system of internal coordinates q_i is given by

$$q_i{}^c = \sum_{j=1} a_{ij} q_j , \tag{38}$$

then the expression for the kinetic energy in the new coordinate system will become

$$2T = \sum_{i=1}^{3N} m_i \left(\sum_i a_{ij} \dot{q}_j \right)^2$$

$$= \sum_{i=1}^{3N} \sum_i \sum_k m_i a_{ij} a_{ik} \dot{q}_j \dot{q}_k$$

$$= \sum_i \sum_k \left(\sum_{i=1}^{3N} m_i a_{ij} a_{ik} \right) \dot{q}_j \dot{q}_k$$

$$= \sum_i \sum_k g_{jk}^{-1} \dot{q}_j \dot{q}_k \quad ,$$

or

$$2T = \sum_{i=1}^{f} \sum_{j=1}^{f} g_{ij}^{-1} \dot{q}_i \dot{q}_j \quad , \tag{39}$$

where

$$g_{ij}^{-1} = \sum_{i=1}^{3N} m_i a_{ij} a_{ik} \quad , \tag{40}$$

and g_{ij}^{-1} is the (ij) element of Wilson's kinetic energy matrix, $\underset{\sim}{G}^{-1}$.

Application of the Lagrangian equation of motion,

$$\frac{d}{dt} \left(\frac{\partial T}{\partial \dot{q}_i} \right) + \left(\frac{\partial V}{\partial q_i} \right) = 0 \quad , \tag{41}$$

to the present problem leads to

$$\sum_{j=1}^{f} g_{ij}^{-1} \ddot{q}_j + \sum_{j=1}^{f} f_{ij} q_j = 0 \quad . \tag{42}$$

Since of interest is a set of solutions of q_i of Equation 42 in a particular form in which every part of the molecule oscillates in unison, the following is substituted:

$$q_j = A_j \sin 2\pi\nu t, \quad [\; j = 1,2,\ldots,f \;] \tag{43}$$

into Equation 42, which then becomes

$$\sum_{j=1}^{f} (f_{ij} - \lambda g_{ij}^{-1}) A_j = 0 \quad [i = 1,2,\ldots f] \tag{44}$$

where

$$\lambda = 4\pi^2 \nu^2 = 4\pi^2 c^2 \omega^2 \qquad (45)$$

The non-trivial solution of the simultaneous linear Equations 44 exist if and only if the following secular equation is satisfied:

$$\left| \underset{\sim}{F} - \lambda \underset{\sim}{G}^{-1} \right| = 0 , \qquad (46)$$

where

$$
\underset{\sim}{F} \equiv
\begin{vmatrix}
f_{11} & f_{12} & \cdot & \cdot & \cdot & f_{1f} \\
f_{21} & f_{22} & \cdot & \cdot & \cdot & f_{2f} \\
\cdot & \cdot & \cdot & \cdot & \cdot & \cdot \\
\cdot & \cdot & \cdot & \cdot & \cdot & \cdot \\
\cdot & \cdot & \cdot & \cdot & \cdot & \cdot \\
f_{f1} & f_{f2} & \cdot & \cdot & \cdot & f_{ff}
\end{vmatrix}
\qquad (47)
$$

and

$$
\underset{\sim}{G}^{-1} \equiv
\begin{vmatrix}
g_{11}^{-1} & g_{12}^{-1} & \cdot & \cdot & \cdot & g_{1f}^{-1} \\
g_{21}^{-1} & g_{22}^{-1} & \cdot & \cdot & \cdot & g_{2f}^{-1} \\
\cdot & \cdot & \cdot & \cdot & \cdot & \cdot \\
\cdot & \cdot & \cdot & \cdot & \cdot & \cdot \\
\cdot & \cdot & \cdot & \cdot & \cdot & \cdot \\
g_{f1}^{-1} & g_{f2}^{-1} & \cdot & \cdot & \cdot & g_{ff}^{-1}
\end{vmatrix}
\qquad (48)
$$

The force constant matrix $\underset{\sim}{F}$ can be defined for a gas molecule with $f = 3N-6$ or $3N-5$ and for a liquid molecule with $f = 3N$. The present purpose is to find such $\underset{\sim}{F}$ matrices which best reproduce the observed vapor pressure isotope effect as well as the spectroscopically observed internal

frequencies. The kinetic energy matrix $\underset{\sim}{G}^{-1}$ is fixed as soon as the molecular geometry and the atomic masses are known. The secular Equation 46 can be alternately solved by solving either

$$\left| \underset{\sim}{F} \underset{\sim}{G} - \lambda \underset{\sim}{I} \right| = 0 , \qquad (49)$$

or

$$\left| \underset{\sim}{G} \underset{\sim}{F} - \lambda \underset{\sim}{I} \right| = 0 . \qquad (50)$$

B) The Schachtschneider and Snyder Program

The Schachtschneider and Snyder program consists of two parts. The first part calculates the $\underset{\sim}{G}$ matrix for every isotopic molecule, given the molecular geometry and the atomic masses. The second part solves the secular equation after reading in the $\underset{\sim}{G}$ matrix calculated in the first part, as well as an $\underset{\sim}{F}$ matrix. The Ishida-Bigeleisen modification of the second part also calculates the vapor pressure isotope effects and several contributions to it at various temperatures.[32] All calculations were performed through the use of an IBM 370/168 computer at the City University of New York/University Computer Center. Communication with the CUNY/UCC was effected through the use of CRT terminals, and the printouts were produced at the Brooklyn College School of Science Data Acquisition Facility.

C) F Matrix for Gaseous Trifluoromethane

Previously published results on the observed and calculated frequencies for gaseous trifluoromethane are outlined in Table XVII. For the present study, the $\underset{\sim}{F}$ matrix of Long, Gravenor, and Jones[33] was chosen as the basis of the normal coordinate analysis for the gaseous molecule. Tables XVIII, XIX, and XX summarize the definition of the internal coordinates, the definition of the symmetry coordinates, and the gaseous $\underset{\sim}{F}$ matrix obtained by Long et al respectively. Figure 30 schematically represents the definition of the internal coordinates. In this figure, atom 4 is in the yz-plane. The frequencies calculated in the present study by using these coordinate definitions and this $\underset{\sim}{F}$ matrix along with the international mass scale based on ^{12}C (i.e., C = 12.000000 amu, H = 1.007825 amu, D = 2.014000 amu, F = 18.998400 amu, and ^{13}C = 13.003335 amu) are tabulated in Table XXI. There is a noticeable disagreement between the frequencies calculated in this study and those of Long et al. A modification of the $\underset{\sim}{F}$ matrix of Long et al was performed by first calculating the differential effects on frequencies of each symmetry $\underset{\sim}{F}$ matrix element. These effects, $\partial\omega_k/\partial \underset{\sim}{F}_{ij}$, are summarized in Table XXII. The final $\underset{\sim}{F}$ matrix and the corresponding gaseous frequencies are tabulated in Tables XXIII and XXIV respectively. Table XXIV shows a significant improvement in the agreement between the calculated and observed gaseous frequencies.

TABLE XVII. Gaseous Freqencies (in cm^{-1}) Observed and Calculated for Trifluoromethane

Molecule	Frequency number	Long [33]		Galasso [34]		D'Cunha [35]	
		obs.	calc.	obs.	calc.	obs.	calc.
CHF_3	ω_1	3035	3036	3031	3030.5	3031	3034.4
	ω_2	1137	1138	1140	1146.4	1140	1141.3
	ω_3	700	702	700	700.8	700	700.7
	ω_4	1376	1379	1372	1379.3	1372	1375.5
	ω_5	1152	1156	1152	1158.3	1152	1155.2
	ω_6	508	508	507	505.4	507	508.4
CDF_3	ω_1	2257	2256	2273	2274.0	2257	2254.5
	ω_2	1110	1110	1109	1103.0	1109	1107.7
	ω_3	693	691	693	691.7	693	692.3
	ω_4	1210	1207	1207	1200.1	1207	1203.2
	ω_5	977	971	974	968.8	974	971.8
	ω_6	502	502	504	505.4	504	502.6

TABLE XVIII. Definition of Internal Coordinates [a]

Coordinate number	Definition
1	C-H stretch
2	C-F stretch
3	C-F stretch
4	C-F stretch
5	H-C-F bend[b]
6	H-C-F bend[b]
7	H-C-F bend[b]
8	F-C-F bend[b]
9	F-C-F bend[b]
10	F-C-F bend[b]

Atom	X Coordinate	Y Coordinate	Z Coordinate
C	0.000000	0.000000	0.000000
H	0.000000	0.000000	1.098000
F_2	1.083050	0.625299	-0.458505
F_3	-1.083050	0.625299	-0.458505
F_4	0.000000	-1.250599	-0.458505

(a) Refer to Figure 30 for the schematic diagram of internal coordinates.

(b) Weighted by the C-F bond length, 1.322 Å.

<u>TABLE XIX. Definition of Symmetry Coordinates</u> [a]

$$S_1 = D$$

$$S_2 = \frac{1}{\sqrt{3}}\, (\, d_2 + d_3 + d_4\,)$$

$$S_3 = \frac{1}{\sqrt{6}}\, (\, \beta_{23} + \beta_{34} + \beta_{24} - \alpha_{12} - \alpha_{13} - \alpha_{14}\,)$$

$$S_4 = \frac{1}{\sqrt{6}}\, (\, 2d_2 - d_3 - d_4\,)$$

$$S_5 = \frac{1}{\sqrt{6}}\, (\, 2\alpha_{12} - \alpha_{13} - \alpha_{14}\,)$$

$$S_6 = \frac{1}{\sqrt{6}}\, (\, 2\beta_{34} - \beta_{23} - \beta_{24}\,)$$

$$S_7 = \frac{1}{\sqrt{2}}\, (\, d_3 - d_4\,)$$

$$S_8 = \frac{1}{\sqrt{2}}\, (\, \alpha_{13} - \alpha_{14}\,)$$

$$S_9 = \frac{1}{\sqrt{2}}\, (\, \beta_{24} - \beta_{23}\,)$$

(a) Refer to Figure 30 for schematic diagram of internal

coordinates.

TABLE XX. F Matrix for Gaseous Trifluoromethane by Long [33]

Coordinate	F Matrix Element (mdyne/$\overset{\circ}{A}$)
F_{11}	5.00
F_{12}	2.03
F_{13}	0.41
F_{22}	7.70
F_{23}	0.44
F_{33}	1.14
F_{44}	5.29
F_{45}	0.43
F_{46}	-0.43
F_{55}	0.46
F_{56}	-0.09
F_{66}	0.82

$R_{C-H} = 1.098 \; \overset{\circ}{A}$

$R_{C-F} = 1.332 \; \overset{\circ}{A}$

$\angle_{H-C-F} = 110°\,08'$

$\angle_{F-C-F} = 108°\,48'$
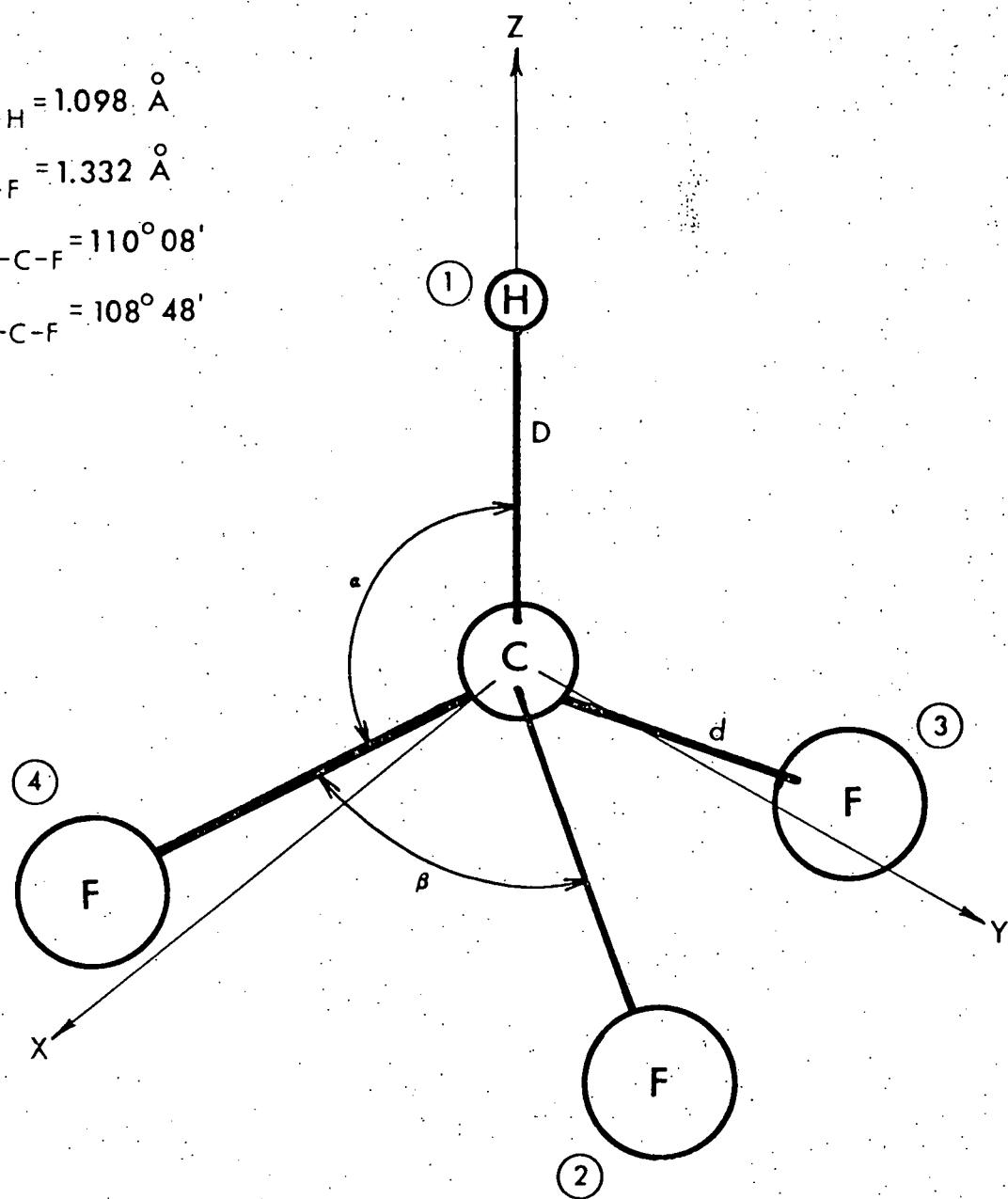
FIGURE 30. INTERNAL COORDINATES FOR TRIFLUOROMETHANE

TABLE XXI. Calculated Frequencies from F Matrix of Long [33]

Molecule	Frequency number	Frequency(cm^{-1})
CHF_3	ω_1	3036.4
	ω_2	1154.7
	ω_3	702.1
	ω_4	1390.3
	ω_5	1150.9
	ω_6	503.1
CDF_3	ω_1	2257.1
	ω_2	1124.8
	ω_3	690.8
	ω_4	1207.4
	ω_5	974.9
	ω_6	497.7

TABLE XXII. Differential Effects of Symmetry Coordinate F Matrix Elements

$$\frac{\partial \omega_k}{\partial F_{ij}} \quad (\text{cm}^{-1} \cdot \text{mdyn}^{-1} \cdot \text{Å})$$

Molecule	Frequency number	F_{11}	F_{12}	F_{13}	F_{22}	F_{23}	F_{33}	F_{44}	F_{45}	F_{46}	F_{55}	F_{56}	F_{66}
CHF_3	ω_1	298	-19	122	0	-4	12	0	0	0	0	0	0
	ω_2	0	-5	12	45	-233	294	0	0	0	0	0	0
	ω_3	11	-33	-78	24	115	135	0	0	0	0	0	0
	ω_4	0	0	0	0	0	0	12	-268	37	1524	-403	28
	ω_5	0	0	0	0	0	0	104	63	208	11	64	105
	ω_6	0	0	0	0	0	0	3	-22	-59	37	194	266
CDF_3	ω_1	214	-30	180	1	-13	38	0	0	0	0	0	0
	ω_2	1	7	-15	47	-221	257	0	0	0	0	0	0
	ω_3	14	-33	-87	22	112	145	0	0	0	0	0	0
	ω_4	0	0	0	0	0	0	100	-418	230	448	-479	139
	ω_5	0	0	0	0	0	0	17	211	11	678	73	2
	ω_6	0	0	0	0	0	0	3	-26	-56	55	236	263

TABLE XXIII. F Matrix of Gaseous Trifluoromethane in

Symmetry and Internal Coordinates

Symmetry Coordinates		Internal Coordinates	
Coord.	F Matrix Element (mdyne/Å)	Coord. [a]	F Matrix Element (mdyne/Å)
F_{11}	5.000000	f_D	5.000000
F_{12}	2.030000	f_d	6.017878
F_{13}	0.410000	f_{dD}	1.172021
F_{22}	7.517634	f_{dd}	0.749878
F_{23}	0.476755	$f_{D\alpha}$	-0.167382
F_{33}	1.140000	$f_{D\beta}$	0.167382
F_{44}	5.268000	f_{α}	0.491320
F_{45}	0.460000	$f_{\alpha\alpha}$	0.039340
F_{46}	-0.430983	f_{β}	0.764617
F_{55}	0.455380	$f_{\beta\beta}$	-0.097309
F_{56}	-0.115000	$f_{d\alpha}$ [b]	0.194294
F_{66}	0.861926	$f_{d\alpha}$' [c]	-0.265706
		$f_{d\beta}$ [b]	0.256033
		$f_{d\beta}$' [c]	-0.180848
		$f_{\alpha\beta}$ [d]	-0.151667
		$f_{\alpha\beta}$' [e]	-0.266667

(a) Refer to Figure 30

(b) Non-prime refers to the bond length adjacent to bond angle

(c) Prime refers to the bond length opposite to the bond angle

(d) Non-prime refers to the bond angle adjacent to bond angle

(e) Prime refers to the bond angle opposite to bond angle

TABLE XXIV. Final Calculated Gaseous Frequencies

Molecule	Frequency number	Frequency(cm^{-1})
CHF_3	ω_1	3036.2
	ω_2	1138.9
	ω_3	701.4
	ω_4	1381.0
	ω_5	1151.8
	ω_6	507.7
CDF_3	ω_1	2256.5
	ω_2	1109.2
	ω_3	690.4
	ω_4	1205.4
	ω_5	973.7
	ω_6	500.7

D) $\underset{\sim}{F}$ Matrix for Liquid Trifluoromethane

As mentioned previously, the external vibrations of a liquid molecule are treated by the cell model as weak harmonic oscillations. They consist of three translational and three rotational motions. The Schächtschneider and Snyder $\underset{\sim}{G}$ matrix program, after calculations of the internal G matrix, computes the center of mass and the three principal axes of the molecule. Furthermore, it calculates the $\underset{\sim}{G}$ matrix elements involving the external motions and the g_{ij}'s representing the interactions between the external and internal motions. Based on the experimental data on the interatomic distances and the atomic bond angles, as shown in Figure 30, the principal moments of inertia, in the units of mdyne per Angstrom per atom mass unit, for $^{12}CHF_3$ are

$$I_A = 89.140306$$

and

$$I_B = I_C = 48.820360$$

The fundamental frequencies of liquid trifluoromethane have been observed, as summarized in Table XXV, but there has been no published liquid $\underset{\sim}{F}$ matrix.

Towards the determination of the liquid $\underset{\sim}{F}$ matrix, the gaseous F matrix was first modified to roughly reproduce the observed liquid frequencies. After a series of calculations of the effects of the diagonal elements for the translational and rotational motions, several sets of

TABLE XXV. Liquid Frequencies Observed for Trifluoromethane

Frequency number	Glockler [36] Frequency(cm^{-1})	Rank [37] Frequency(cm^{-1})
ω_1	3062	3062
ω_2	1117	1117
ω_3	697	697
ω_4	1376	1376
ω_5	——	1160
ω_6	508	508

these diagonal external force constants, f_{tr} and f_{rot}, were chosen, and the effects of the various internal-external interaction force constants for each set of f_{tr} and f_{rot} selected were studied. This determined the set of external diagonals and internal-external interaction elements of the liquid $\underset{\sim}{F}$ matrix that best reproduced the vapor pressure isotope effect observed in the experimental part of the present study. A final adjustment to the internal part, $\underset{\sim}{F}_{ii}$, was then made to finally adjust the liquid internal frequencies to the observed frequencies.

As a first step, the gaseous $\underset{\sim}{F}$ matrix was modified to roughly reproduce the observed liquid frequencies tabulated in Table XXV. For this purpose, certain values for the diagonal elements for the translational and rotational motions had to be chosen, but the effects of any reasonable changes in these external force constants on the internal frequencies were found to be negligible. The tentative $\underset{\sim}{F}_{ii}$ matrix obtained by using $f_{tr} = 0.300000$ mdyn/$\overset{\circ}{A}$ and $f_{rot} = 0.050000$ mdyn-$\overset{\circ}{A}$ is tabulated in Table XXVI. This is the $\underset{\sim}{F}_{ii}$ used in the subsequent $\underset{\sim}{F}_{liq}$ adjustment procedures, until the last step mentioned in above outline.

The next step was a study of the effects of f_{tr} and f_{rot} on the $^{13}C/^{12}C$ isotope effect in trifluoromethane. During this stage of the study, that part of of the $\underset{\sim}{F}_{liq}$

TABLE XXVI. Internal Part of the Tentative Liquid $\underset{\sim}{F}$ Matrix

for Trifluoromethane

Coordinate[a]	$\underset{\sim}{F}$ Matrix Element (mdyn/$\overset{o}{A}$)
f_D	4.820698
f_d	6.247256
f_{dD}	0.900410
f_{dd}	0.498351
$f_{D\alpha}$	-0.310438
$f_{D\beta}$	0.310438
f_α	0.489509
$f_{\alpha\alpha}$	0.041347
f_β	0.765351
$f_{\beta\beta}$	-0.096575
$f_{d\alpha}$[b]	0.194294
$f_{d\alpha}$,[c]	-0.265706
$f_{d\beta}$[b]	0.256033
$f_{d\beta}$,[c]	-0.180848
$f_{\alpha\beta}$[d]	-0.125241
$f_{\alpha\beta}$,[e]	-0.240241

(a) Refer to Figure 30

(b) Non-prime refers to the bond lenfth adjacent to bond angle

(c) Prime refers to the bond length opposite to bond angle

(d) Non-prime refers to the bond angle adjacent to bond angle

(e) Prime refers to the bond angle opposite to bond angle

matrix representing the internal-external interaction, F_{ie}, was set to be a null matrix. The diagonal translational element was varied between 0.01000 and 3.000000 mdyn/$\overset{\circ}{A}$, and the three equal rotational elements were varied between 0.001000 and 3.000000 mdyn-$\overset{\circ}{A}$, representing unrealistically high and low values for external forces. Table XXVII summarizes the results of these studies. Table XXVII shows the magnitude and slope of $\ln(P'/P)$ based on these F_{liq} matrices and the F_{gas} matrix of Table XXIII. It is obvious that the F_{liq} matrix in the absence of force constant elements representing interactions between internal and external motions cannot predict the observed inverse vapor pressure isotope effect and the observed positive slope of the plot of $\ln(P'/P)$ versus temperature. As will become obvious in the latterpart of this subsection when possible effects of some significant changes in F_{ii} will be discussed, this conclusion on the importance of F_{ie} remains unalterable.

In the next series of studies, the internal-external interaction force constants were included. A symmetry consideration indicated that the translational motion in the direction of the C-H axis, T_z, interacts significantly with the C-H stretch, C-F stretches, H-C-F bends, and F-C-F bends. Accordingly, the differential effects of variations in the F matrix elements representing these internal-external interactions on $\ln(P'/P)$ were calculated. The results obtained, using $f_{tr} = 0.300000$ mdyn/$\overset{\circ}{A}$ and

TABLE XXVII. Effects of the Translational and Rotational

Force Constants on the $^{13}C/^{12}C$ Vapor Pressure Isotope Effect

in Trifluoromethane

f_{tr} (mdyn/$\overset{\circ}{A}$)	f_{rot} (mdyn-$\overset{\circ}{A}$)	$\ln (P'/P)$ [a]		
		@ T_1	@ T_2	Δ
0.01	0.001	0.011807	0.009386	-0.002421
0.01	0.01	0.011812	0.009389	-0.002423
0.01	0.1	0.011864	0.009421	-0.002443
0.01	1.0	0.012360	0.009733	-0.002627
0.01	3.0	0.013340	0.010374	-0.002966
0.1	0.001	0.012103	0.009569	-0.002534
0.1	0.01	0.012108	0.009572	-0.002536
0.1	0.1	0.012160	0.009604	-0.002556
0.1	1.0	0.012657	0.009916	-0.002741
0.1	3.0	0.013637	0.010557	-0.003080
1.0	0.001	0.014979	0.011365	-0.003614
1.0	0.01	0.014984	0.011369	-0.003615
1.0	0.1	0.015036	0.011401	-0.003635
1.0	1.0	0.015533	0.011712	-0.003823
1.0	3.0	0.016514	0.012354	-0.004160
3.0	0.001	0.020851	0.015146	-0.005705
3.0	0.01	0.020856	0.015150	-0.005706
3.0	0.1	0.020908	0.015181	-0.005717
3.0	1.0	0.021405	0.015493	-0.006012
3.0	3.0	0.022386	0.016135	-0.006251

(a) T_1 = 161.1° K and T_2 = 204.6° K, corresponding to the lowest and highest temperatures respectively at which the distillation study was performed. Δ is the difference of $\ln (P'/P)_{@T_2}$ minus $\ln (P'/P)_{@T_1}$.

f_{rot} = 0.100000 mdyn-$\overset{\circ}{A}$, are tabulated in Table XXVIII.
Ohter choices of F_{tr} and f_{rot} yielded almost identical
differential effects as those summarized in Table XXVIII,
although the general magnitude of $\ln$ (P'/P), in the
absence of $\underset{\sim}{F}_{ie}$, was strongly dependent on the choice of
these external diagonal elements. In all cases, an
increase in the slope of the plot of $\ln$ (P'/P) versus
temperature is accompanied by a shift toward a larger
inverse vapor pressure isotope effect. Using these
differential parameters, The following, which best fit
the experimantal vapor pressure isotope effect data, were
obtained:

$$f(T_z,C-H) \quad = \quad -0.840000 \text{ mdyn/}\overset{\circ}{A}$$

$$f(T_z,C-F) \quad = \quad 0.840000 \text{ mdyn/}\overset{\circ}{A}$$

$$f(T_z,H-C-F) \quad = \quad 0.300000 \text{ mdyn/}\overset{\circ}{A}$$

$$F(T_z,F-C-F) \quad = \quad -0.300000 \text{ mdyn/}\overset{\circ}{A}$$

The introduction of these non-vanishing internal-
external interaction force constants, however, shifted the
internal frequencies to a slight degree. Therefore, a
slight modification in the $\underset{\sim}{F}_{ii}$ was necessitated. The
final $\underset{\sim}{F}$ matrix thus obtained is presented in Table XXIX.
The liquid internal frequencies that the $\underset{\sim}{F}_{liq}$ matrix
predicts are tabulated in Table XXX. These frequencies
should be compared with the experimental values listed in
Table XXV. In Figure 31, the vapor pressure isotope effect
calculated (solid line) by using this $\underset{\sim}{F}_{liq}$ matrix and the
$\underset{\sim}{F}_{gas}$ matrix of Table XXIII in conjunction with the exact

TABLE XXVIII. Differential Effects of Internal-External Interaction Force Constants

Involving T_z : f_{tr} = 0.3 mdyn/Å, f_{rot} = 0.1 mdyn-Å[a]

$\underset{\sim}{F}_{ie}$ Elements[d]				$\ln (P'/P)$				
$f(T_z,CH)$	$f(T_z,CF)$	$f(T_z,HCF)$	$f(T_z,FCF)$	@ T_1[b]	@ T_2[b]	Δ[b]	Δ_1[c]	Δ_2[c]
0	0	0	0	0.012813	0.010009	-0.002804	———	———
0.01	0	0	0	0.012824	0.010018	-0.002806	0.000011	0.000009
0	0.01	0	0	0.012760	0.009969	-0.002791	-0.000053	-0.000040
0	0	0.01	0	0.012640	0.009883	-0.002757	-0.000173	-0.000126
0	0	0	0.01	0.012991	0.010137	-0.002854	0.000178	0.000128

(a) For $\underset{\sim}{F}_{ii}$, see Table XXVI

(b) $T_1 = 161.1^{\circ}$ K and $T_2 = 204.6^{\circ}$ K, corresponding to the lowest and highest temperatures respectively at which the distillation study was performed. Δ is the difference of $\ln (P'/P)_{T_2}$ minus $\ln (P'/P)_{T_1}$.

(c) $\Delta_1 = \left[\ln (P'/P)_{T_1} \text{ with } f_{ie} = 0.01 \right] - \left[\ln (P'/P)_{T_1} \text{ with } \underset{\sim}{F}_{ie} = \underset{\sim}{0} \right]$

$\Delta_2 = \left[\ln (P'/P)_{T_2} \text{ with } f_{ie} = 0.01 \right] - \left[\ln (P'/P)_{T_2} \text{ with } \underset{\sim}{F}_{ie} = \underset{\sim}{0} \right]$

(d) In units of mdyn/Å.

TABLE XXIX.   Liquid and Gaseous F Matrix for Trifluoromethane

Force Constants	F Matrix Elements[a]	
	Gas	Liquid
Internal		
Diagonal		
C-H stretch	5.000000	4.814698
C-F stretch	6.017878	6.206256
H-C-F bend	0.491320	0.489509
F-C-F bend	0.764617	0.765351
Interaction		
C-H str x C-F str	1.172021	0.859410
C-F str x C-F str	0.749878	0.474351
C-H str x H-C-F bend	-0.167382	-0.310438
C-H str x F-C-F bend	0.167382	0.310438
C-F str x adj H-C-F bend	0.194294	0.194294
C-F str x opp H-C-F bend	-0.265706	-0.265706
C-F str x adj F-C-F bend	0.256033	0.256033
C-F str x opp F-C-F bend	-0.180848	-0.180848
H-C-F bend x H-C-F bend	0.039340	0.041347
F-C-F bend x F-C-F bend	-0.097309	-0.096575
H-C-F bend x adj F-C-F bend	-0.151667	-0.125241
H-C-F bend x opp F-C-F bend	-0.266667	-0.240241
External		
Diagonal		
Translation	———	0.300000
Rotation	———	0.100000[b]
Internal-External Interaction		
C-H str x T_z	———	-0.840000
C-F str x T_z	———	0.840000
H-C-F bend x T_z	———	0.300000
F-C-F bend x T_z	———	-0.300000

(a) Unless otherwise noted, in units of mdyn/Å.

(b) In units of mdyn-Å.

TABLE XXX. Liquid Frequencies Calculated from $\underline{F}$ Matrix of Table XXIX

| Frequency number	$^{12}CHF_3$ Frequency (cm^{-1})	$^{13}CHF_3$ Frequency (cm^{-1})
ω_1	3062.4	3046.3
ω_2	1116.7	1097.0
ω_3	697.0	692.9
ω_4	1376.1	1366.6
ω_5	1159.9	1133.6
ω_6	507.8	506.8
ω_{tr}	125.8	124.4
ω_{tr}	85.3	84.7
ω_{tr}	85.3	84.7
ω_{rot}	59.0	58.9
ω_{rot}	59.0	58.9
ω_{rot}	43.6	43.6

FIGURE 31. CELL MODEL VAPOR PRESSURE ISOTOPE EFFECT IN CHF_3

Bigeleisen formulae, Equations 3 and 5 is compared with the experimental values of $\ln (P'/P)$. According to Equations 12 and 13, the $F_{\sim liq}$ matrix of Table XXIX yields the following values of A and B, the coefficients appearing in Bigeleisen's two term approximation for $\ln (P'/P)$, Equation 11: A = 19.25, B = 1.31. Agreement btween these calculated values fo A and B and those obtained by the least-squares fit of the experimental vapor pressure data to the two term equation is apparently poor. This point will be discussed again at the end of this subsection. The effect of a 10% decrease in f_{tr} has also been plotted (dashed line) in Figure 31. A 10% change in f_{rot} is too insignificant to appear in the plot at that same scale.

Differential effects of other force constant elements in $F_{\sim ie}$ are similar to those interactions involving the T_z coordinate. Some examples in support of this observation are presented in Tables XXXI, XXXII, and XXXIII. The final $F_{\sim liq}$ matrix was chosen not to include these other internal-external interaction force constant elements. The interactions between any two external motions, i.e., translation-translation, rotation-rotation, or translation-rotation, have been found to have differential effect values an order of magnitude smaller than those of the internal-external interactions. Therefore, the external-external interactions have not been included in the final result.

It is noted in Table XXIX for the final $F_{\sim liq}$, that

TABLE XXXI. Differential Effects of Internal-External Interaction Force Constants

Involving T_x, R_x and R_y : $f_{tr} = 0.3$, $f_{rot} = 0.1$ [a]

$\underset{\sim}{F}_{ie}$ Elements[b,c]	@ T_1 [d]	@ T_2 [d]	Δ [d]	Δ_1 [e]	Δ_2 [e]
		$\ell n\ (P'/P)$			
$f_{13,5} = 0.1$; $f_{13,6} = 0.1$; $f_{13,7} = 0.2$	0.012040	0.009431	-0.002804	-0.000773	-0.000578
$f_{13,8} = 0.2$; $f_{13,9} = 0.1$; $f_{13,10} = 0.1$	0.013620	0.010597	-0.003023	0.000807	0.000588
$f_{13.5} = 0.1$; $f_{14,6} = 0.1$; $f_{14,7} = 0.2$	0.013151	0.010271	-0.002880	0.000338	0.000262
$f_{16,5} = 0.1$; $f_{16,6} = 0.1$	0.012801	0.010001	-0.002800	-0.000012	-0.000008
All $f_{ie} = 0$	0.012813	0.010009	-0.002804	——	——

(a) For $\underset{\sim}{F}_{ii}$, see Table XXVI.

(b) In units of mdyn/Å.

(c) For coordinate definitions, see Table XVIII.

(d) $T_1 = 161.1^{\circ}$ K and $T_2 = 204.6^{\circ}$ K, corresponding to the lowest and highest temperatures respectively at which the distillation study was performed. Δ is the difference of $\ell n\ (P'/P)_{T_2}$ minus $\ell n\ (P'/P)_{T_1}$.

(e) $\Delta_1 = \left[\ell n\ (P'/P)_{T_1} \text{ with } f_{ie} = 0.1 \right] - \left[\ell n\ (P'/P)_{T_1} \text{ with } \underset{\sim}{F}_{ie} = \underset{\sim}{0} \right]$

$\Delta_2 = \left[\ell n\ (P'/P)_{T_2} \text{ with } f_{ie} = 0.1 \right] - \left[\ell n\ (P'/P)_{T_2} \text{ with } \underset{\sim}{F}_{ie} = \underset{\sim}{0} \right]$

TABLE XXXII. Differential Effects of Internal-External Interaction Force Constants

Involving T_x, R_x, and R_y : $f_{tr} = 0.3$, $f_{rot} = 0.05$ [a]

F_{ie} Elements [b,c]	ln (P'/P)				
	@ T_1 [d]	@ T_2 [d]	Δ [d]	Δ_1 [e]	Δ_2 [e]
$f_{13,5} = 0.1$; $f_{13,6} = 0.1$; $f_{13,7} = 0.2$	0.012011	0.009413	-0.002598	-0.000773	-0.000578
$f_{13,8} = 0.2$; $f_{13,9} = 0.1$; $f_{13,10} = 0.1$	0.013592	0.010579	-0.003013	0.000807	0.000588
$f_{14,5} = 0.1$; $f_{14,6} = 0.1$; $f_{14,7} = 0.2$	0.013123	0.010253	-0.002870	0.000338	0.000262
$f_{16,5} = 0.1$; $f_{16,6} = 0.1$	0.012772	0.009983	-0.002789	-0.000013	-0.000008
All $f_{ie} = 0$	0.012785	0.009991	-0.002794	——	——

(a) For F_{ii}, see Table XXVI.

(b) In units of mdyn/$\overset{\circ}{A}$.

(c) For coordinate definitions, see Table XVIII.

(d) $T_1 = 161.1^{\circ}$ K and $T_2 = 204.6^{\circ}$ K, corresponding to the lowest and highest temperatures respectively at which the distillation study was performed. Δ is the difference of ln $(P'/P)_{T_2}$ minus ln $(P'/P)_{T_1}$.

(e) $\Delta_1 = [$ln $(P'/P)_{T_1}$ with $f_{ie} = 0.1] - [$ln $(P'/P)_{T_1}$ with $F_{ie} = 0]$

$\Delta_2 = [$ln $(P'/P)_{T_2}$ with $f_{ie} = 0.1] - [$ln $(P'/P)_{T_2}$ with $F_{ie} = 0]$

TABLE XXXIII. Differential Effects of Internal-External Interaction Force Constants

Involving T_x, R_x, and R_y : $f_{tr} = 0.1$, $f_{rot} = 0.05$ [a]

$\underset{\sim}{F}_{ie}$ Elements [b,c]	ℓn (P'/P)				
	@ T_1 [d]	@ T_2 [d]	Δ [d]	Δ_1 [e]	Δ_2 [e]
$f_{13,5} = 0.1$; $f_{13,6} = 0.1$; $f_{13,7} = 0.2$	0.011355	0.009007	-0.002348	-0.000777	-0.000577
$f_{13,8} = 0.2$; $f_{13,9} = 0.1$; $f_{13,10} = 0.1$	0.012942	0.010176	-0.002766	0.000810	0.000590
$f_{14,5} = 0.1$; $f_{14,6} = 0.1$; $f_{14,7} = 0.2$	0.012470	0.009849	-0.002621	0.000338	0.000263
$f_{16,5} = 0.1$; $f_{16,6} = 0.1$	0.012119	0.009579	-0.002540	-0.000013	-0.000007
All $f_{ie} = 0$	0.012132	0.009586	-0.002546	————	————

(a) For $\underset{\sim}{F}_{ii}$, see Table XXVI.

(b) In Units of mdyn/$\overset{o}{A}$.

(c) For coordinate definitions, see Table XVIII.

(d) $T_1 = 161.1^o$ K and $T_2 = 204.6^o$ K, corresponding to the lowest and highest temperatures respectively at which the distillation study was performed. Δ is the difference of ℓn (P'/P)$_{T_2}$ minus ℓn (P'/P)$_{T_1}$.

(e) $\Delta_1 = [\ell n$ (P'/P)$_{T_1}$ with $f_{ie} = 0.1]$ $-$ $[\ell n$ (P'/P)$_{T_1}$ with $\underset{\sim}{F}_{ie} = \underset{\sim}{0}]$

$\Delta_2 = [\ell n$ (P'/P)$_{T_2}$ with $f_{ie} = 0.1]$ $-$ $[\ell n$ (P'/P)$_{T_2}$ with $\underset{\sim}{F}_{ie} = \underset{\sim}{0}]$

the C-H and the C-F stretching force constants for the liquid are 4.814698 mdyn/Å and 6.206256 mdyn/Å respectively, in contrast to the corresponding values for gaseous trifluoromethane of 5.000000 mdyn/Å and 6.017878 mdyn/Å respectively. While f_{C-H} decreased upon condensation, f_{C-F} increased. On the other hand, it can be noted that in Tables XVII and XXV the frequency for the C-H stretching mode (ω_1) increases from 3035 cm^{-1} to 3062 cm^{-1} upon condensation, while the frequencies involving the C-F stretching motions decrease upon condensation. The natural choice for f_{C-H} and f_{C-F}, therefore would involve an increase in the former and a decrease in the latter upon condensation. The $\underset{\sim}{F}_{liq}$ fitting process, similar to those to that described above, using an increased C-H stretching force constant, lead to another $\underset{\sim}{F}_{liq}$ matrix, tabulated as "$\underset{\sim}{F}_{liq}(I)$" in Table XXXIV. The vapor pressure isotope effect that this $\underset{\sim}{F}_{liq}$ yields (dashed line) is compared to the results obtained from the $\underset{\sim}{F}_{liq}$ of Table XXIX (solid line) in Figure 32. The increase in f_{C-H} upon condensation leads either to a) a too shallow slope when the magnitude of $\ln (P'/P)$ is comparable to those in the experimental data, or b) too large an inverse effect when the slope is comparable to that of the experimental data.

As a further alternative, the effects of an increase in both f_{C-H} and f_{C-F} have been investigated. Table XXXV summarizes the effects of f_{tr} and f_{rot} when $\underset{\sim}{F}_{ii}$ constructed from the internal elements listed uder "$\underset{\sim}{F}_{liq}(II)$" in Table

TABLE XXXIV. Trial Liquid F Matrices for Trifluoromethane

Force Constants	F Matrix Elements[a]	
	$F_{liq}(I)$	$F_{liq}(II)$
Internal		
Diagonal		
C-H str	5.069799	5.079799
C-F str	6.000442	6.070442
H-C-F bend	0.475929	0.475929
F-C-F bend	0.751771	0.751771
Interaction		
C-H str x C-F str	0.982035	1.070196
C-F str x C-F str	0.653696	0.723596
C-H str x H-C-F bend	-0.167382	-0.167382
C-H str x F-C-F bend	0.167382	0.167382
C-F str x adj H-C-F bend	0.194294	0.194294
C-F str x opp H-C-F bend	-0.265706	-0.265706
C-F str x adj F-C-F bend	0.256033	0.256033
C-F str x opp F-C-F bend	-0.180848	-0.180848
H-C-F bend x H-C-F bend	0.027767	0.027767
F-C-F bend x F-C-F bend	-0.110155	-0.110155
H-C-F bend x adj F-C-F bend	-0.138821	-0.138821
H-C-F bend x opp F-C-F bend	-0.253821	-0.253821
External		
Diagonal		
Translation	0.300000	0.300000
Rotation	0.050000[b]	0.050000[b]
Internal-External Interaction		
C-H str x T_z	-0.080000	-0.030000
C-F str x T_z	0.080000	0.030000
H-C-F bend x T_z	0.040000	0.010000
F-C-F bend x T_z	-0.040000	-0.010000

(a) Unless otherwise noted, in units of mdyn/$\overset{\circ}{A}$.

(b) In units of mdyn-$\overset{\circ}{A}$.
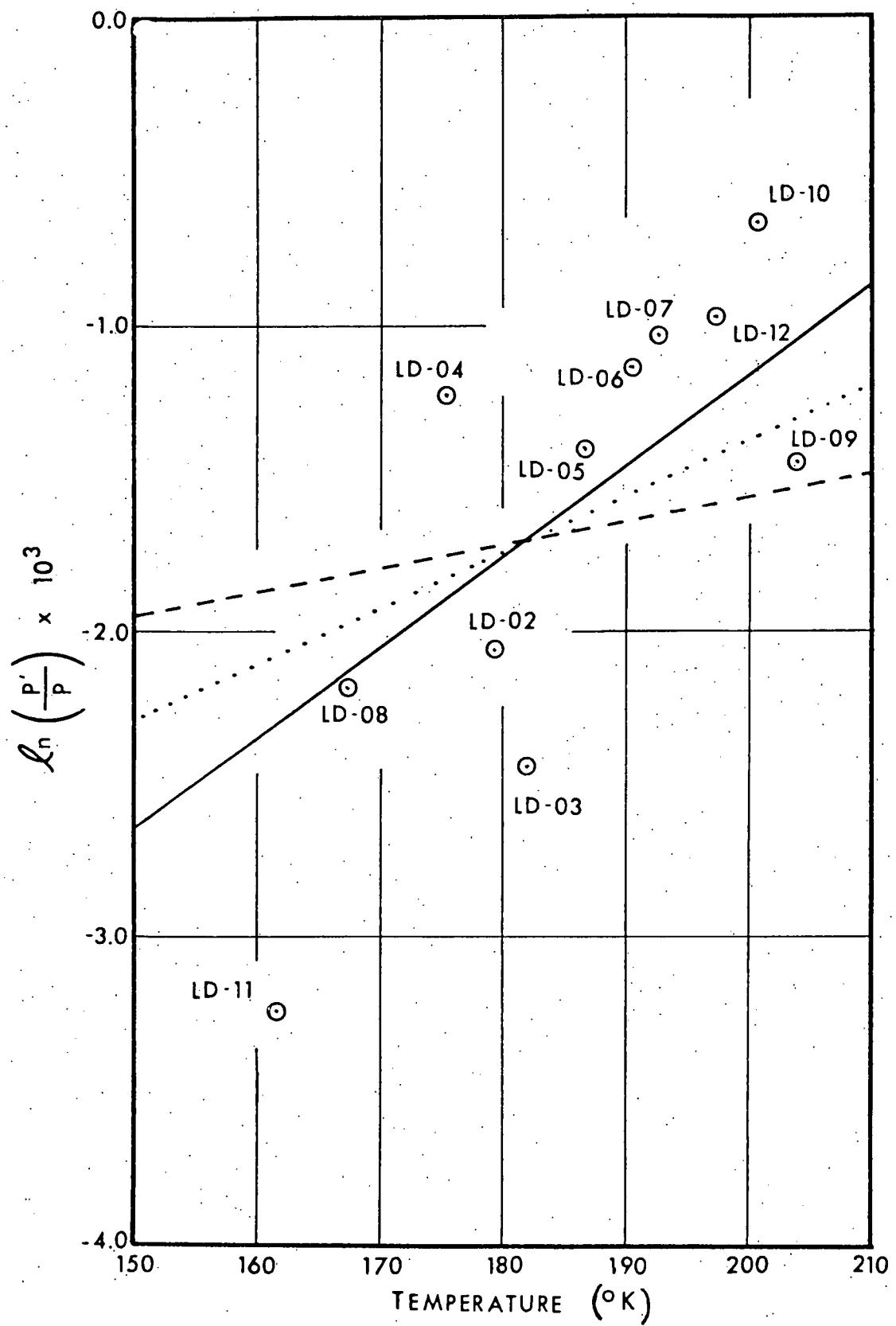
FIGURE 32. EFFECTS OF CHOICE OF $F_{\sim liq}$ ON $\ell_n\left(\frac{P'}{P}\right)$ IN CHF_3

TABLE XXXV. Effects of the Translational and Rotational
Force Constants on $\ln (P'/P)$ for Trial Liquid $\underline{F}$ Matrix

f_{tr} (mdyn/Å)	f_{rot} (mdyn-Å)	$\ln (P'/P)$ [a]		
		@ T_1	@ T_2	Δ
0.01	0.001	-0.001208	-0.000925	0.000283
0.01	0.01	-0.001203	-0.000922	0.000281
0.01	0.1	-0.001151	-0.000890	0.000261
0.01	1.0	-0.000655	-0.000578	0.000077
0.01	3.0	0.000326	0.000063	-0.000263
0.1	0.001	-0.000911	-0.000742	0.000169
0.1	0.01	-0.000906	-0.000739	0.000167
0.1	0.1	-0.000854	-0.000707	0.000147
0.1	1.0	-0.000358	-0.000395	-0.000037
0.1	3.0	0.000623	0.000246	-0.000377
1.0	0.001	0.001965	0.001054	-0.000911
1.0	0.01	0.001970	0.001057	-0.000933
1.0	0.1	0.002022	0.001090	-0.000932
1.0	1.0	0.002518	0.001401	-0.001117
1.0	3.0	0.003499	0.002043	-0.001456
3.0	0.001	0.007836	0.004834	-0.003002
3.0	0.01	0.007841	0.004837	-0.003004
3.0	0.1	0.007893	0.004869	-0.003024
3.0	1.0	0.008390	0.005181	-0.003209
3.0	3.0	0.009371	0.005823	-0.003548

(a) $T_1 = 161.1^{\circ}$ K and $T_2 = 204.6^{\circ}$ K, corresponding to the lowest and highest temperatures respectively at which the distillation study was performed. Δ is the difference of $\ln (P'/P)_{T_2}$ minus $\ln (P'/P)_{T_1}$.

XXXIV is used. None of the internal-external interaction constants were included. Tables XXXVI and XXXVII are summaries of the differential effects of the interaction force constants involving T_z and the internal coordinates. These illustrate the general observation that the differential effects of the internal-external interaction force constants are similar for different choices of F_{ii} and F_{ee}. However, these different choices significantly effect the magnitude of $\ln (P'/P)$. Thus, the choice of F_{ii} and F_{ee} of Table XXIX sets the level of $\ln (P'/P)$ at a sufficiently positive (normal) level with $F_{ie} = 0$, so that sufficiently large F_{ie} elements could be included in order to achieve a reasonably large slope without going too far into the inverse region. The choice of F_{ii} and F_{ee} of $F_{liq}(II)$ in Table XXXIV leads to an agreement with the experiment which is intermediate in slope between F_{liq} of Table XXIX and $F_{liq}(I)$ of Table XXXIV, as shown by the dotted line in Figure 32.

The importance of the effect of the non-classical rotation of gaseous molecules towards $\ln \frac{s}{s'}f_g$ was pointed out by Bigeleisen, Cragg, and Jeevanandam[12] in relation to the vapor pressure isotope effect in methane. When this effect is explicitly included, Equation 3 becomes

$$\ln \frac{P'}{P} = \ln \frac{s}{s'}f_c - \ln \frac{s}{s'}f_g{}^o - \ln f_R \qquad (51)$$

where $\frac{s}{s'}f_g{}^o$ is the reduced partition function of the

TABLE XXXVI. Differential Effects of Internal-External Interaction Force Constants

for Trial Liquid $\underset{\sim}{F}$ Matrix : f_{tr} = 0.3 mdyn/$\overset{o}{A}$, f_{rot} = 0.05 mdyn-$\overset{o}{A}$[a]

$\underset{\sim}{F}_{ie}$ Elements[b]				$\ell n \ (P'/P)$				
$f(T_z,CH)$	$f(T_z,CF)$	$f(T_z,HCF)$	$f(T_z,FCF)$	@ T_1[c]	@ T_2[c]	Δ[c]	Δ_1[d]	Δ_2[d]
0	0	0	0	-0.000230	-0.000320	-0.000090	——	——
0.01	0	0	0	-0.000209	-0.000303	-0.000094	0.000021	0.000017
0	0.01	0	0	-0.000285	-0.000361	-0.000076	-0.000055	-0.000041
0	0	0.01	0	-0.000403	-0.000446	-0.000043	-0.000173	-0.000126
0	0	0	0.01	-0.000053	-0.000191	-0.000138	0.000177	0.000129

(a) For $\underset{\sim}{F}_{ii}$, see Table XXXIV ("$\underset{\sim}{F}_{liq}(II)$").

(b) In units of mdyn/$\overset{o}{A}$.

(c) T_1 =161.1^o K and T_2 = 204.6^o K, corresponding to the lowest and highest temperatures respectively at which the distillation study was performed. Δ is the difference of $\ell n \ (P'/P)_{T_2}$ minus $n \ (P'/P)_{T_1}$.

(d) $\Delta_1 = \left[\ell n \ (P'/P)_{T_1} \text{ with } f_{ie} = 0.01\right] - \left[\ell n \ (P'/P)_{T_1} \text{ with } \underset{\sim}{F}_{ie} = \underset{\sim}{0}\right]$

$\Delta_2 = \left[\ell n \ (P'/P)_{T_2} \text{ with } f_{ie} = 0.01\right] - \left[\ell n \ (P'/P)_{T_2} \text{ with } \underset{\sim}{F}_{ie} = \underset{\sim}{0}\right]$

TABLE XXXVII. Differential Effects of Internal-External Interaction Force Constants

for Trial Liquid $\underset{\sim}{F}$ Matrix : $f_{tr} = 0.1$ mdyn/$\overset{O}{A}$, $f_{rot} = 0.05$ mdyn-$\overset{O}{A}$[a]

$\underset{\sim}{F}_{ie}$ Elements[b]				$\ell n\ (P'/P)$				
$f(T_z,CH)$	$f(T_z,CF)$	$f(T_z,HCF)$	$f(T_z,FCF)$	@ T_1[c]	@ T_2[c]	Δ[c]	Δ_1[d]	Δ_2[d]
0	0	0	0	-0.000883	-0.000725	0.000158	———	———
0.01	0	0	0	-0.000862	-0.000708	0.000154	0.000021	0.000017
0	0.01	0	0	-0.000938	-0.000766	0.000172	-0.000055	-0.000041
0	0	0.01	0	-0.001057	-0.000851	0.000206	-0.000174	-0.000126
0	0	0	0.01	-0.000705	-0.000595	0.000110	0.000178	0.000130

(a) For $\underset{\sim}{F}_{ii}$, see Table XXXIV ("$\underset{\sim}{F}_{liq}$(II)").

(b) In units of mdyn/$\overset{O}{A}$.

(c) $T_1 = 161.1^{O}$ K and $T_2 = 204.6^{O}$ K, corresponding to the lowest and highest temperatures respectively at which the distillation study was performed. Δ is the difference of $\ell n\ (P'/P)_{T_2}$ minus $\ell n\ (P'/P)_{T_1}$.

(d) $\Delta_1 = \left[\ell n\ (P'/P)_{T_1}\ \text{with}\ f_{ie} = 0.01\right] - \left[\ell n\ (P'/P)_{T_1}\ \text{with}\ \underset{\sim}{F}_{ie} = \underset{\sim}{0}\right]$

$\Delta_2 = \left[\ell n\ (P'/P)_{T_2}\ \text{with}\ f_{ie} = 0.01\right] - \left[\ell n\ (P'/P)_{T_2}\ \text{with}\ \underset{\sim}{F}_{ie} = \underset{\sim}{0}\right]$

internal vibrations of the gaseous molecule and

$$f_R = \frac{\left(Q_{qm}/Q_{cl}\right)_R}{\left(Q_{qm}'/Q_{cl}'\right)_R} \tag{52}$$

For a symmetric top molecule, the reduced partition function of the non-classical rotor, $\left(Q_{qm}/Q_{cl}\right)_R$, is given by[39]

$$\frac{Q_{qm}}{Q_{cl}} = e^{\sigma_B/4} \left\{ 1 + \frac{1}{12}\left[1 - \frac{B}{A}\right]\sigma_B + \frac{7}{480}\left[1 - \frac{B}{A}\right]^2 \sigma_B^2 + \cdots \right\} \tag{53}$$

where

$$\sigma_B = \frac{hcB}{kT} \tag{54}$$

$$A = \frac{h}{8\pi^2 c I_A} \tag{55}$$

$$B = \frac{h}{8\pi^2 c I_A} \tag{56}$$

Use of $I_A = 1.48019 \times 10^{-38}$ erg-sec^2 and $I_B = 8.10673 \times 10^{-39}$ erg-sec^2 for $^{12}CHF_3$, and $I_A = 1.48019 \times 10^{-38}$ erg-sec^2 and $I_B = 8.12771 \times 10^{-39}$ erg-sec^2 for CHF_3 in Equation 52 leads to

$$\ln f_R = \frac{3.08 \times 10^{-3}}{T} - \frac{3.423 \times 10^{-5}}{T^2} \tag{57}$$

It is apparent that the non-classical rotational correction for $^{13}C/^{12}C$ substitution in CHF_3 is insignificant primarily due to its large molecular weight and moments of inertia.

The disagreement between the calculated and the

least-squares fit values of A and B of Bigeleisen's two term approximation, Equation 11, as pointed earlier, is not significant per se. First, Bigeleisen's two term expression for $\ln (P'/P)$ is an approximation to the exact expression, Equation 3. Second, the large degree of scatter of the experimental points led to large uncertainties in the least-squares fit values of A and B. The true test for an agreement between experiment and theory lies in a comparison of the calculated $\ln (P'/P)$, according to Equation 3, and the experimental values. Even the solid line in Figures 31 and 32, however, does not quite follow the trend of the experimental points. This discrepancy is probably a consequence of the simplifying assumptions implied in the simple cell model of the liquid. In this model, a single liquid molecule represents the entire liquid and this molecule interacts with the remainder of the phase which is structureless. The present liquid force field calculation has strongly indicated the existence of an unusually higher degree of interaction between the representative molecule and the remainder of the phase as exemplified by the large shifts in the diagonal $\underline{F}$ matrix elements upon condensation and the existence of large internal-external interaction force constants. This would suggest a significant degree of molecular association, perhaps through hydrogen bonding of molecules. Such a liquid system cannot be well represented by the simple cell model. The disagreement is probably due to this

inadequacy of the model used.

V. CONCLUSION

The vapor pressure difference between the vapor pressure of $^{12}CHF_3$, P', and the vapor pressure of $^{13}CHF_3$, P, between the temperatures of 161° K and 205° K, may be expressed as

$$\ell n \frac{P'}{P} = \frac{(217 \pm 66)}{T^2} - \frac{(0.89 \pm 0.36)}{T} \tag{58}$$

according to Bigeleisen's two term equation, Equation 11.

The inclusion of the second-order term in Cohen's Long Time Kinetics Theory, Equation 20, affords a closer least-squares fit of the experimental isotopic ratios of samples within approximately the first 100 minutes of time zero of the distillation. After this initial period, the effect of this modification is insignificant.

According to the cell model, the experimentally obtained data of ℓn (P'/P) is not reproduced in the absence of internal-external interaction force constants, within reasonable limits of the external force constants. The experimental data can be adequately reproduced with the gaseous and liquid $\underset{\sim}{F}$ matrices summarized in Table XXIX through the use of Wilson's $\underset{\sim}{F}$ $\underset{\sim}{G}$ matrix method.

VI. ACKNOWLEDGEMENT

VII. REFERENCES

1-Report to United States Atomic Energy Commission, LA-4391, "A Carbon-13 Production Plant Using Carbon Monoxide Distillation", D.E. Armstrong, A.C. Briesmeister, B.B. McInteer, R.M. Potter (1970).

2-J.P. Agrawal, Separation Science, 6(6), 819 (1971).
J.P. Agrawal, Ibid., 6(6), 831 (1971).
A.R. Gupta and T.I. Taylor, Annual Progress Report to United States Atomic Energy Commission, CU-15-62 (1962).
M.R. Ghate and T.I. Taylor, Annual Progress Report to United States Atomic Energy Commission, CU-755-6 (1969).
M.R. Ghate and T.I. Taylor, Ibid., CU-755-7 (1970).

3-R.A. Schwind, Chem Prog Eng, 50, 75 (1969); United States Atomic Energy Commission Report MLM-1886, Mound Laboratory, Feb. 1972.

4-C.A. Hutchinson, D.W. Stewart, H.C. Urey, J Chem Phys, 8, 532 (1940).

5-J.S. Drury, L.L Brown, A.A. Palko, United States Atomic Energy Commission Report ORNL 4306 (1968).

6-M.R. Ghate and T.I. Taylor, Annual Progress Report to United States Atomic Energy Commission COO-3263 (1973).

7-K.Clausius and G. Dickel, Naturwiss, 26, 546 (1938).

8-J. Bigeleisen and M.G. Mayer, J Chem Phys, 15, 261 (1947).

9-Chem & Eng News, 53, #19 17 (1975).

10-J. Bigeleisen, J Chem Phys, 34, 1485 (1961).

11-K. Cohen, The Theory of Isotope Separation as Applied to the Large Scale Production of U-235, McGraw-Hill Book Co., N.Y. (1951).

12-J. Bigeleisen, C.B. Cragg, M. Jeevanandam, J Chem Phys, 47, 4335 (1967).

13-P. Baertschi, W. Kuhn and H. Kuhn, Nature, 171, 1018 (1953)

14-M. Wolfsberg, J Chem Phys, 60, 15 (1963).

15-T. Ishida, United States Atomic Energy Commission Report NYO-4266-1 (1972).

16-T. Ishida, United States Atomic Energy Commission Report COO-3127-1 (1973).

17-T. Ishida, United States Atomic Energy Commission Report C00-3127-4 (1974).

18-J. Bigeleisen, Advan Chem Ser, $\underline{89}$, 1 (1969).

19-T. Ishida and H. Wieck, United States Atomic Enery Commission Report C00-3127-11 (1975).

20-C.J. Rodden, ed.,"Analytical Chemistry of the Manhattan Project", McGraw-Hill Book Co., N.Y. (1950).

21-J. Bigeleisen, Private Communication.

22-J. Bigeleisen, S.V. Ribnikar, J Chem Phys, $\underline{35}$, 1297 (1961).

23-J. Bigeleisen, M.J. Stern, A. Van Hook, J Chem Phys, $\underline{38}$, 497 (1963).

24-Unpublished data of Allied Chemical Corp. (1970).

25-J. Bigeleisen, F.P. Brooks, T. Ishida, and S.V. Ribnikar, Rev Sci Instr, $\underline{39}$, 353 (1968).

26-T.Ishida and H. Wieck, United States Atomic Energy Commission Report C00-3127-2 (1973).

27-M. Benedict and T.H. Pigford, <u>Nuclear Chemical Engineering</u>, McGraw-Hill Book Co., N.Y. (1957).

28-M.E. Rose, Phys Rev, $\underline{91}$, 610 (1953).

29-E.B. Wilson, J.C. Decius, and P.C. Cross, <u>Molecular Vibrations</u>, McGraw-Hill Book Co., N.Y. (1955).

30-Constructed by Mr. H. Wieck.

31-J.H. Schachtschneider and R.G. Snyder, Spectrochim Acta, $\underline{19}$, 117 (1963).

32-T. Ishida and J. Bigeleisen, private communication.

33-D.A. Long, R.B. Gravenor, and D.T.L. Jones, Trans Faraday Soc, $\underline{60}$, 1509 (1964).

34-V. Galasso, G.DeAlti, and G. Costa, Spectrochim Acta, $\underline{21}$, 669 (1965).

35-R. D'Cunha, J Mol Spectroscopy, $\underline{43}$, 282 (1972).

36-G. Glockler and W.F. Edgell, J Chem Phys, $\underline{9}$, 224 (1941).

37-D.H. Rank, E.R. Shull, and E.L. Pace, J Chem Phys, $\underline{18}$, 885 (1950).

38-M.J. Stern, W.A. Van Hook, and M. Wolfsberg, J Chem Phys, <u>39</u>, 3179 (1963).

39-G. Herzberg, <u>Molecular Spectra and Molecular Structure, Vol II.</u>, Van Nostrand Co. Inc., N.Y. (1945).